Anti-lock braking control design using a Nonlinear Model Predictive approach and wheel information

Francesco Pretagostini

Master of Science Thesis

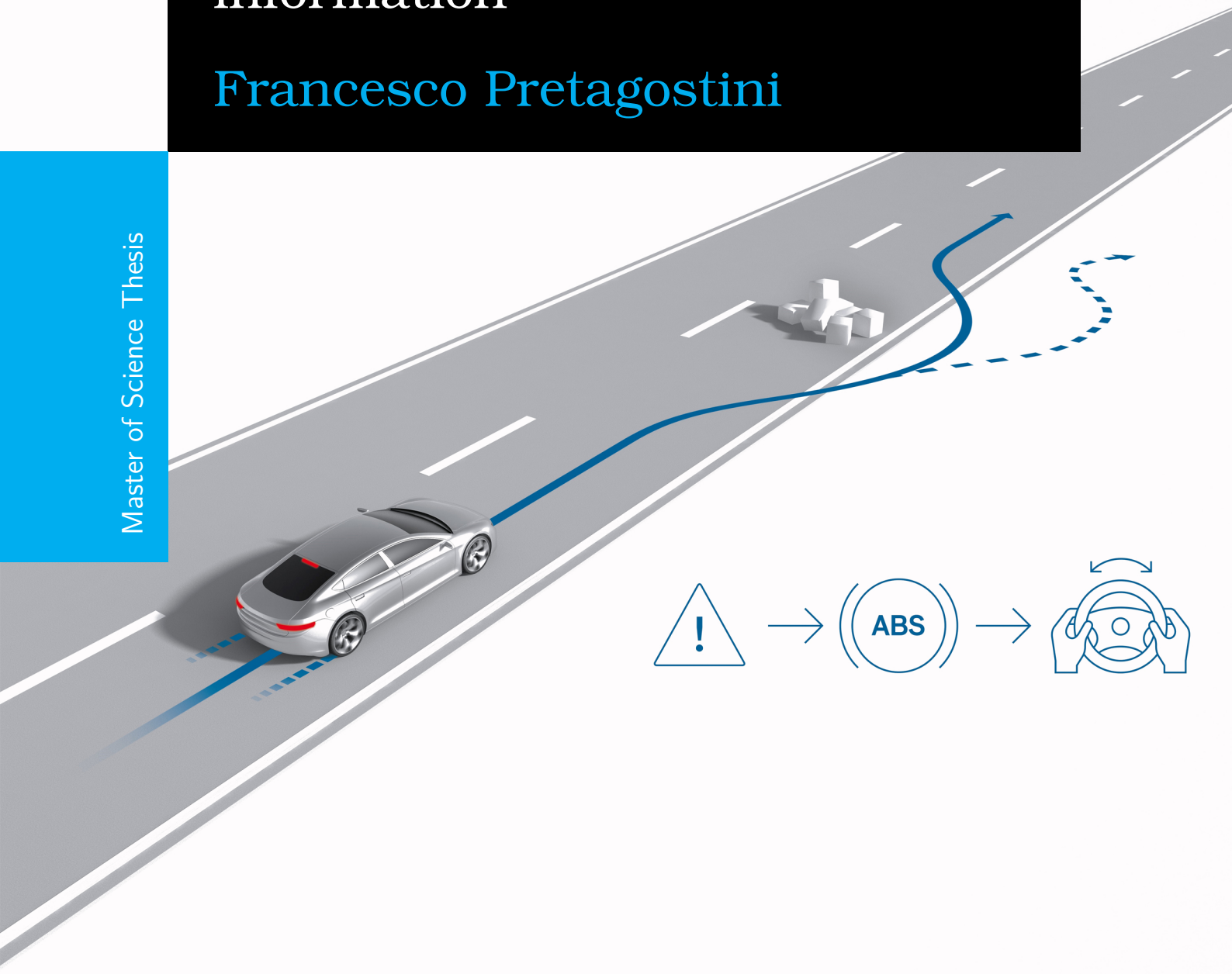

TU Delft Delft University of Technology

Department of Cognitive Robotics (CoR)

Anti-lock braking control design using a Nonlinear Model Predictive approach and wheel information

Master of Science Thesis

For the degree of Master of Science in Vehicle Engineering at Delft University of Technology

Francesco Pretagostini

October 26, 2018

Faculty of Mechanical, Maritime and Materials Engineering (3mE) · Delft University of Technology

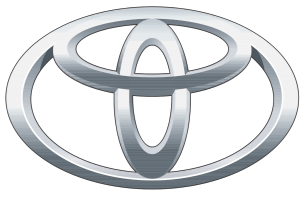

The work in this thesis was supported by Toyota Motor Europe. Their cooperation is hereby gratefully acknowledged.

Abstract

Over the past century, cars have become a fundamental part of our society. With the increasingly larger number of vehicles on the road, safety is, now more than ever, a topic of paramount importance. It is estimated that every year 26,000 people are killed on European roads, corresponding to a social cost of 100 billion euros. In the last two decades, awareness about this issue has however increased substantially, and great effort is now put into improving these numbers.

The introduction of driver assistance systems in recent years has led to a significant decrease in fatal accidents. One of the first implemented ones was Anti-lock Braking System (ABS), introduced on the market in 1978. ABS is an active safety system nowadays mandated on every new car sold in Europe. By preventing wheel lock during emergency braking, the system allows for shorter braking distances and steering ability retention.

Despite the fact that forty years went by since ABS introduction, the control strategy behind it has changed very little, still retaining a rule based approach. Extensive review of literature of the subject, highlighted the possibility that significant improvements could be achieved if the control strategy was to be redesigned in a way that takes advantage of the many technological improvements achieved in the last decade.

The aim in this thesis is to verify this statement and quantify any potential improvement in Anti-lock Braking System. In order to achieve the research objective, a novel ABS algorithm was designed. The controller, based on state of the art hardware, uses a model predictive control approach and potentially available wheel force information as the pillars of its design. A supervisory activation logic is also developed to replicate full ABS functionalities and keep the driver in the loop. The controller is then tested on Toyota's high-end vehicle simulator and benchmarked against the current industrial state of the art.

The vehicle simulator has its core in a multibody model augmented with kinematics and compliance measurements, and it is largely validated against experiments. A complex multiphysics model of the brake system, together with the short wavelength rigid ring tire model, complete the setup.

A comprehensive set of manoeuvres, including friction jumps and rough road braking scenarios, is developed to assess performance and robustness of the proposed controller. Addi-

tionally, a list of aspect-specific performance metrics is drafted and deployed to accurately investigate the simulations results and identify relative gains with respect to the benchmark in different instances of the braking manoeuvre.

The analysis showed substantial reduction of the braking distance and improved steering ability in each of the simulated scenarios. Furthermore, robustness of the controller against external factors, such as high frequency noise generated by road irregularities or friction transitions, is demonstrated to be comparable to that of industrial state of the art controllers.

Based on the now verified potential of the proposed controller, and a list of the future engineering steps mapping the way until an eventual controller deployment on the market is identified.

Table of Contents

List of Figures

List of Tables

Acknowledgements

Writing this last section of my thesis definitely bring me mixed feelings. On the one hand, I am relieved this work is finally completed and curious about what the future is going to bring next. On the other, it means these amazing two years spent between Delft and Brussels are coming to an end. A time in which I have learned so much, made so many amazing experiences, and had the opportunity of meeting wonderful people. A time from which I will always bring memories with me. For this, I would like to thank the people that have contributed to this work and experience.

First and foremost, I would like to thank my supervisor Barys Shyrokau for always stimulating my knowledge, and for his assistance while working on this thesis. However, I mostly have to thank him for introducing me to the subject of vehicle dynamics controls. A subject I became extremely passionate about, and that probably wouldn't have appreciated without meeting him first, and having him as a guide later.

Additionally, I would like to thank my manager at Toyota, Giovanni Berardo, for becoming my mentor throughout my year in Brussels and for teaching me some important managerial qualities I will always keep with me. Furthermore, I would like to thank my colleagues from TME chassis division for making me feel part of a group and for their tireless will to share their knowledge with me. Although many should be given, a special mention goes to Yugo Kiyasu for his constant advise, many late night conversations about my work, and for keeping me motivated in the most difficult times.

Moreover I would like to thank my friends, those who where in Delft and those that weren't, for making my journey a lot easier, and for the fantastic moments already spent together and the many ones to come. My family also deserves a big thank you. I would not have had the opportunity of writing this work if it wasn't for my parents. They therefore deserve all of my gratitude for backing my choices unconditionally. Last, but certainly not least, I would like to thank Myrthe for her emotional support during the last two months of this work and for taking my mind off my work whenever it was getting too much.

Delft, University of Technology
October 26, 2018

Francesco Pretagostini

"Prediction is very difficult, especially if it's about the future."
— *Niels Bohr*

Chapter 1

Introduction

Since its first invention, the automobile has transformed from a luxury product accessible to very few people to one of the most important means of transportation. While over the years the technology used in cars has changed much, one thing has not: a human drives the car. In fact, the vast majority of vehicle crashes can be attributed to human error, with loss of control being one of the main causes. The introduction of driver assistance systems has led to a considerable decrease in road accidents. These systems are designed to take control over selected tasks in an emergency situation, in the attempt to keep the vehicle controllable for the driver. However, they are yet far from being perfect and their capability continuously extends with the technological progress.

1-1 Road safety

Over the past century the automobile has become an integral part of modern society, enabling affordable mobility to the masses. Statistics speak for themselves: according to the ACEA, [11], there are around 291 million vehicles on Europe's roads, or one for every two people; for the US, the NHTSA recorded over 268 million registered passenger vehicles in 2016, which travelled a combined 5 trillion kilometers [12].

This unprecedented level of mobility however, does not come without its cost: during 2016 in the EU only, 26,000 people lost their lives on the road [1], see Figure 1-1, while a total of 37,461 people died in the US [13]. If the prospective is enlarged to less developed countries too, numbers are even worse: estimates by the World Health Organization suggest that, on a yearly basis, road crashes kill 1.25 million people –nearly 3400 road fatalities per day –and injure up to 50 million [14].

Fortunately, in the last two decades awareness about this issue has increased substantially and great effort from all areas is put into improving these very sad numbers. Road safety research has increased exponentially since the 1950s [2], see Figure 1-2.

At policy levels ambitious targets are being set by regulatory bodies. The European commission targeted to reduce the number of annual road fatalities to 27,000 by 2010 and 15,750 by

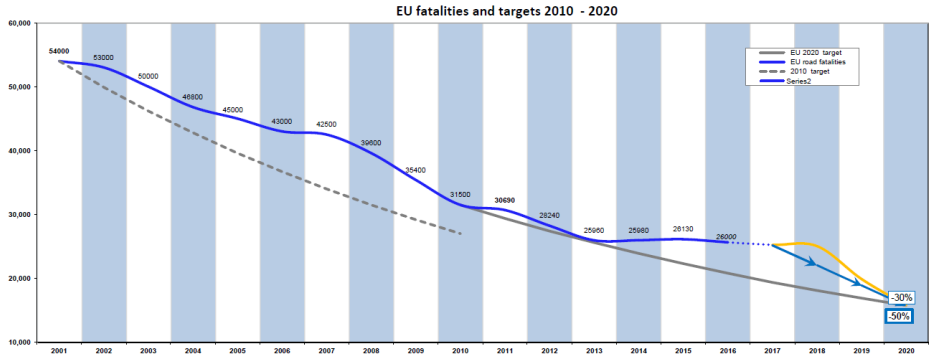

Figure 1-1: Evolution of EU28 fatalities 2000-2016 and targets 2010-2020 [1]

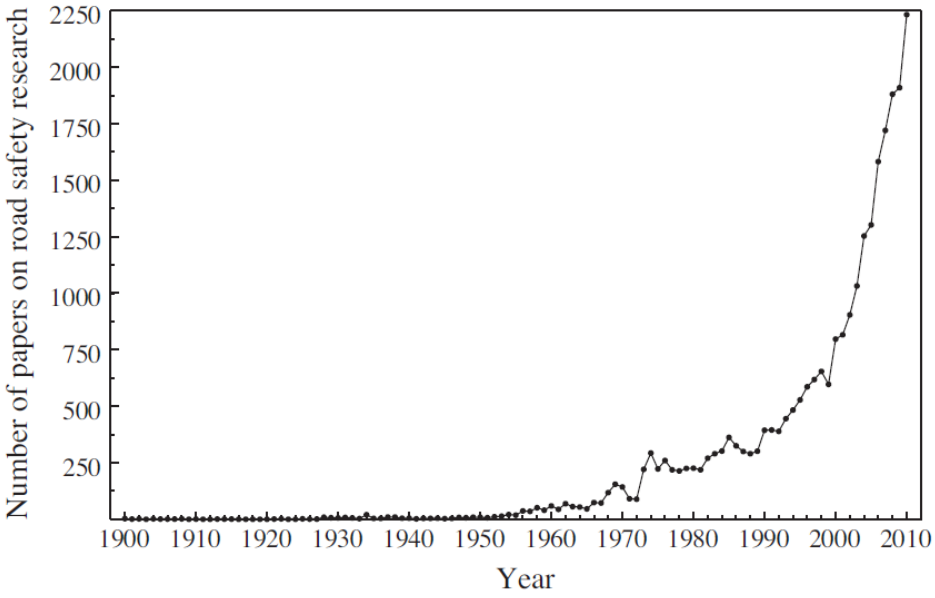

Figure 1-2: Yearly number of articles on road safety from 1990 to 2010 [2]

2020 [1]. The first goal was unfortunately missed and, by looking at Figure 1-1, a plateau seems to be reached in the recent years. A similar behaviour is shown by statistics regarding the US, where according to "traffic safety facts" the number of fatalities have increased in the last two years [12].

There are however, multiple ways to improve road safety further. These can be categorized in three macro-areas. The first regards intervention on improving the road infrastructure, for example placing street lighting, improving road surface quality or installing road signs. The latter twos are concerned the vehicles themselves. Vehicle safety systems are divided into passive and active systems. Passive safety aims at reducing injuries and preventing deaths after an impact; good example of passive safety systems are: seat-belts, airbags, crash structures, etc. On the other hand, active safety is concerned with preventing those incidents from happening instead of alleviating their effects. Events such as high speed lane changes or sudden changes in tire friction can make it difficult for a untrained driver to keep control of the vehicle and often result in crashes. A large number of incidents of this kind can be

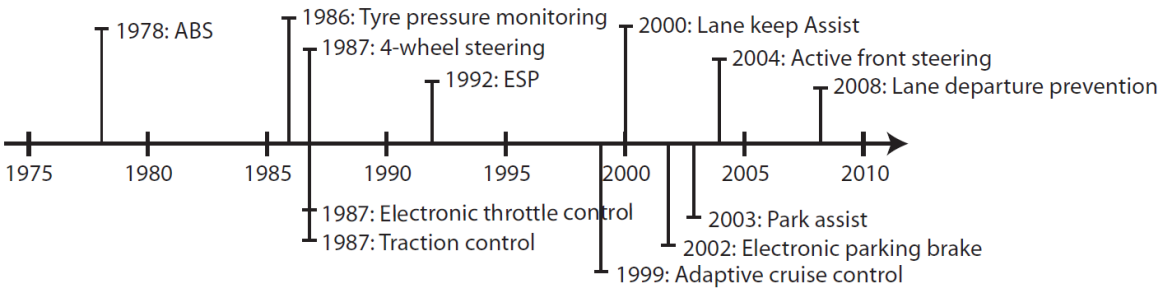

Figure 1-3: Introduction of various driver assistance systems throughout the years [3]

reduced in severity, or even completely avoided, if vehicles are made easier to control in such situations.

Active safety systems, also known as Advanced Driver Assistance Systems (ADAS), started appearing back in the 1980s and have since resulted in significant reductions in the human cost of automobiles. These systems, including Anti-lock Braking System (ABS), Traction Control System (TCS), Electronic Stability Control (ESC), and Roll Stability Control (RSC) utilize control over the drive and brake systems of the vehicle to augment the driver's actions and improve the handling response of the car. A time-line of the various driver aids and their introduction throughout the years is shown in Figure 1-3.

This thesis will focus on one of the previously mentioned active safety systems, namely, the ABS.

1-2 ABS introduction

The Anti-Lock Braking System (ABS) is an active safety technology used to control wheel dynamics during severe braking. The system aims at maximizing braking performance while keeping the vehicle's ability to steer and thus the capability of controlling it in the lateral direction.

Practically, when a driver applies the brake pedal on a moving vehicle, the wheels tend to slow down relative to the ground, causing tire slip. The slip results in the generation of longitudinal tire-road force. As the brake apply is increased, the wheel slip, hence the brake force, increases proportionally. This continues until the maximum braking capability of the particular tire and road surface is reached. Upon further application of the brake input, wheel slip moves to its unstable region, eventually ending in wheel lock [15]. The coefficient of road adhesion then falls to its sliding value, and the tire's ability to sustain lateral force is reduced to almost null. As a result, the stopping distance will be longer and the directional stability of vehicle in turning manoeuvres will be lost [16].
This is a quick and simplistic way of looking at combined slip dynamics but it explains well the need of ABS; for a more detailed explanation of the phenomenon the reader may refer to [7].

1-2-1 ABS requirements & challenges

The ABS control objective is practically achieved by monitoring the applied brake torque by means of pressure modulation. Being a safety system, ABS must satisfy a wide range of requirements which are well summarized in [17]:

- The closed-loop brake control system must be capable of maintaining steering response and vehicle stability at all times, regardless of the road conditions;
- ABS should be capable of utilizing the friction between tires and road surface to maximum effect;
- The brake control system must remain operational through the vehicle's entire speed range;
- The controller must allow for rapid adaption to changes in road friction;
- The demands for vehicle stability, steering response and optimal braking must be kept at all times, also on bumpy roads.

Additionally, ABS specifically poses unique challenges [18]:

- Depending on road conditions, the maximum allowable braking force may vary over a wide range;
- The vehicle velocity and thus longitudinal wheel slip signal, crucial for controller performance, is both highly uncertain and noisy;
- The coefficient of friction between tire and road cannot be accurately measured and need to be estimated;
- On rough roads, the wheel slip ratio varies widely and rapidly due to tire bouncing;
- The torque-pressure relation is non-linear due to variations in disc-pad friction coefficient;
- A certain degree of uncertainty is also associated with vehicle parameters (e.g. mass, CoG location, etc.);
- The plant to be controlled (elastically suspended wheel, braking servo system and actuators) introduces significant delays which limit the controller's bandwidth.

Besides, the main difficulty arises from the strong non-linearity of the tire, a result of tire force saturation. Due to the long list of problems to overcome, a wide variety of approaches have been proposed since the first reliable automotive application by Bosch in 1978 [19], [20].

1-2-2 ABS control variables

In the literature regarding ABS, three control variables have been traditionally used:

- Wheel acceleration — $\dot{\omega}$;
- Longitudinal wheel slip —λ;
- Tire longitudinal force —F_x.

The use of the angular acceleration comes from the fact that it can be easily measured with a wheel encoder. Furthermore, controllers of this type are able to keep the wheel slip in a neighbourhood of the optimal point, without explicitly using the value of optimal wheel slip, λ^*. However, these algorithms are only able to track the optimum λ^* and not to stabilize the system around any arbitrary reference. Consequently, the selection of the set point is extremely crucial, and, since it is impossible to find a unique value for every road condition, a set point adaption must be implemented. Additionally, the control action can be dynamically critical if the road surface changes rapidly and the thresholds are often based of heuristic arguments, resulting in a complex tuning procedure [5].

Regulation of the wheel slip is simpler from the dynamical point of view and is less sensitive to friction coefficient estimation errors. Moreover, slip control has the interesting feature that the applied torque converges to a fixed value, hence, wheel slip control shows no oscillations like for the wheel acceleration case [21], [22]. Nonetheless, the slip measurement requires the estimation of vehicle speed, which is often noisy. Therefore, noise sensitivity of the controller is a critical issue in this case, especially at low speed [19].

ABS systems could be made more robust and less complex if wheel load information are used. Specifically in an ABS context, wheel force information would allow to measure the friction coefficient peak and remove some tedious and sometimes unreliable estimation steps [23]. Load-sensing bearings or intelligent tires with embedded MEMS accelerometers, allow to measure wheel forces with sufficient accuracy and bandwidth, making suitable for the application in vehicle dynamics control of consumer cars in the near future. As a note, it would as well be possible, for a more cost effective market implementation, to replace sensors by creating appropriate force estimators; however, with the drawback of added implementation complexity.

1-2-3 ABS actuation

The design of braking control systems is clearly highly dependent on the brake actuators characteristics and performance.

The most common brake layout found in passenger cars is Hydraulically Applied Brakes (HAB), shown in Figure 1-4a. Brake servo assistance is generated by the brake booster: a hollow housing with a movable rubber diaphragm creating two chambers, one of which is pressure varying. The process of filling up the rear chamber with atmospheric air when the brakes are applied, introduces significant delays in the brake actuation. The ABS function is realized by controlling the on/off solenoid valves; the system uses the volume accumulator to dump pressure and the driver force to increase it, while the pump is only used to bring the

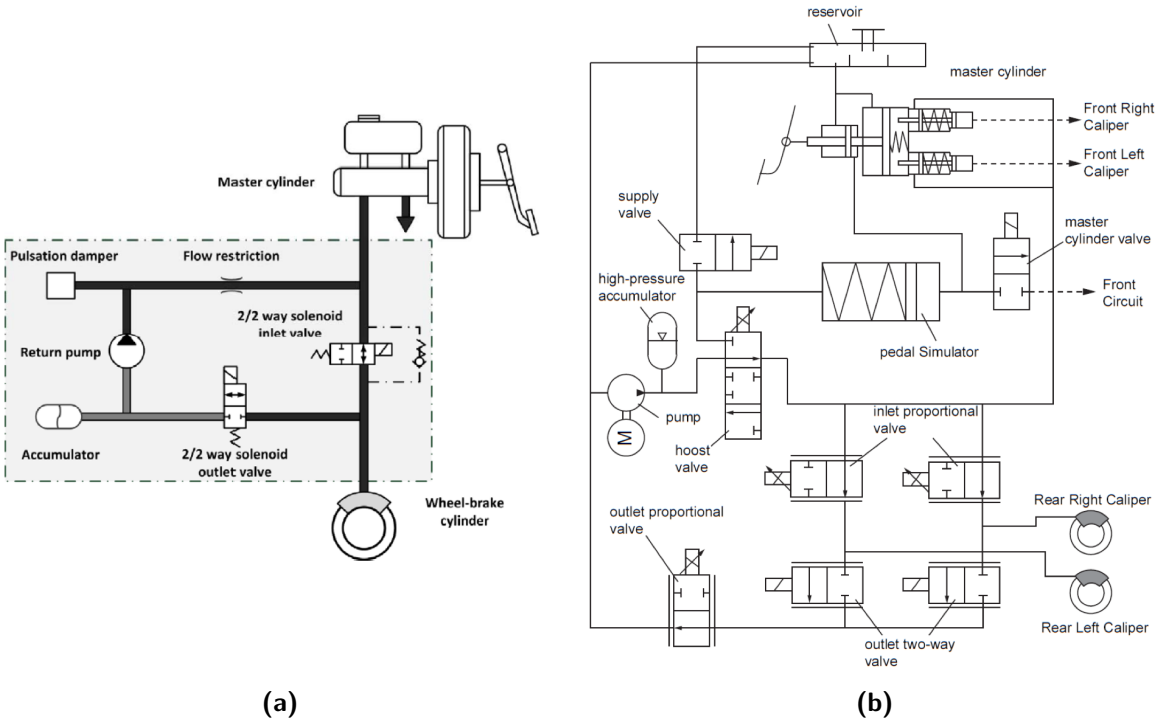

Figure 1-4: Brake system layouts: (a) Conventional hydraulically actuated brakes , (b) Electro-hydraulically actuated brakes, [4]

excess fluid back into the master cylinder reservoir, see Figure 1-4a. This layout is generally not capable of achieving a certain pressure target reliably ,hence, pressure modulation is usually realized in a stairway-fashion making it most suitable for rule based, fuzzy logic and neural network.

The advent of hybrid vehicles and active safety system is causing the gradual shift from conventional hydraulic to Electro-Hydraulic Brake (EHB) systems. These systems are generally characterized by a faster response compared to conventional hydraulic systems and allow for continuous pressure modulation, therefore making it possible to formulate braking control as a classical regulation problem. The system's key element is the boost valve, an electronically controlled proportional valve, downstream the high pressure accumulator, see Figure 1-4b. By proportionally opening and closing this element it is possible to achieve a specific target pressure.

Lastly, in Electro –Mechanical Brake (EMB) systems the "wet" part of the brakes is completely removed and substituted with electric motors on the calipers. The layout is more compact, lighter and faster than both the two previously presented ones; however, the challenges of a large operational range (up to 40 kN), actuator saturation, load-dependent friction, and nonlinear stiffness make it challenging for the EMB to be conveniently applicable to consumer cars.

To decide which layout to use in this work, the three just presented systems where analyzed and ranked in terms of: design simplicity, production cost, system size, real-world feasibility and control possibilities. Results are shown in Table 1-1 The scoring system is such that

Table 1-1: Suitability evaluation of different brake actuators

	Simplicity	Response	Cost	Size	Feasibility	Control	Tot. score
HAB	$\oplus\oplus$	$\ominus\ominus$	$\oplus\oplus$	$\ominus\ominus$	$\oplus\oplus$	$\ominus\ominus$	0
EHB	$\ominus$	$\oplus$	$\oplus$	$\oplus$	$\oplus\oplus$	$\oplus\oplus$	6
EMB	$\oplus$	$\oplus\oplus$	$\ominus$	$\oplus\oplus$	$\ominus\ominus$	$\oplus\oplus$	4

$\oplus\oplus$ is worth 2 points, $\oplus$ is equivalent to a +1, $\ominus$ detracts 1 point and $\ominus\ominus$ equates to a -2. The scores are based both on Toyota's internal objective data and material generated in the field of the EU project Electric-Vehicle Control of Individual Wheel Torque for On- and Off-Road Conditions (E-VECTOORC), [24]. As it can be seen EHB ranks first as it provides the flexibility and controllability of a by-wire system but does not show all the feasibility limitations associated to EMB. For this reason, Electro–Hydraulics Brakes (EHB) will be the go-to system for this thesis.

1-3 ABS control strategies in literature

The focus is now shifted into analyzing the main ABS control trends proposed by researchers and OEMs. There are two macro directions found in literature: the first one, comprising of dynamic threshold based and fuzzy logic controllers, achieves the control objective by discretely modulating brake pressure for each wheel; the second one, including PID, robust, sliding mode, optimal, model based and model predictive controllers, assumes the possibility of continuously modulating brake pressure and, thus, brake torque.

Logic threshold controllers are widely used in ABS applications. The advantages of this control method come from the heuristic and tuneable control laws and low hardware requirements (see Figure 1-4a) [25]. Rules are identified from practical experience as well as intensive simulation studies. The approach does work rather well in practice; however, although initial LUT-values and their range of variability can be assessed in simulation environment, extensive testing is needed to fine tune the control logic.

Threshold based algorithms can be well represented using the concept of Finite State Machines (FSM). A number of states, each associated with a certain control action, is defined a-priori and the jump from one state to the other is triggered by the control variable overcoming a certain predefined threshold, see Figure 1-5. Three control actions are generally defined: apply, dump and hold pressure. A more detailed explanation of the working principles behind these algorithms can be found in [26] and [27].

Commercially available ABS systems are all of this kind, and event-triggering thresholds are usually dynamical values of slip and deceleration, or a switching surface defined using a weighted sum of the two [28]. Because road conditions vary over a large range of friction levels, the thresholds need to be redefined for each of them (i.e. dry, wet, snow, etc.), resulting in an adaption of logic based on the output of a friction estimator.

Furthermore, the inclusion of rules related to the functions of Electronic Brake Distribution (EBD), Autonomous Emergency Braking (AEB), TCS, jerk compensation, μ-split, braking while turning, and many others, make the state machine extremely intricate.

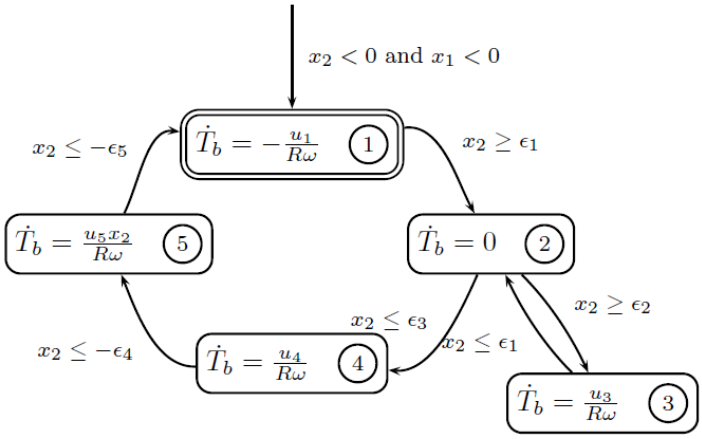

Figure 1-5: Rule Based ABS finite state machine from [5]

From this brief analysis, it becomes clear that the number of tuning parameters for a commercial Rule-Based (RB) application is incredibly high, and only companies with years of experience in their development and tuning are able to provide this kind of Anti-lock Braking System controllers. Nonetheless, some academic examples of Rule-Based ABS control are found in [5], [22] and [29].

Next to industrial applications, multiple other control strategies have been proposed in the vast field of ABS control research, each of the control methods was thoroughly analyzed prior to the start of this thesis work. A short summary of their advantages and disadvantages is now presented. A more detailed discussion may be found in [30] and [31].

- Fuzzy logic controllers can be a good way of approaching estimation of vehicle parameters but are not well suited for full ABS design since they heuristic nature makes them very difficult to tune and requires large training sets. An interesting approach in which rules are not based on experience but rather adopted automatically according to the wheel slip by means of Adaptive Network-based Fuzzy Inference System (ANFIS) is presented in [32]. Lastly, the recent trends towards integrated chassis control are impossible to achieve with this technology.

- Neural networks require even larger and more accurate training data to achieve adequate performance and robustness. On the vehicle system, this is extremely pricey, or even, economically unthinkable.

- PIDs struggle with non-linearities and can go unstable if countermeasures are not in place. Additionally, they lack a feed-forward term causing them to be slow.

- Optimal control requires a significant computational effort to solve the optimization problem. Additionally, it is not as robust as Model Predictive Control (MPC) with respect to modelling errors, and lacks feed-forward ability.

- Sliding mode controllers are very robust but present chattering issues. When this is addressed by a method that does not introduce significant trade-offs, for example in the

Integral Sliding Mode Controller (ISMC) case as in [33], they represent the best reactive wheel slip controllers in terms of performances and robustness.

- Robust controllers allow the design to be simpler since no adaption is necessary for the controller to be stable; however, little can be said about their performances compared to the other mentioned control strategies due to the lack of publications on the topic. Again, being reactive, they are very sensitive to actuator's bandwidth and general performance.
- Model predictive control represents an opportunity to improve dynamic performance and robustness of state of art controllers; however, the computational burden, especially if a non-linear prediction model is used, needs to be addressed.

In conclusion, because of all of the above reasons, MPC is believed to be the field with the most potential, and little has been so far investigated in terms of possibilities (i.e. only simple linear model have been proposed). The advance in microcontrollers processing power and the drive towards a model based integrated chassis control means that its major drawback, computational effort, is decreasing in importance and could be outweighed by its performance benefits. These tough still need to be effectively proved by means of detailed, trustworthy simulation at first, and Hardware In the Loop (HiL) or field testing in case simulation shows a promising outcome.

1-4 Thesis goal

As previously mentioned, ABS individually controls brake torque to keep each tire at its optimal slip or, where the maximum braking force is generated. Reducing the distance in which a vehicle is able to stop can, per se, dramatically reduce the likelihood of a crash; however, in a situation in which this is not sufficient, ABS should keep the vehicle steerable at all times during the braking so that an avoidance manoeuvre could be attempted.

Steering is however only used in this work to maintain the vehicle straight during braking, or in other words, no obstacle avoidance manoeuvre is specifically simulated to both reduce the complexity of the problem and avoid ESC-effects when comparing the proposed controller with the benchmark provided by Toyota.

Optimal wheel slip tracking should be achieved regardless of the external conditions. In other words, the controller should be robust to:

- Tire-road friction conditions (high-, medium-, low- μ)
- Road state (e.g perfectly smooth road, wavy roads, cobblestones, etc.)
- Sudden changes in available grip (μ-jump)

Keeping what was just mentioned in mind, the main research question of this project can be formulated as follows:

> *How can nonlinear model predictive control and wheel force information improve nowadays ABS algorithms?*

To answer this question, several objectives have been set:

- Develop a brake system transient model in Dymola © multi-physics software to accurately replicate brake system transient behaviour;
- Extend Toyota's vehicle model, developed in Simpack ©, to allow it to be paired with the brake system model and ABS controller;
- Develop and tune a nonlinear model predictive ABS controller and cast it in a way that is equivalent to the bechmark Rule-Based controller provided by Toyota;
- Exploit multiple co-simulation strategies to allow the mentioned systems to communicate among each other and produce an accurate replica of the most important effect influencing ABS braking;
- Compare the two control strategies on a variety of ABS braking scenarios;
- Clearly identify strength and weaknesses of the proposed controller by means of thorough analytical analysis of test results by means of effect-specific performance indicators.

Now that research questions and objectives have been defined, a short section highlighting the contribution of this work to Toyota Motor Europe (TME) scope is presented.

1-5 Thesis contributions

There are multiple aspects in this work that represent an interest for Toyota Motor Europe chassis control and chassis brake divisions.

First of all, this is the first time a multi-phisics model of the brake system is realized; the model will be used, in addition to what done in this work, to conduct parametric analysis on how different systems' design elements (e.g. from suspensions and brakes) affect the vehicle behaviour.

Moreover, introduction of the control logic in the vehicle model will allow closer replication of the real vehicle behaviour in limit braking and handling manoeuvres. General exploitation of multiple co-simulation tools was also of significant importance for Toyota Motor Europe's model based design activities, in fact this is the first time s-function, Inter-Processor Communication (IPC) and Functional Mock-up Unit (FMU) are used in the same simulation within an vehicle dynamics framework.

On the control side, the realization of a MPC Anti-lock Braking System that is as close as possible in design philosophy to an implementable controller will clearly show, not only the performance differential between rule based and model-based controller, but also give an idea what kind of hardware requirements and costs would be needed to implement such a control strategy.

Moreover, this work will also start investigating what performance benefits would be obtained by a controller that uses wheel information (e.g. tire forces and road friction) as a element of its design.

Lastly, this would be the first time a in-house model-based ABS controller is developed in TME.

1-6 Thesis outline

This thesis consists of seven chapters leading to a complete answer to the earlier stated research question.

1. Chapter 1 introduced some key concepts related to ABS, motivated the choices made for the control strategy and brake hardware, as well as formulating the research objectives and contributions.
2. Chapter 2 focuses on accurate modelling of the vehicle's behaviour and that of its subsystems.
3. Chapter 3 presents the validation of the used simulations models and introduces the final co-simulation layout.
4. Chapter 4 explores the theory behind Nonlinear Model Predictive Control. Moreover, a first implementation of the ABS, focusing on control of the wheel corner is examined with the intent of more easily explaining some fundamental aspects regarding the final controller.
5. Chapter 5 formulates the proposed full-car ABS controller. Its key aspects are well described and some necessary subsystems for its correct functioning introduced.
6. Chapter 6 describes on how the proposed controller was assessed in simulation and discusses the findings obtained for each of braking scenario. Moreover, it briefly discusses the working principle of the benchmark logic: a RB (Rule-based) controller that replicates the one found on the vehicle simulated in this work.
7. Chapter 7, presents some more general conclusions, as well as, recommendations for future research in this field of study.

Chapter 2

Modelling of the vehicle and its subsystems

When a new control strategy is designed, simulation can be an incredibly powerful development tool as it gives designers the required flexibility and repeatability that field testing simply would not be able to achieve. However, it is very important to understand what are the key aspects that should be replicated to produce a result that is as close as possible to the real word case.

It was generally noticed that the majority of literature discussing ABS, especially that presenting advanced control strategies, often relies on oversimplified vehicle models that are capable of providing a first idea of how the controller would behave but fail to replicate some of the effects that may lead to unstable or even unusable controllers in a real word situation (e.g. subsystem nonlinearities and delays, as well as road-related parameters fluctuation).
On the other hand, in research and industrial literature concerning vehicle modelling, a broad spectrum of complexity is observed as this is linked to the required application and development stage. For example, if a preliminary study for an active suspension system is planned, a quarter car model (one or two degrees of freedom vertical model) might be the appropriate tool. However, if simulation of the complete vehicle behaviour is wished, e.g. for a vehicle handling study, we might opt for a planar vehicle model or for a 14 DoF one (including pitch and roll) depending on how detailed our aim is. When making this choice there is usually a trade-off between modelling accuracy and available resources (of computational power, time or budget for example).

For this specific application, as the full vehicle behaviour needs to be simulated, a variety of options is available. The number of degrees of freedom and, accordingly, the number of differential equations varies from two for the classical bicycle model up to 38 DoF models for complex investigations [34], passing through the application of the 8 DoF [35, 36], and rarely the 14 DoF [37, 38]. In addition, in case of multibody commercial software (e.g. MSC.ADAMS or Simpack), this number can grow up to 160.

Due to the multitude of effects influencing the vehicle dynamics during an ABS stop (e.g. brake system behaviour, suspension kinematics and compliance, load paths, etc.), either a

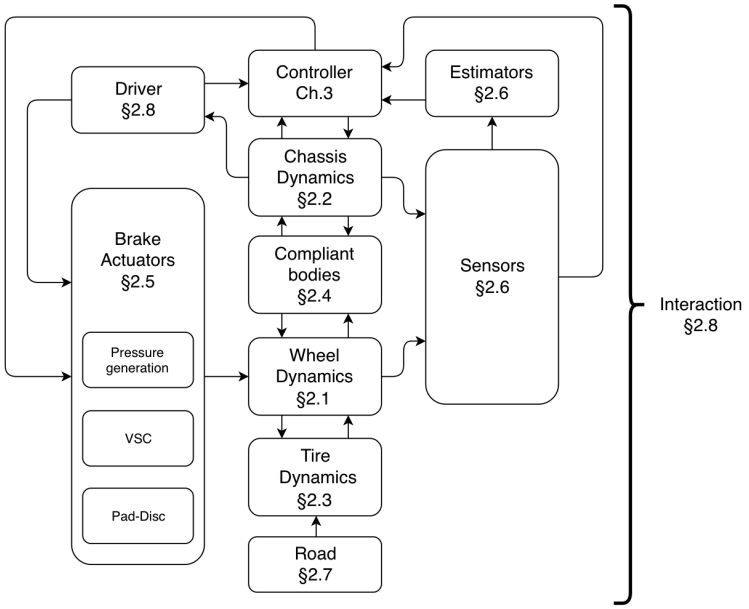

Figure 2-1: Overview of system's components and corresponding paragraph

complicated analytical model or a multibody model including these elements was required to predict anything close to the real vehicle output. Because of its extremely modular structure, the multibody approach was finally chosen, as this would more easily allow for incorporation of the subsystems responsible for each of the above-mentioned effects.

The final model, developed in Simpack, includes representations of the vehicle's body, subframes, suspension arms, struts, anti-roll bars, steering system, engine, drive-train and tires. Additionally, some of the elements are structurally compliant and others may present elaborate behaviour captured in empirical models. Examples of the latter include elastomeric elements, dampers, tires, and human beings.

In the next sections, the main components of the selected simulation set-up, see Figure 2-1, will be presented, and their choice motivated by a brief discussion of the main concerns to produce an accurate replication of vehicle behaviour.

2-1 Chassis dynamics

The vehicle's chassis is the main body to which all other components attach. In the model, this is composed by a mass-less body to which four "trim masses" are rigidly connected. These, after an iterative procedure, are set such that the vehicle sprung mass, inertias and some other important parameters are identical to the real vehicle. The procedure allows to lump the mass of some components attached to the chassis that do not need more detailed modelling. Examples of this are the seats, windows, dashboard, etc. Additionally some other components, such as engine and transmission, which originate vibrations that should be caught by simulation, are modelled as independent masses suspended by compliant elements, rubber bushings, and should therefore be removed by the chassis mass.

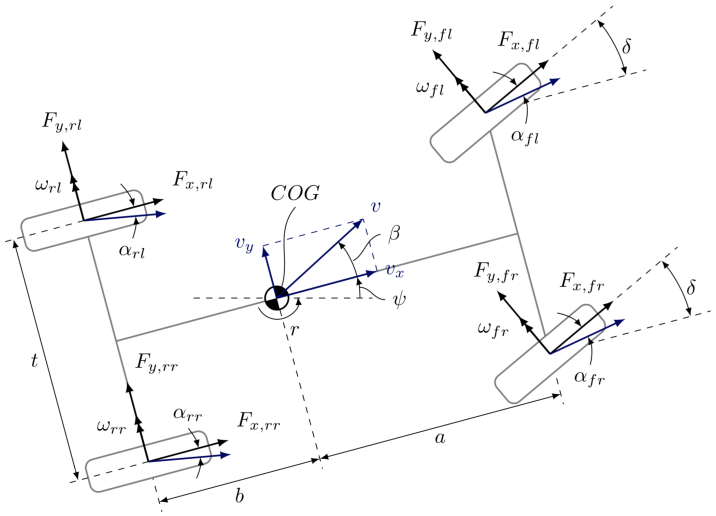

Figure 2-2: Planar free body diagram for passenger car, [6]

Moreover, since the torsional stiffness of the vehicle structure could influence the full vehicle simulations, front and rear half body parts are connected by a revolute joint aligned along the longitudinal axis of the vehicle and located at the CoG. The relative rotation of the two body masses is resisted by a torsional spring with a stiffness corresponding to the chassis' torsional stiffness.

As mentioned, some of the components do have relative motion among them (e.g. engine-body, engine-trasmission, etc.) but given this movement is usually small, they can be seen as a unique element having 6 DoF for descrictive purposes (longitudinal, lateral, vertical, roll, pitch and yaw motions).

Chassis equations of motion

Assuming the vehicle is travelling on a smooth flat road and the road disturbances are equal to zero, the following equations describe the dynamics of the vehicle body [39, 40]. These equations can be derived by drawing a Free Body Diagram (FBD); the one describing longitudinal, lateral and yaw dynamics is shown in figure Figure 2-2, the FBD concerning pitch and vertical dynamics are reported in Figure 2-3 and Figure 2-4 respectively, while the FBD for roll dynamics is omitted.

Longitudinal motion:

$$m_t\left(\frac{dv_x}{dt} - v_y\frac{d\psi}{dt} + v_z\frac{d\theta}{dt}\right) - m_s\left(\frac{d\phi}{dt}\frac{d\psi}{dt} + \frac{d^2\theta}{dt^2}\right)h_s\cos\phi = \sum F_x \tag{2-1}$$

Lateral motion:

$$m_t\left(\frac{dv_y}{dt} - v_x\frac{d\psi}{dt} + v_z\frac{d\phi}{dt}\right) - m_s\left(\frac{d\theta}{dt}\frac{d\psi}{dt} + \frac{d^2\phi}{dt^2}\right)h_s\cos\phi = \sum F_y \tag{2-2}$$

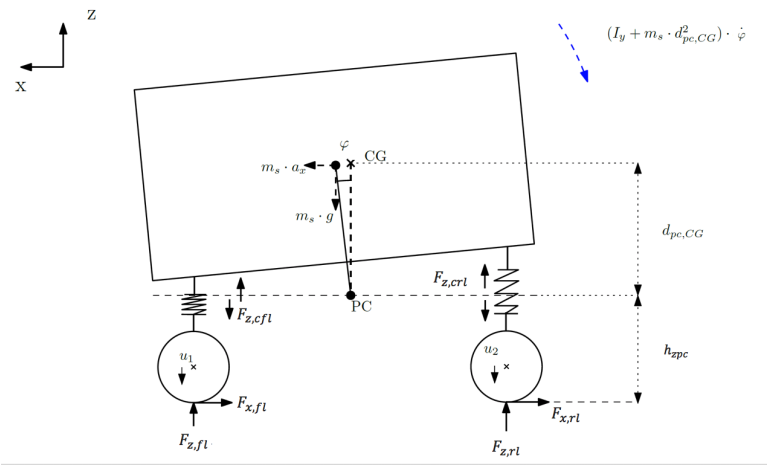

Figure 2-3: Pitch free body diagram for passenger car, [6]

Yaw motion:

$$I_{zz,s}\frac{d^2\psi}{dt^2} + I_{xz,s}\left(\frac{d\theta}{dt}\frac{d\psi}{dt} - \frac{d^2\phi}{dt^2}\right) + m_s a_x h_s \sin\phi = \sum M_\phi \tag{2-3}$$

Roll motion:

$$I_{xx,s}\frac{d^2\phi}{dt^2} - I_{xz,s}\left(\frac{d\phi}{dt}\frac{d\theta}{dt} + \frac{d^2\psi}{dt^2}\right) - m_s a_y h_r \cos\phi = \sum M_\phi \tag{2-4}$$

Pitch motion:

$$I_{yy_s}\frac{d^2\theta}{dt^2} - (I_{zz_s} - I_{xx_s})\frac{d\psi}{dt}\frac{d\psi}{dt} + I_{xz_s}\left(\frac{d^2\phi}{dt^2}\frac{d^2\psi}{dt^2}\right) + m_s a_x h_p \cos\theta = \sum M_\psi \tag{2-5}$$

Vertical motion:

$$m_s\left(\frac{dv_z}{dt} - v_x\frac{d\theta}{dt} + v_y\frac{d\phi_z}{dt}\right) + m_s\left(\frac{d^2\phi}{dt^2} + \frac{d^2\theta}{dt^2}\right)h_s\cos\phi = \sum F_z \tag{2-6}$$

The right hand side of the system of equations is given below:

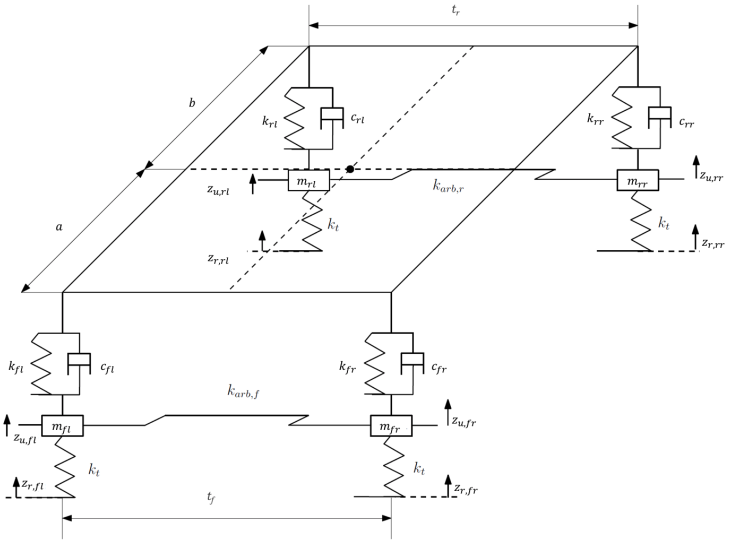

Figure 2-4: Vertical free body diagram for passenger car, [6]

$$
\begin{aligned}
\sum F_x &= \sum_{ij=1}^{4} F_{x,ij} - F_x^{aero} \\
\sum F_y &= \sum_{n=ij}^{4} F_{y,ij} - F_y^{aero} \\
\sum M_\psi &= a(F_{y,FL} + F_{y,FR}) - b(F_{y,RL} + F_{y,RR}) + \frac{t_f}{2}(F_{x,FL} - F_{x,FR}) + \frac{t_r}{2}(F_{x,RL} - F_{x,RR}) + \sum_{ij=1}^{4} M_{zw,ih} \\
\sum M_\phi &= m_s g h_s \sin\phi - \frac{t_f}{2}(F_{z,FL} - F_{z,FR}) - \frac{t_r}{2}(F_{z,RL} - F_{z,RR}) \\
\sum M_\theta &= m_s g h_p \sin\theta - a(F_{z,FL} + F_{z,FR}) + b(F_{z,RL} + F_{z,RR}) \\
\sum F_z &= \sum_{ij=1}^{4} F_{z,ij} - F_z^{aero}
\end{aligned}
\tag{2-7}
$$

In the previous equations, the full vehicle mass is calculated as follows:

$$
m_t = m_s + m_{uf} + m_{ur} \tag{2-8}
$$

The tire projections along the vehicle axes, $F_{x,ij}$, $F_{y,ij}$ are related to the tire forces along the wheel axes as follows:

$$
\begin{bmatrix} F_{x,i} \\ F_{y,i} \end{bmatrix} = \begin{bmatrix} \cos\delta_{ij} & -\sin\delta_{ij} \\ \sin\delta_{ij} & \cos\delta_{ij} \end{bmatrix} \begin{bmatrix} F_{x,ij} \\ F_{y,ij} \end{bmatrix}, i = 1, ...4 \tag{2-9}
$$

Weight transfer - Static and Inertial

An interesting effect, generating form the chassis being elastically suspended, is weight transfer. Since, the more load is present on a corner, the more tire forces can be exploited, this is of particular relevance for ABS. As no lateral manoeuvres are analyzed in this work, longitudinal weight transfer is of most interest. However, for completeness, equations for both longitudinal and lateral effects will be briefly presented.

The load transfer due to longitudinal acceleration, F_z^{long}, is calculated as:

$$F_z^{long} = \frac{m_s h_s + m_{uf} h_{uf} + m_{ur} h_{ur}}{2L} a_x \tag{2-10}$$

Similarly those due to lateral accelerations, $F_{z,front}^{lat}$ and $F_{z,rear}^{lat}$ are:

$$\begin{aligned} F_{z,front}^{lat} &= \left(\frac{m_s h_f l_r}{L} + m_{uf} h_{uf} \right) \frac{a_y}{t_f} \\ F_{z,rear}^{lat} &= \left(\frac{m_s h_f l_f}{L} + m_{ur} h_{ur} \right) \frac{a_y}{t_r} \end{aligned} \tag{2-11}$$

The load transfers owed to roll stiffness and roll damping, $F_{z,front}^{roll}$ and $F_{z,rear}^{roll}$, are defined by the suspension characteristics as follows:

$$\begin{aligned} F_{z,front}^{roll} &= -\frac{1}{t_f} \left(K_{\phi,f} \phi + c_{\phi,f} \frac{d\phi}{dt} \right) \\ F_{z,rear}^{roll} &= -\frac{1}{t_r} \left(K_{\phi,r} \phi + c_{\phi,r} \frac{d\phi}{dt} \right) \end{aligned} \tag{2-12}$$

Similarly, the load transfers due to pitch behaviour, $F_{z,front}^{pitch}$ and $F_{z,pitch}^{roll}$, are:

$$\begin{aligned} F_{z,front}^{pitch} &= 0.5 t_f \left(K_{\theta,f} \theta + c_{\theta,f} \frac{d\theta}{dt} \right) \\ F_{z,rear}^{pitch} &= 0.5 t_r \left(K_{\theta,r} \theta + c_{\theta,r} \frac{d\theta}{dt} \right) \end{aligned} \tag{2-13}$$

2-2 Corner dynamics

Of the six DoF that the wheel possesses, the rotational one around the wheel $y-$axis is definitely the most interesting one from a ABS prospective and will therefore be discussed in this section. Vertical dynamics of the corner, on the other hand, will be briefly touched in section 2-4. The other 4 degrees of freedom, being the rotation of the front wheels about their vertical axis (steering) and those allowed by the compliance of the hub and suspensions will not be treated as they are not of particular importance for a discussion concerning ABS; however, taking them into account in the multibody model will allow for better accuracy of the simulation results.

The wheel assembly behaviour in the rotational direction around the $y-$axis is described by:

$$I_{yy,u}\dot{\omega}_{ij} = R_w F_{x,ij} - T_{b,ij} - T_{drag} \tag{2-14}$$

An additional useful concept to define for future discussions, is that of longitudinal wheel slip, i.e. the normalized relative velocity between the road and the tire, which, in case of zero tire sideslip angle is defined as:

$$\lambda := \frac{v - \omega_{ij} R_w \cos(\alpha_{ij})}{max\{v, \omega_i R_w \cos(\alpha_{ij})\}} \tag{2-15}$$

where v is the wheel ground contact point velocity and $\omega_{ij} R_w$ is the linear speed of the tire (with radius R_w and angular speed ω_{ij}) at the contact point. The presence of a non-zero slip is due, in general, to traction and braking forces exerted on the tire. As this work focuses on braking manoeuvres (hence $v \leq \omega_{ij} R_w$) and considers scenarios of small tire sideslip angle, where $\cos(\alpha_t) \approx 1$, Eqn. (2-15) can be simplified to:

$$\lambda \approx \frac{v - \omega R_w}{v} \tag{2-16}$$

with $\lambda \in [0, 1]$. In particular, $\lambda = 0$ corresponds to a pure rolling wheel and $\lambda = 1$ to a locked one.

2-3 Tire dynamics

As tires are the main way for a vehicle to exert forces on the environment, having models that accurately predict the way the tire generates longitudinal and lateral forces is critical for obtaining a model with good accuracy.

The first tire models in literature were only concerned the steady-state relation between the slip and the developed force, and were physically derived from variants of the brush model, [41]. These models assume the generated force to be instantaneous; however, a tire does not respond instantaneously to changes in slip; a certain distance must be traveled before the steady-state levels of forces and moments are reached. This relaxation behavior is caused mainly by the flexibility of the tire structure.

The dynamic behavior of the tire has lately gained a large interest. In applications such as state-of-the-art active safety systems that intervene in limit conditions by controlled braking actions where the transient properties of the tire affects the vehicle dynamics.

One of the most famous empirical, transient tire models is the Magic Formula (MF), developed by H.B. Pacejka in conjunction with Volvo [13]. Pacejka fitted measurement data to a model to obtain an accurate estimate of these forces [42]. The basic formula when only longitudinal motion is considered is shown in Eqn. 2-17, [8].

$$F_{x0} = D_x \sin C_x \arctan(1 - E)(B_x \lambda + \arctan B_x \lambda) \tag{2-17}$$

Where:

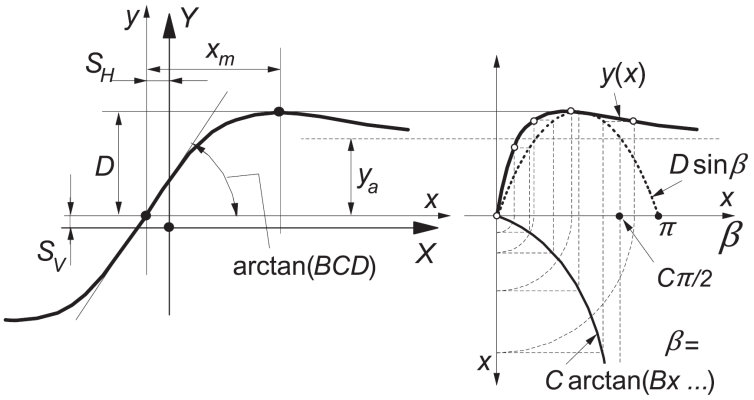

Figure 2-5: Curve produced by the original sine version of the Magic Formula, Eqn. (2-17), [7]

$$\begin{aligned} \lambda &= \lambda + p_{H_{x2}} df_z \\ D_x &= F_z(pD_x 1 + p_{D_{x2}} df_z)\Delta_{\mu x} \\ C_x &= p_{C_{x1}} \\ E_x &= p_{E_{x1}} + p_{E_{x2}} df_z + p_{E_{x3}} df_z^2 \\ K_x &= F_x p_{K_{x1}} \\ B_x &= K_x/(C_x D_x) \end{aligned} \tag{2-18}$$

Here, λ is the longitudinal slip and $df_z = \frac{F_z - F_{z0}}{F_{x0}}$, with F_{x0} being the nominal load. The p coefficients are parameters used for curve fitting and the Δ are optional scaling parameters. The equation showed in this report is for longitudinal dynamics only, however, the original Magic Formula can determine forces and moments in all directions.

Figure 2-5 shows the influence of each parameters on the overall shape of the slip-force characteristic. In the formula D is known as the peak factor and indicates the peak value of the friction function; the parameters C, B and E are known as respectively the shape, stiffness and curvature factor.

Over the years, the model has been modified several times to become the most successful tire friction model. It's most recent form is the Short Wavelength Intermediate Frequency Tire (SWIFT) model, described in [7] and developed by TU-Delft and TNO, is a collection of methods employed to extend the MF-tire concept, with dynamic properties and ability to handle uneven roads. The model can handle frequencies up to 60 Hz and wavelengths larger than 0.2 m. Additionally, it acts on longitudinal slip, lateral slip, camber, and turn slip.

As can be seen in Figure 2-6a, the tire belt is modelled as a rigid body/ring which is elastically suspended with respect to the rim. This can be done since, when considering a maximum frequency of approximately 60–100 Hz, the deformations of the tire belt can be neglected. Residual springs are introduced between the ring and contact patch to ensure that the overall stiffness of the tire (and relaxation lengths) are correct. The ring has a flexible attachment to the rim, with stiffnesses in all directions.

For short wavelengths, the finite length of the contact patch must also be considered. This is accomplished by using the slip model, which accounts for the contact patch transients.

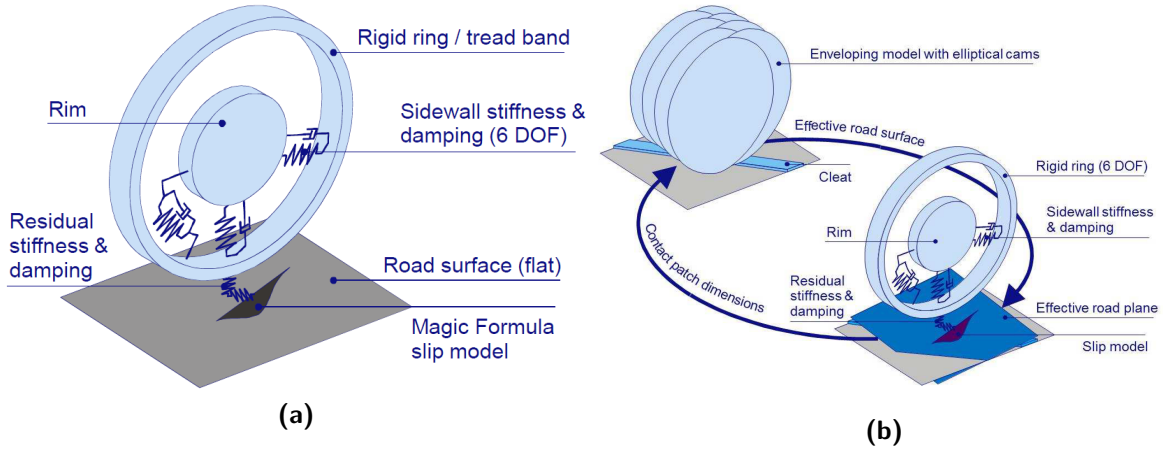

Figure 2-6: MF-Swift: (a) inclusion of belt dynamics, (b) enveloping for uneven road surface, [8]

To improve the transient properties even further, the stiffness in the contact patch rubber is modelled as a first order differential equation with a time constant corresponding to the size of the adhesion area in the patch.

When rolling over short obstacles and rough roads, tire geometry and elasticity give rise to highly nonlinear behavior of the tire forces and changes in the effective rolling radius. To incorporate this enveloping behavior, the concept of effective road surface is used. This is entirely identified by the plane height, slope, curvature and banking. An obstacle-enveloping model, consisting of elliptical cams that touch the actual road surface, is used to generate it, see Figure 2-6b. To be able to manage inclination of the surface, two cams (tandem) are necessary. Finally, the single point rigid ring model contacts this road surface and the slip forces from the Magic Formula act on it.

When choosing among the tire models it is important to consider the purpose of the particular application. The structure and software implementation of MF-Swift allow the user to select the level of complexity according to the simulation scenarios (e.g. basic handling, control testing, rough roads, road load simulations, etc.) making it the appropriate tool for the diverse nature of the simulation scenarios used in this research.

2-4 Compliant bodies

An aspect which is often overlooked in ABS literature is the effect of compliant bodies on the overall dynamics of the vehicle. While in common driving and handling manoeuvres it is reasonable to neglect this effects or to lump them into a characteristic equation (e.g. as it commonly done for anti-roll bars), the forces to which the vehicle is subjected in ABS braking to are too high to assume that this won't affect the vehicle dynamics.

In this work, flexible bodies behaviour, compliance of suspension and that of steering parts are measured on dedicated test benches (i.e. a suspension test bench and a Kinematics and compliance (KnC) rig). The observed behaviour is then replicated either by correct modelling

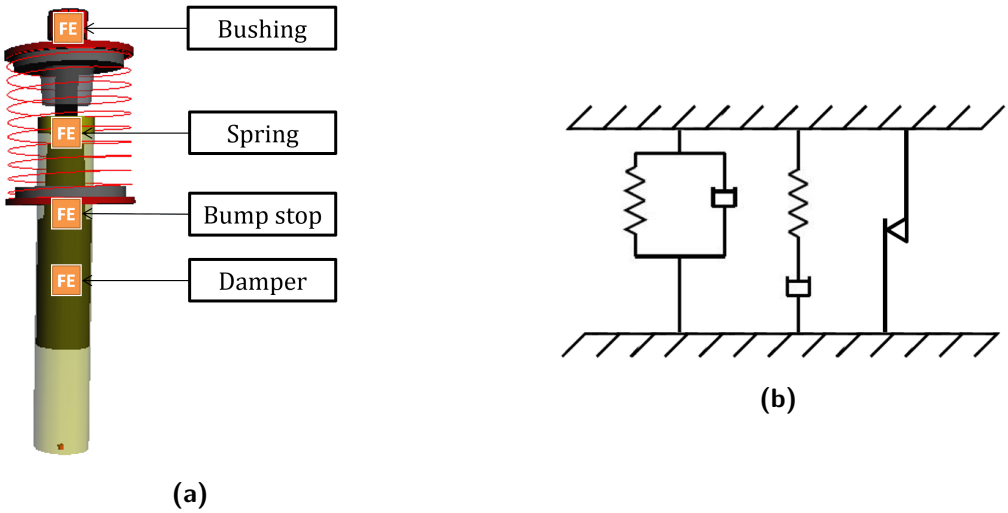

Figure 2-7: Schematic view of: (a) spring damper system model, a) bushing model

of the element (e.g. for springs and dampers or suspension arms) or by the insertion of compliant constraints at specific model locations (e.g. between the wheel hub and the wheel hub bearing). The main compliant elements affecting longitudinal dynamics are now briefly described and their modelling explained.

Spring Damper System (SDS)

The SDS is commonly associated with vertical dynamics of the vehicle; however, it is of fundamental importance for each of the other five motions as well. As the majority of the vehicle mass is elastically suspended, the SDS plays a fundamental role in the vehicle's weight transfer phenomena as well as in pitch/roll response and, therefore, needs to be modelled accurately enough.

After careful review of all the options, it was decided that an additional FMU connecting the vehicle simulator to an accurate physical model of the damper would have implied substantial compromises in the model's running time. For this reason it was chosen to opt for a simpler approach that replicates on the bench measured non-linear characteristics of each element (i.e. spring, damper, bump-stop, bushings). A schematic showing the final model is shown in figure Figure 2-7a, here FE stands for Force Element.

The suspension force at the strut, $F_{s,i}$, is consequently defined as:

$$F_{z,ij} = K_{ij}(z_{u,ij} - z_{b,ij}) + C_{s,ij}(\dot{z}_{u,ij} - \dot{z}_{b,i}j) + F_{bumpstop} + F_{bush} \tag{2-19}$$

Where the wheel vertical motion comes form:

$$\begin{aligned}
0.5m_{uf}\ddot{z_{u,FL}} &= K_t(\xi_{FL} - z_{u,FL}) - F_{s,FL}SWF_{FL} - F_z^{long} - F_z^{lat} \\
0.5m_{uf}\ddot{z_{u,FR}} &= K_t(\xi_{FR} - z_{u,FR}) - F_{s,FR}SWF_{FR} - F_z^{long} + F_z^{lat} \\
0.5m_{ur}\ddot{z_{u,RL}} &= K_t(\xi_{RL} - z_{u,RL}) - F_{s,RL}SWF_{RL} + F_z^{long} - F_z^{lat} \\
0.5m_{ur}\ddot{z_{u,RR}} &= K_t(\xi_{RR} - z_{u,RR}) - F_{s,RR}SWF_{RR} + F_z^{long} + F_z^{lat}
\end{aligned} \tag{2-20}$$

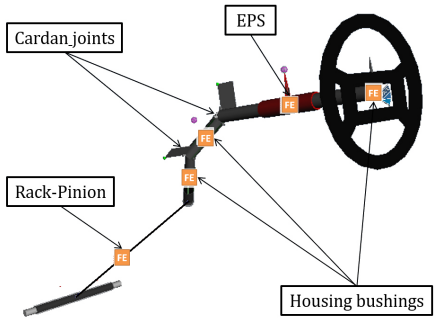

Figure 2-8: Schematic view of the steering model

and the body corners positions for small angles are approximately:

$$\begin{aligned} z_{b1} &= z_a + 0.5t_f\phi - l_f\theta \\ z_{b2} &= z_a - 0.5t_f\phi - l_f\theta \\ z_{b3} &= z_a + 0.5t_r\phi - l_r\theta \\ z_{b4} &= z_a - 0.5t_r\phi - l_r\theta \end{aligned} \tag{2-21}$$

Ball joints and bushings

Bushings are cushions made of elastomeric materials commonly mounted on vehicle suspension and steering joints to absorb road inputs, control the amount of movement and reduce noise and vibration. However, the flexibility of rubber also introduces an element of play in the suspension system. This may result in non-negligible changes in the corner behaviour during high-load conditions (cornering and braking), adversely affecting the vehicle's handling. The way bushings are modelled in this work is by a Kelvin-Voigt element, a Maxwell cell and a logarithmic function arranged in a parallel configuration, as shown in figure 2-7b. For ball joints modelling on the other hand, only the parallel spring-damper is retained as the viscoelastic behaviour is negligible.

Steering

As for bushings and suspensions, the importance of a correct steering model is often overlooked when discussing longitudinal vehicle dynamics. The flexibility of the steering column and steering linkages, together with the mass and inertia in the system, makes it prone to vibrations that can upset the ABS controllers as they are carried onto the wheel assembly. A snapshot of the steering model is shown in figure Figure 2-8.

2-5 Brake actuators

Accurate modelling of the brake actuators and replication of the delays and nonlinearities associated to it, is of paramount importance when studying longitudinal dynamics. Additionally, ABS performance is closely related to the capabilities of the brake system itself. As

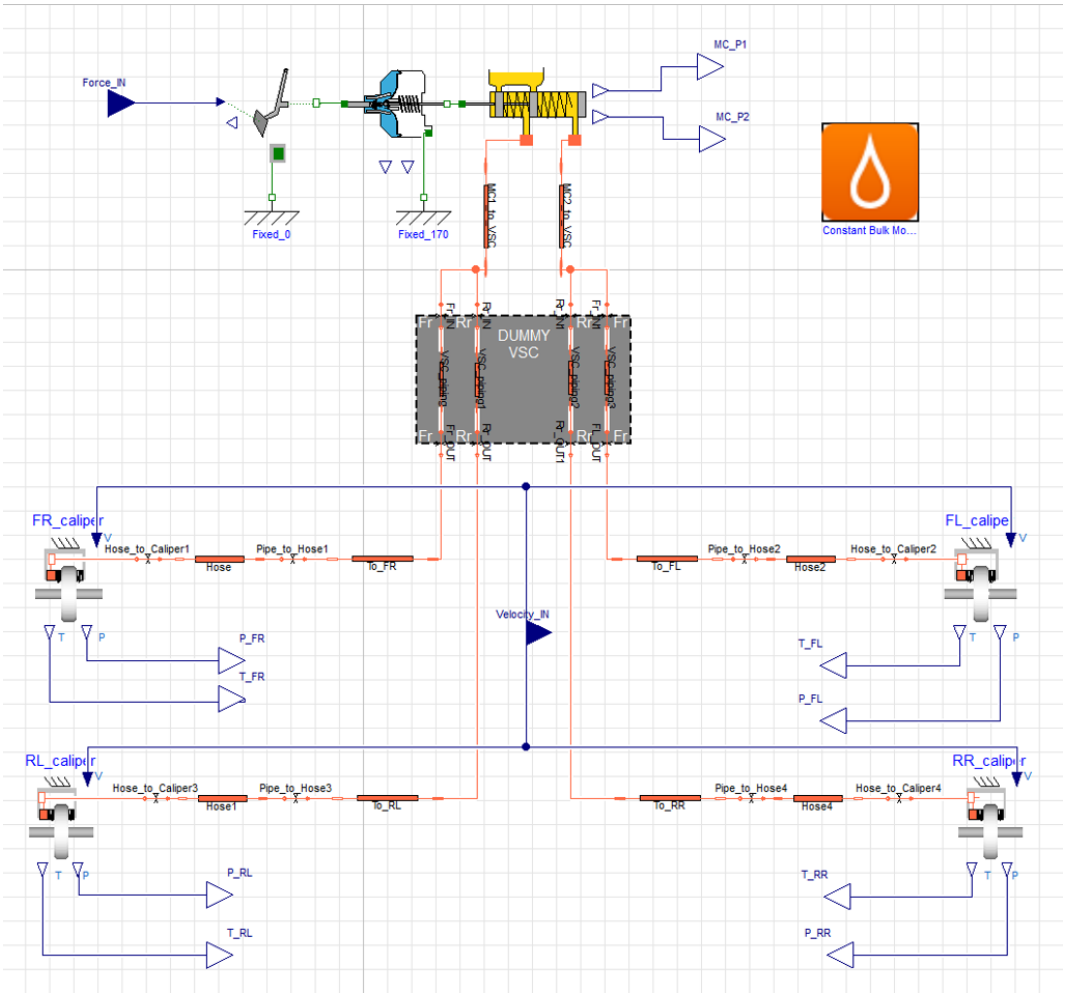

Figure 2-9: Outer-most view of the brake system model

mentioned in the previous chapter, two different actuator types will be used. Specifically, the current rule based ABS logic works with conventional hydraulic brake system, while the controller proposed in this work is based on the assumption of being able to continuously modulate brake pressure, a feature EHB is capable of. In the next two sections the modelling approaches used to replicate the response of these two actuator topologies is briefly discussed.

Conventional Hydraulically Applied Brakes

Modelling of the conventional brake system was realized following a multi-physics approach since HAB uses hydraulic, pneumatic and mechanical components to generate the necessary pressure.

This component is the result of an extensive modelling process, of which only the basic aspects will be introduced here. The effect of hysteresis on brake distance for a new disk brake mechanism does not exceed 5% in most critical cases [43]; therefore, it is neglected in this study.

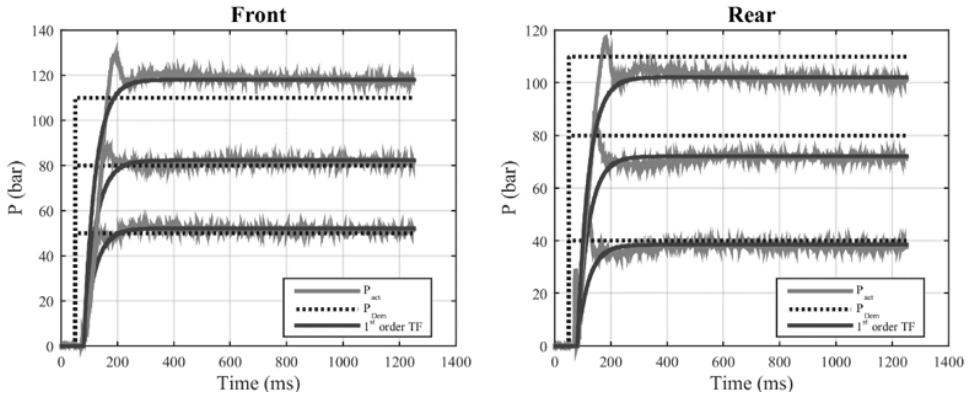

Figure 2-10: EHB response to step pressure demand

The model outermost view is shown in Figure 2-9. As can be seen, it comprises of the following basic elements:

- Brake pedal - simple, purely mechanical component;
- Brake booster - complex mechanical-pneumatic component responsible for brake assistance;
- Master cylinder - simple mechanical and hydraulic component responsible for brake fluid displacement;
- VSC passive model - simple hydraulic model replicating pressure losses and delay of VSC hydraulic unit when deactivated;
- Brake lines and brake hoses - simple hydraulic model responsible for pressure losses and delay generated as the fluid is transported to the calipers;
- Calipers - simple hydraulic model replicating brakes piston displacement and fluid consumption as the brake are applied.

Electro–Hydraulics Brakes

For the modelling of Electro–Hydraulics Brakes a different approach was taken as the nonlinearity and variability of this system is much more contained compared to HAB. The reason for this is the substitution of the brake booster, an highly nonlinear and variable component, with a much more precise electronically controlled high pressure accumulator mated to a proportional output valve. After investigation of the available options, it was decided that a first order transfer function with additional pure delay was capable of replicating the behaviour of the system in a accurate enough way.

The parametrization of the system, resulting from an extensive identification procedure on a full brake system test bench is obtained from [24]. For confidentiality reasons the parameter cannot be disclosed; however, a comparison of the model's output and test results in response to a step input for different pressure targets is shown in Figure 2-10.

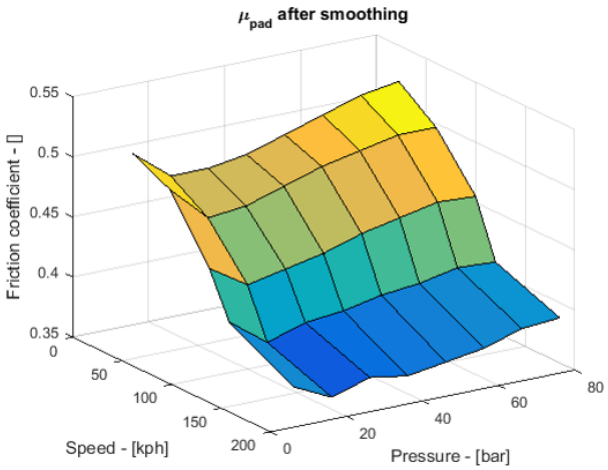

Figure 2-11: Friction coefficient LUT

Pad-Disc friction

Both brake actuator models output wheels pressures; however, the vehicle model inputs are brake torques. A simple conversion was therefore developed to replicate the pad-disc contact and transform wheel pressures into respective brake torques. The conversion uses the following well known physical relationship:

$$T_{b,ij} = 2\mu_{pad,ij}(v, p, T)R_w A_{pist} P_{ij} + T_{drag} \tag{2-22}$$

The pad-disc friction coefficient is dependent on vehicle velocity, pressure and temperature. In the model this dependency is expressed by a 3-dimensional look-up table, of which pressure and velocity dependency is shown in figure Figure 2-11. The relationship is obtained by analyzing AK master data (a standard industry test for friction coefficient measurement). The thermal power created by the brakes is calculated according to eq. (2-23), where α_{env} is an empirically calculated coefficient which accounts for the fact that part of the generated heat is transferred directly to the environment and not to the disc.

$$\dot{Q}_{ij} = \alpha_{env} T_{b,ij} \omega_{ij} \tag{2-23}$$

Subsequently, the well known heat transfer equations for convection and radiation evaluates the instantaneous power dissipation. By integrating equation (2-24), the temperature variation is found.

$$\Delta T_d = \frac{1}{m_d C_{pd}} \int \dot{Q}_{in} - \dot{Q}_{out} dt \tag{2-24}$$

The temperature change is then added to the temperature at the previous time step to calculate the current temperature of the disc, which is then used as an entry from the friction coefficient LUT.

2-6 Sensors and estimators

A detailed modelling of sensors is outside the scope of this thesis; however, errors and noise on available and estimated information can be harmful to the controller's performances and should therefore be taken into account. The general approach taken in this work is to alter the information coming from the vehicle simulator so to match signal quality available in the vehicle. In the next sections, each sensor and its accuracy is shortly discussed.

Load Sensing Bearings

In the collaboration with industrial partner SKF, TU Delft developed rolling bearings on which deformation is measured at several load indicative locations using strain gauges. Based on the measured strains, the loads $F_{x,ij}$ and $T_{b,ij}$ necessary for the presented controller, can be reconstructed. As the brake torque $T_{b,ij}$ is exerted on the rotary degree of freedom of the bearing, it cannot be measured directly. Nonetheless, the brake torque prescribed from the controller and corrected by measurement of the effects of tangential force $F_{TD,ij}$ can be used instead. The reconstruction of loads consists of two steps. First, all signals are filtered and calibrated such to obtain the unbiased signal contents of interest. Afterwards, the loads are determined by transformation of these signals. More information on this process can be found in [44, 45].

In the scope of this work, load sensing bearings were modelled by superimposing a random amplitude sinusoidal signal (with frequency equal to $50Hz$) on the forces coming from the multibody vehicle simulator. In particular, the maximum amplitude of the noise was chosen to be 10% of the current forces; this largely overestimates the noise normally presented by load sensing bearings but was needed to make sure the controller is robust enough to handle worse-case scenario (i.e. when sensing is performed on rough roads).

Inertial Measurement Unit (IMU) and wheel encoders

The IMU provides body specific accelerations and angular rates to all requesting devices. It uses a combination of accelerometers and gyroscopes, generally one MEMS rotational rate sensors and a MEMS two axis accelerometer.

Wheel encoders on the other hand, are electro-mechanical devices that convert the angular motion of a shaft to digital output signals. There are two main types of rotary encoders: absolute and incremental. For wheel rotational velocity purposes an incremental encoder is commonly used, this provides information about the motion of the shaft, which typically is processed elsewhere into information such as position, speed and acceleration.

For both IMU and encoder information, noise was modelled as a zero-mean white noise with parameters set such that rms value from the supplier's data sheet was matched. Parameters are not reported for confidentiality reasons.

Chassis velocity estimation

Since to create the slip signal, vehicle velocity is necessary, and no cheap sensor is available for direct measurement at a frequency high enough to be suitable for controls, this variable is

commonly estimated. The problem has traditionally been tackled by pursuing three different kinds of approaches: devising algorithms based on intuitive procedures linked to the physics of problem (e.g. fastest wheel speed), setting up genuine black-box approaches based on input/output data (e.g. neural networks) and stating model-based filtering problems solved via classical identification techniques and observer design methods (e.g. Kalman filters) [19].

As common passenger cars still use physically related approaches due to their robustness, it was chosen to replicate this kind. This is done by subtracting a random value (chosen inside a interval taken from experiments) to the velocity signal being sampled at a frequency of $250Hz$.

2-7 Road modelling

Obtaining a detailed simulation of the vehicle performance requires a model that not only characterizes the vehicle but also accounts for variability of the surfaces the vehicle on which is travelling. As will be discussed in future chapters, this work, considers both braking manoeuvres on smooth and rough roads. The two approaches used for their modelling are briefly introduced in the next to sections.

Smooth road

Modelling of smooth roads is fairly simple; however, one should consider the fact that road friction coefficient is never constant, regardless of the environmental and pavement conditions. In order to account for this variably, a random variation of friction coefficient within a boundary of 10% of its average values is considered. The tire-road friction is then extrapolated from a look-up table as the simulation runs. For the interpolation between to successive points a step is used and the road is quantified every 16 cm, which was found to be the average contact length of the tire within the analyzed braking scenarios.

3D road - CRG

For modelling of 3D road surfaces, the software OpenCRG is used in combination with some laser-scanned rough road from Toyota's database. OpenCRG is an open source standardized 3D road data representation defined in the plane by its direction (heading, yaw angle). Curved Regular Grid (CRG) represents road elevation data close to an arbitrary road centre line. The reference line may be complemented by slope or superelevation and is defined by consecutive heading angles. Columns of the grid are longitudinal cuts parallel to the reference line. Rows, on the other hand, represent a lateral cut orthogonal to the reference line. This approach, compared to common x-y coordinates, allows for compact storage and sufficient accuracy, even for long tracks [46]. An example, showing one of the two roads later introduced, is shown in Figure 2-12

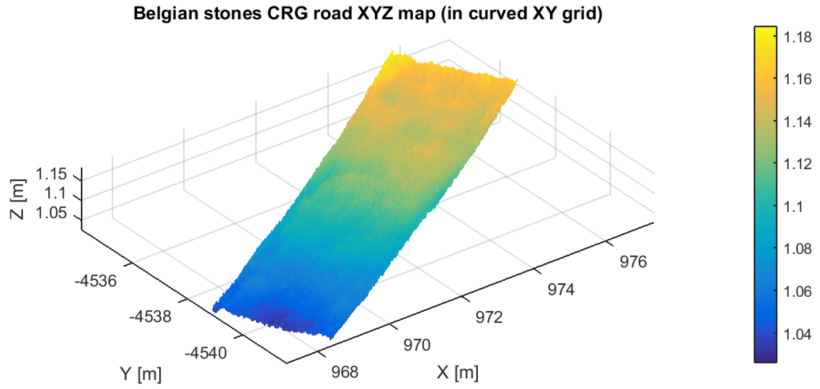

Figure 2-12: Laser scanned Belgian cobblestones road

2-8 Driver modelling

In order to control the vehicle's heading, maintain a constant velocity, and initiate the braking manoeuvre, a simple driver model is set up. For brake actuation, a ramp function (with slope equal to the maximum HAB pressure generation rate) is applied until the moment the ABS activates, at which point the driver is overruled and the controller decides the torque. For lateral dynamics, a controller using the steering wheel angle as an input is used. The controller comprises of a yaw angle feedforward and feedback part and lateral position feedback. Internally a track is used in order to evaluate the controller's feedforward action. The controller is implemented by a PI for yaw angle and PD for lateral position which manage to replicate steering of a non-professional driver wheel enough for the specific application.

2-9 Summary

Chapter 2 introduced the modelling aspects behind the realization of the vehicle simulator. From an ABS point of view, the key elements necessary for accurate vehicle dynamics behaviour replication are: vehicle, brake system, tires, sensors, road and driver. Each of these aspects were well discussed in this chapter and implemented in the vehicle simulator used for this work. Approaches behind the formulation of each element are summarized here:

- Vehicle - A multi-body model augmented with kinematics and compliance measurement. Among others, the vehicle model represents: chassis, engine, transmission, corners and steering;
- Brakes - Either a multi-physics model or a transfer function for HAB and EHB respectively;
- Tires - Short wavelength rigid ring model (MF Swift) in conjunction with a properly parameterized tire property file;
- Sensors - Gaussian white noise in superimposed to the signals coming from IMU and wheel encoders. Wheel force signals are combined with a amplitude-varying high frequency sinusoidal instead;

- Road - Laser-scanned profiles simulated deploying a CRG approach;
- Driver - PID controller tuned in a way that replicated an everyday driver in terms of respinsiveness.

Chapter 3

Models validation and co-simulation

Simulation models, being approximate imitations of real-world systems, never exactly resemble them. As a consequence, every time a new model is developed, it should be verified and validated to a degree needed for the intended purpose or application.

Verification and validation is an iterative process that starts after functional specifications have been documented and initial model development is completed. The final validation outcome is presented in this chapter and the models suitability for the scope of this work is discussed. On the other hand, the verification step is omitted.

3-1 Subsystems validation

The two main subsystem models, brake system and vehicle, are compared to experiments in the next pages. As will be described, overall accuracy of the simulations is adequate, nonetheless, some deviations are present at specific conditions.

3-1-1 Brake system model - static brake applications

In order to validate the brake system model a series of static brake applications were performed by a driver on an instrumented vehicle. The system was tested with and without the vacuum line connected so to first obtain good correlation of the mechanical and hydraulic part, and then of the full system with pneumatic booster assistance. Because of the high nonlinearity of the booster component the applications were performed targeting different pressure levels (12.5,30,50,140 bar) and repeated for multiple application rates (10,50,100,150 mm/s).

Overall performances of the brake systems model is satisfactory; however, it was noticed that correlation improves significantly as the application rates and target pressures increase.

In Figure 3-1 results are shown for a target pressure of 30 bar. As mentioned, for higher pressure levels, more compatible with ABS braking forces, performances improve, and results are substantially better than those shown in Figure 3-1; Nonetheless, the application at 30 bar functions well to highlight the main identified criticalities:

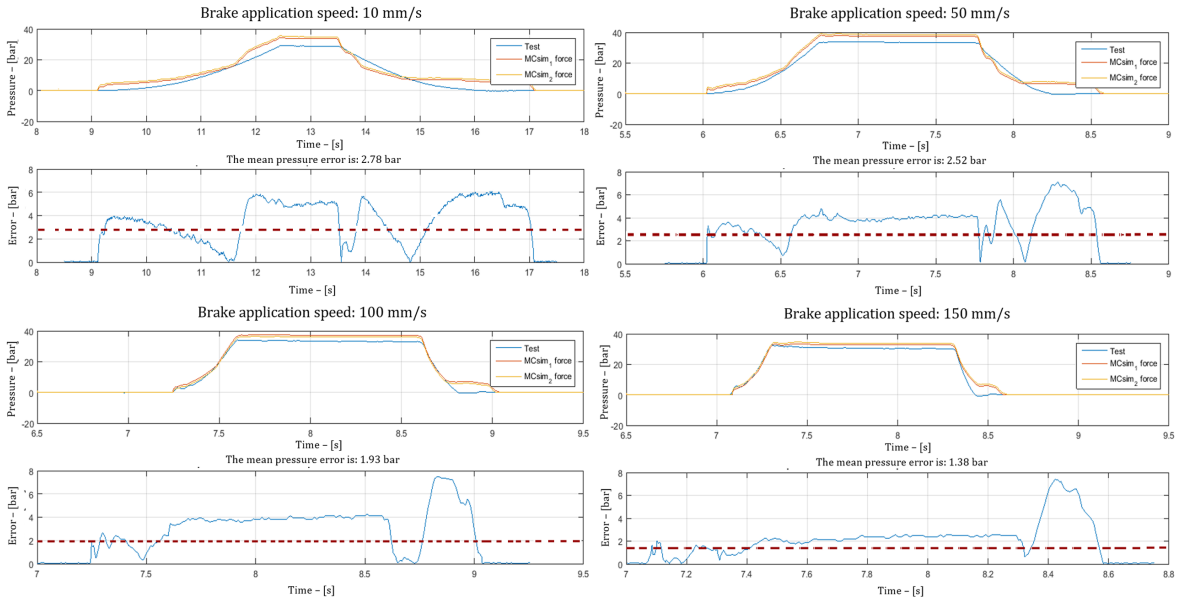

Figure 3-1: Brake system model correlation with experimental results

- The booster pneumatic valves are modelled according to Sanville flow model (ISO 6358). This model is developed for circular cross-section 2-way valves, yet the valves in the booster are not circular, neither properly 2-way, resulting in some modelling error. To account for partial opening of the valve, the flow rate is assumed to be linearly proportional with the valve aperture. This is not a strong assumption and constitutes the reason why at low application speed, when the valve is not fully open, correlation is poor;
- During the validation measurements, the brake force was applied by a human and not by a brake robot. As for a human it is fairly difficult to keep the perpendicularity between the foot and the load cell axis, results are compromised whenever this alignment is lost. Since this phenomenon is mainly prone to appear in the return phase (where the foot-load cell alignment is more difficult to control), it is believed that the apparent error seen in Figure 3-1 is partially caused by this problem as well.

In conclusion, the model accurately represents first order dynamics of the brake system and, specifically at pressure levels and application rates of common ABS braking manoeuvres, it is able to validly replicate the brake system behaviour.

3-1-2 Vehicle model - kinematics, compliance, handling, braking

The original vehicle model used in this work was developed by Toyota Motor Europe. The model, targeted at handling and ride comfort assessment, was therefore validated by them. The validation process comprises of a first correlation of the wheel kinematics. When this correlation is satisfactory, the focus is shifted to matching the vehicle compliance obtained by measurement of the vehicle on a KnC rig. Lastly, a series of manoeuvres is performed on a test track to check the vehicle lateral and yaw response to the driver's steering input at different longitudinal velocities.

Due to confidentiality, neither the kinematics nor compliance validation data can be shown. Nonetheless, as some maneuvers for lateral correlation are rather standardized, a selection of them (at 60 and 100 km/h) are reported in Figure 3-2. As can be seen, good correlation is achieved for handling dynamics throughout the vehicle speed range.

Since no real validation was performed for longitudinal dynamics in TME, after modification of the vehicle model to adapt it for co-simulation with the brake system model, the vehicle simulator was correlated with a series of tests replicating a variety of brake applications outside the ABS range of intervention. Only the most significant of those is shown in this report. Figure 3-3, shows a high friction, high deceleration stop from 70 km/h. As can be seen, except for a sightly different exit velocity, again caused by the brake model misbehaving on the release phase, the vehicle simulator is capable of well replicating both longitudinal and pitch dynamics of the real vehicle. Since the tested vehicle is equipped with torque transducers, alongside other more traditional sensors, the correct functioning of the transformation from pressure to torque can be verified as well.

3-2 Subsystems co-simulation

Since subsystems have been developed in different simulation suits, namely, MATLAB Simulink ®, Simpack ® and Dymola ®, a way to make these subsystems communicate with each other is needed if the full vehicle behaviour is to be simulated.

After some investigation, Simulink was found to be the most convenient host environment as it is the most popular tool among the three software. The other two programs are then connected to Simulink by means of two different approaches, namely FMI and IPC. Certainly FMI could have been used for both connections; however, from a simulation run-time prospective, this was not a convenient solution. In the next two sections, the basic principles of these two co-simulation approaches are explained, lastly, the final layout is introduced.

Functional Mock-up Interface (FMI)

The FMI standard is an open and tool-independent standard for exchange of models between tools generated using a combination of xml-files and compiled C-code. The FMI defines a C interface that is implemented by an executable called Functional Mock-up Unit (FMU). A simulation environment, such as Simulink in this case, can then use the FMI to create an instance of the FMU and simulate it together with other native models. The FMI standard currently specifies two types of protocols: FMI for Model Exchange (import and export), and FMI for Co-Simulation (master and slave). In this work, the latter approach is used as it was found to be both quicker and more stable.

Inter-Processor Communication (IPC)

SIMAT is a proprietary co-simulation interface between Simpack and MATLAB Simulink; by using IPC, it enables simultaneous simulation of the Simpack vehicle model and Simulink subsystem models (brake FMU included). IPC is a mechanism which allows models to communicate with each other and synchronize their actions at the processor level. Specifically, the

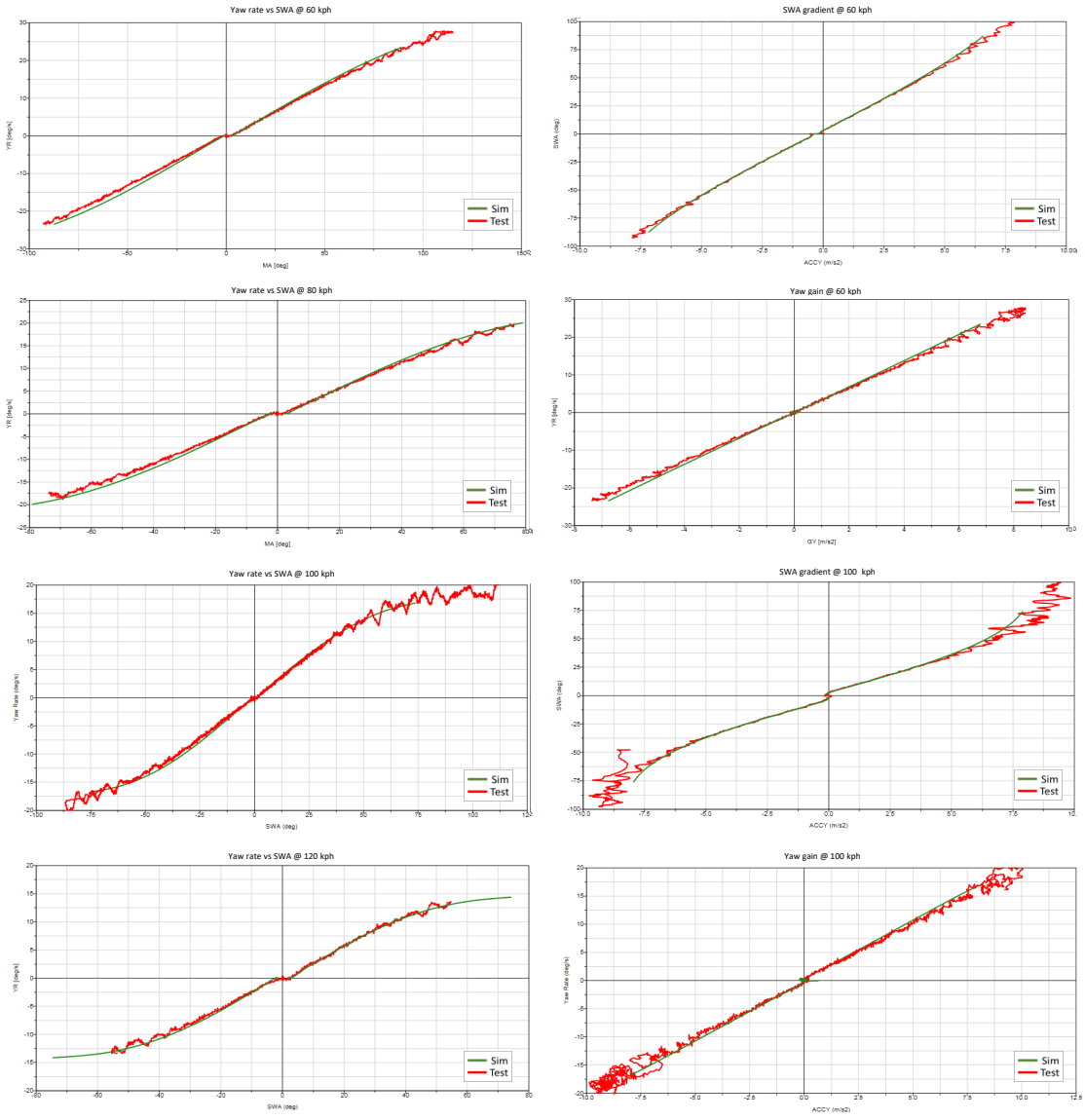

Figure 3-2: Vehicle model handling validation

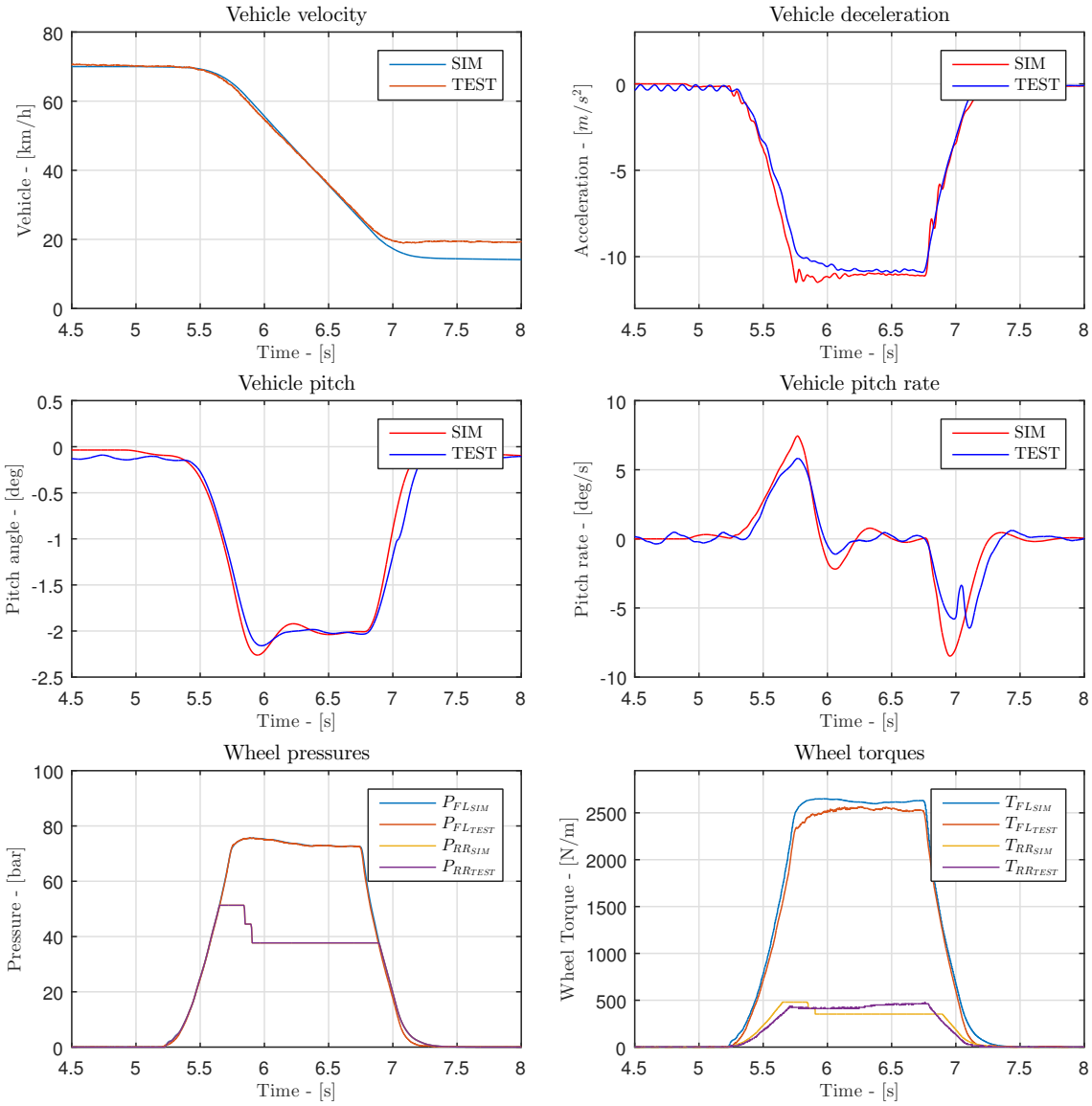

Figure 3-3: Vehicle model longitudinal validation

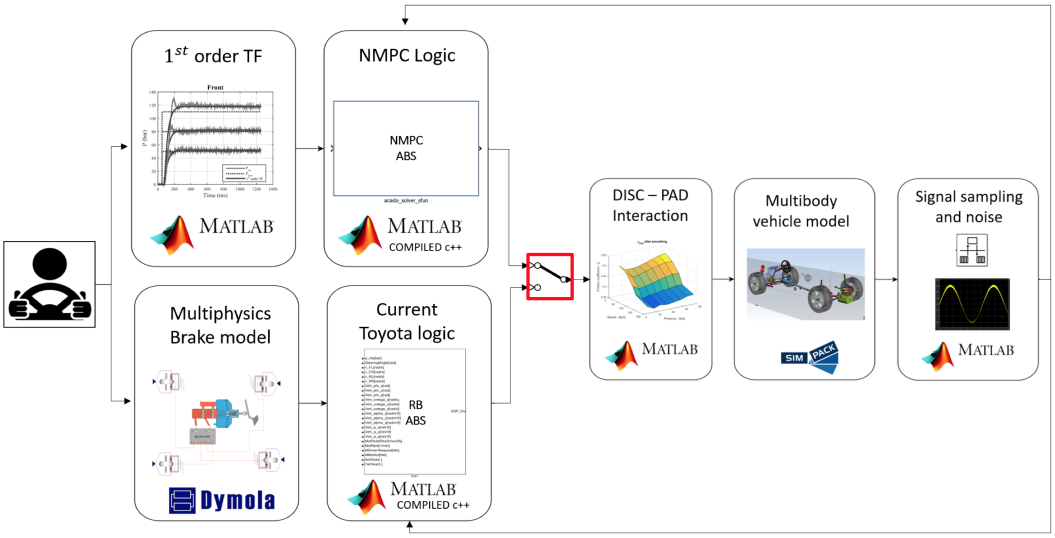

Figure 3-4: ABS co-simulation tool-chain

two co-simulation partners exchange their results with a given time step using the TCP/IP protocol.

Co-simulation toolchain

After discussion of the interface methods, the toolchain required for full vehicle simulation is introduced. The main aim was to develop a modular co-simulation environment where switching between the current RB logic and continuous NMPC controller is as simple as possible. Referring to Figure 3-4, it can be seen that this is achieved by solely interchanging the brake system and controller blocks while leaving the other subsystems unaltered. Two initialization scripts were developed to make sure the loading process of the necessary parameters and connection of the blocks is automated. In this way, performing a simulation is as simple as running the initialization script and answering a series of prompt questions characterizing the braking manoeuvre.

3-3 Co-simulation validation

In the previous sections the correct behaviour of each subsystem was verified through comparison with real world tests, nonetheless, it is best practice to verify that their interaction and common output is also as reliable.

In order to do this, a high friction 130-0 km/h full ABS braking is simulated and compared against six comparable vehicle tests performed on two different test dates, the comparison is shown in Figure 3-5. Due to the sizeable variability present in the test outcome as a result of slightly different environmental and brake corner conditions, and for ease of reading, tests are plotted in gray dashed lines, while simulation output is colored. Overall, a good level of matching is observed in the vehicle state variables, particularly at higher speed (above 20

km/h). Additionally, by looking at the wheel pressure and torque graphs, ABS modulation patterns are clearly similar to those observed in the vehicle tests. The increased mismatch in the low speed region is supposed to come from the tire property file being mainly identified for lateral dynamics, while fewer tests were performed for the longitudinal one. This most probably results in a simulated tire that is more difficult to control than its real-world counterpart at low speeds.

Despite the fact that a better prediction of lower speed behaviour could be obtained with a more accurate tire property file, as the main aim of this work is to quantify relative gains and not absolute performances, the proposed co-simulation is judged to be capable enough for the scope.

3-4 Summary

This chapter introduced the validation process that lead to confirmation of the suitability of the subsystem models introduced in chapter 2.

Firstly, the brake system model was compared against static brake applications preformed on a real vehicle. Then, the correct behaviour of the vehicle model was verified by correlation of the simulation output with kinematics, compliance, handling and braking test results. Furthermore, the final vehicle simulation layout was described alongside the methods used for contemporary simulation of each subsystem. Lastly the resulting full vehicle simulator, containing brake actuators, rule based ABS logic and vehicle model, was compared to a further real world test. The co-simulation validation supported what was already highlighted by simulation of the single subsystems and confirmed the suitability of the models for relative performance assessment.

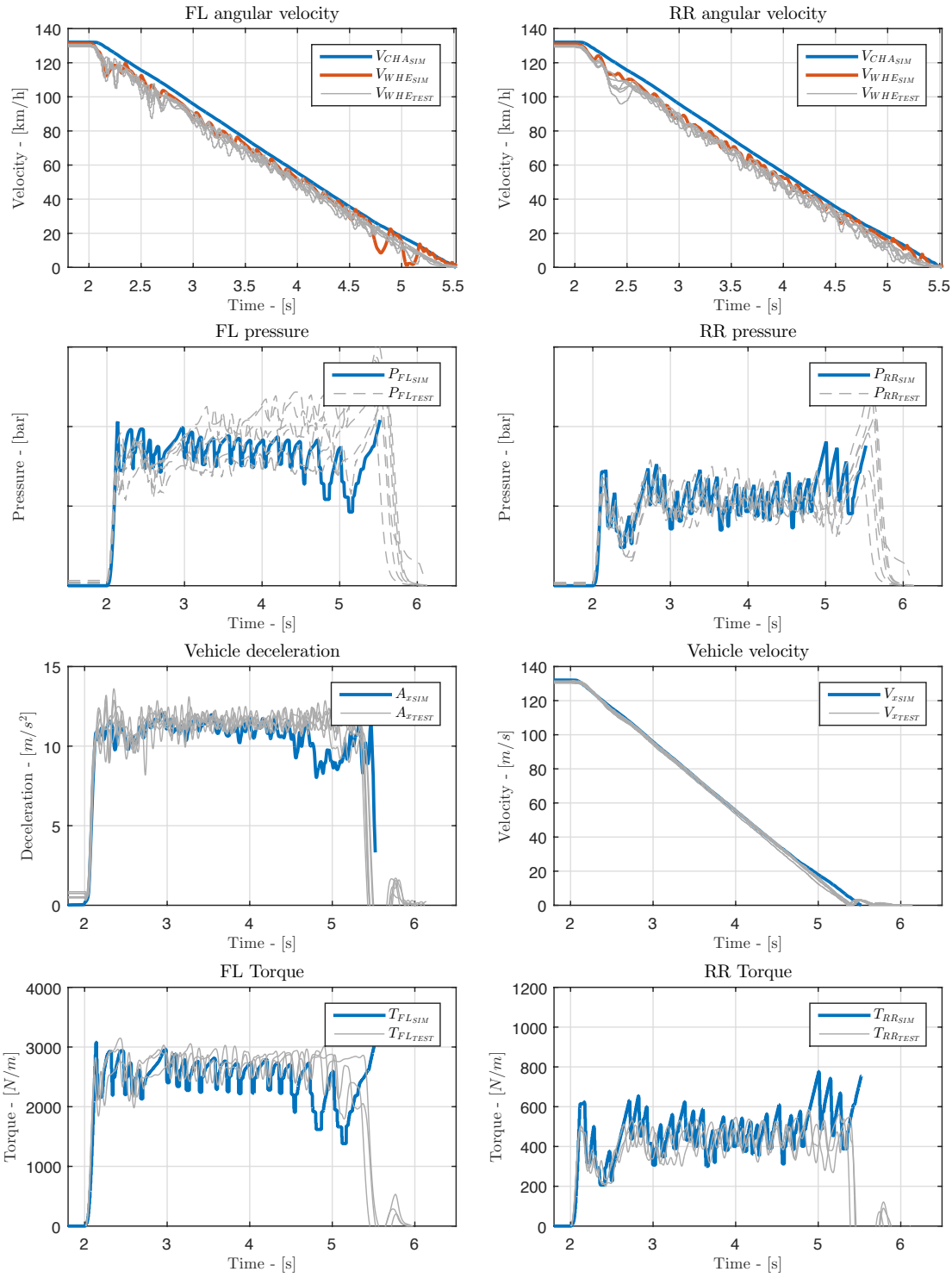

Figure 3-5: High speed AMS validation

Chapter 4

Nonlinear Model Predictive Control - Introduction & first implementation

4-1 Model predictive control

In this thesis a model predictive control framework is used to generate feasible and optimal wheel torques. MPC offers an elegant and modular framework, which makes it easy to extend control problems. This resulted into a structured development process starting with control of the wheel corner and ending with the full car. Additionally, since constraints can be included in the formulation, optimal brake torques are always selected within actuator capabilities. Furthermore, using a model based approach results in few tuning parameters associated with physical quantities, which in turn, enable the designer to avoid long and tedious tuning processes.

In the next sections, model predictive control and its key elements, as well as the used software for its implementation, are introduced.

4-1-1 Introduction

Model Predictive Control (MPC) is a model based approach that is gaining popularity for control of dynamical constrained systems. A model predictive controller uses a, either linear or nonlinear, dynamical model of the system to predict its future behavior over a finite time interval, that is,the prediction horizon. The predicted future behavior is then optimized via control inputs with respect to a given optimality criterion reflecting some control objectives. The criterion is formulated as a cost function and system's constraints, and solved at each sampling period. After computation of the optimal control sequence, only the first control move is applied in closed loop. In the next sampling interval, the entire process is repeated using the most recent state measured.
This concept, known as Receding Horizon Control (RHC), incorporates a feedback aspect in the MPC [47, 48]. The working principle is well illustrated in Figure 4-1.

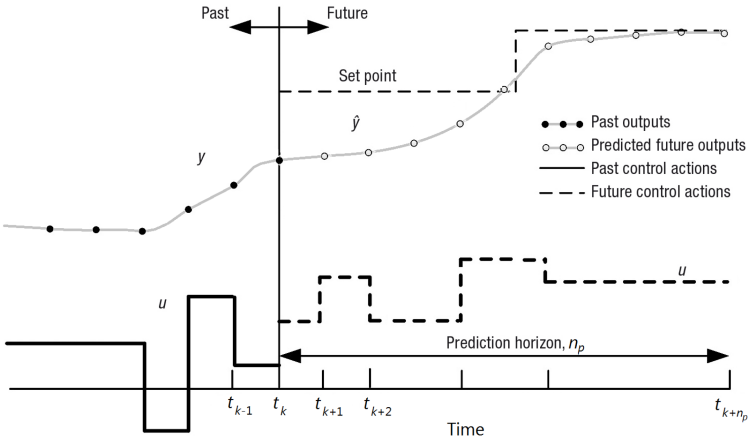

Figure 4-1: Model Predictive control illustration, [9]

The use of linear prediction models can sometimes be oversimplified with respect to the plant that it is supposed to represent. When this is the case, sufficient accuracy of predictions cannot be achieved, which results in large plant-model mismatch and a consequent loss of performance or even stability. Because of the high nonlinearity of the slip dynamics, in this work Nonlinear Model Predictive Control (NMPC) is deployed. NMPC differs from the more general MPC scheme in the fact that a nonlinear process model is used for prediction.

4-1-2 Prediction model

As previously mentioned, the controller necessitates a system model to operate. The quality of this model largely determines the performance of the MPC controller.

In this work a nonlinear, continuous time, state-space model is considered. This class is defined by a set of ordinary differential equations (ODEs) of the following form:

$$\dot{\mathbf{x}}(t) = \mathbf{f}(\mathbf{x}(t), \mathbf{u}(t)) \tag{4-1}$$

and an algebraic output equation:

$$\mathbf{y}(t) = \mathbf{g}(\mathbf{x}(t), \mathbf{u}(t)) \tag{4-2}$$

where $\mathbf{x}(t) \in \mathbb{R}^n$, $\mathbf{u}(t) \in \mathbb{R}^m$, and $\mathbf{y}(t) \in \mathbb{R}^p$ are the state, control input and system output, at time $t \geq 0$, respectively. Functions $\mathbf{f} : \mathbb{R}^{n+m} \mapsto \mathbb{R}^n$ and $\mathbf{g} : \mathbb{R}^{n+m} \mapsto \mathbb{R}^p$ are vector valued, continuous, at least once differentiable functions.

4-1-3 Optimal control problem formulation

Optimization based braking torques, $T_{b_{\text{cmd}}}$, result from iteratively solving a constrained Optimal Control Problem (OCP). In its general form, the OCP is formulated as follows:

$$\underset{y(\cdot),u(\cdot)}{\text{minimize}} \underbrace{\int_{t_0}^{t_0+T_P} \Big(||y(t) - y_{\text{ref}}(t)||_Q^2 + ||u(t) - u_{\text{ref}}(t)||_R^2 \Big) dt + ||y(t_0+T_P) - y_{\text{ref}}(t_0+T_P)||_P^2}_{\text{J}} \tag{4-3a}$$

subject to

$$x(t_0) = \widetilde{x}_0 \qquad \text{Initial conditions} \tag{4-3b}$$
$$\dot{x}(t) = f(x(t), u(t)) \qquad \text{Vehicle dynamics} \tag{4-3c}$$
$$y(t) = g(x(t), u(t)) \qquad \text{Output mapping} \tag{4-3d}$$
$$\underline{x}(t) \leq x(t) \leq \bar{x}(t) \qquad \text{State constraints} \tag{4-3e}$$
$$\underline{u}(t) \leq u(t) \leq \bar{u}(t) \qquad \text{Actuator constraints} \tag{4-3f}$$
$$Q \in \mathbb{R}^p_{\geq 0}, \qquad R \in \mathbb{R}^m_{\geq 0}, \qquad P \in \mathbb{R}^p_{\geq 0} \tag{4-3g}$$

The solution of the OCP is the result of minimizing the cost function J as in (4-3), in which: Q, P are non-negative definite weight matrices penalizing the deviations of the outputs (y) from their reference values (y_{ref}), and R is positive definite weight matrix penalizing the deviations of the inputs u from their reference values (u_{ref}). The weight matrices can therefore be used as tuning parameters. Defining the OCP in (4-3) consists of following three three main parts:

- Choosing and setting up the prediction model in (4-3c);
- Designing constraints as in (4-3e) and (4-3f);
- Tuning the MPC weights of (4-3g)

4-1-4 Optimal control problem as a numerical optimization problem

An important step in the practical solution of (4-3) is to transform it into suitable form for numerical solution. The goal is to obtain a finite dimensional optimization problem using an appropriate parameterization of the original problem. A short explanation is now given, nonetheless a clear in depth discussion of the topic can be found in [49].

The prediction horizon is divided into N_p sampling periods, giving rise to a shooting grid $t_0 < t_{k+1} < \ldots < t_0 + N_p$. The shooting grid can be defined arbitrarily; however, equidistant grids are the most frequently used. Then, the input trajectory is parameterized with a suitable basis function on each sub-interval. This is described by a vector of parameters $\mathbf{u}_i$, where i corresponds to the interval's index. The simplest and most used approach is to use piece-wise constant function where:

$$\mathbf{u_i} = \mathbf{q_i} \qquad \text{for} \qquad t \in \langle t_i, t_{i+i}) \tag{4-4}$$

The Optimal Control Problem can now be solved with either of two direct methods: single- or multiple-shooting.

In the single shooting method, model simulation and optimization are done sequentially. The nonlinear model is numerically integrated first to find the sensitivity of the cost function to the problem parameters $\mathbf{u}_i$. In this way, dynamic constraints (4-3b) and (4-3d) are effectively eliminated from the problem formulation (simulated trajectories automatically meet the dynamic constraints). Secondly, the optimization is carried out. The main advantage of this method is its implementation simplicity and the fact that the iterates during the optimization are always feasible [50].

In the multiple shooting method on the other hand, the optimization problem parameters are not only control trajectory parameters $\mathbf{u}_i$, but also the states at the beginning of each sub-interval, $\mathbf{s}_i$ [51]. The model equations are then integrated on the sub-intervals and the resulting trajectories are optimized separately. The optimization problem has an additional set of equality constraints enforcing continuity of state trajectory between the sub-intervals:

$$\mathbf{x}(t_i + 1) = \mathbf{s}_{i+1} \tag{4-5}$$

The multiple shooting approach provides better handling of unstable and highly nonlinear systems than single shooting approach. At the same time, the optimization problem is structured in a way that is beneficial for the optimization solver. On the other hand, the number of variables is increased. Given the highly nonlinear nature of wheel system the latter approach is selected.

The optimization problem that is obtained can be written as follows:

$$\underset{q_k,\dots,q_{k+N_p}}{\text{minimize}} \sum_{i=k}^{k+N_p-1} J_{i,d}(\mathbf{q}_i, \mathbf{x}_i) + J_{f,d}(\mathbf{q}_{k+N_P}, \mathbf{x}_{k+N_P}) \tag{4-6}$$

subject to the same conditions as for (4-3).

The cost function is now expressed as a sum of functions $J_{i,d}$ and a terminal function $J_{f,d}$. The form of these functions depends on the original cost function in (4-3) and the transformation method used. In case of single or multiple shooting, the functions are integrals over individual shooting sub-intervals that will be evaluated numerically. In this way, the state and input trajectories are considered only at times used by the numerical integrator. The sub-intervals can either belong to a fixed grid or be arbitrary time instants given by a solver variable step selection. In this work a regular grid was chosen for simplicity.

Other more efficient methods to transform the problem (4-3) into a finite dimensional problem are also available. The main idea is to have the functions $J_{i,d}$ and $J_{f,d}$ defined on discrete samples of state and input trajectories only. This is achieved by simulation of the model (4-1) and subsequent linearization and discretization of its dynamics. In this way, the cost function computation does not require integration over time, but only a sum over discrete sampling time instants. This is actually, how the problem is handled by the chosen NLP solver (`QP OASES`) since much less computational resources are needed if the integration is removed. However, the detailed description of this process is outside of the scope of this thesis. The interested reader may refer to [52].

4-2 Corner braking control - problem set up

In this section, the first ABS control implementations is shown. The main focus is put on preliminary investigation of the NMPC framework applied to ABS control. As discussed in

the next pages, this simpler set up is used to answer important implementation questions without the burden of a complex simulation model that would take several minutes to run. Hence, the aim is to keep the controller and simulation environment as simple as possible for fast performances, but at the same time incorporating the main dynamics and nonlinear elements. Doing so, the findings can be easily carried over to the final controller and vehicle simulator.

4-2-1 Wheel rotational dynamics and longitudinal slip

For the preliminary design and testing of braking control algorithms, a simple but effective model known as the single-corner model is typically used. This is obtained by combining Eqn. (2-14) with the longitudinal equation for the wheel corner:

$$\begin{cases} \dot{\omega} = \frac{R_w F_x - T_b}{I_w} \\ \dot{v} = -F_x/m_c \end{cases} \tag{4-7}$$

As λ, v and ω are linked by the algebraic relationship (2-16), it is possible to replace the state variable ω with λ:

$$\begin{cases} \dot{\lambda} = -\frac{1-\lambda}{v m_c} F_x - \frac{R_w^2}{I_w v} F_x + \frac{R_w}{v I_w} T_b \\ \dot{v} = -\frac{F_x}{m_c} \end{cases} \tag{4-8}$$

Since the longitudinal dynamics of the vehicle is much slower than the rotational dynamics of the wheel due to large differences in inertia, v can be considered as a slowly-varying parameter. Under this assumption, the second equation of the system (4-8) can be neglected, so that the model reduces to a first-order model of the wheel slip dynamics. It is worth noticing that the single-corner model relies on the following simplifications:

- The four wheels are treated as dynamically decoupled;
- The suspension dynamics are neglected;
- The wheel radius is assumed to be constant;
- Straight-line braking is considered (i.e. the friction forces' dependence on the camber angle γ and on the tire sideslip angle α_t is neglected).

4-2-2 Stability analysis

In order to study the stability of the system, this needs to be linearized first. If the variables $\delta T_b = T_b - \bar{T}_b$, $\delta\lambda = \lambda - \bar{\lambda}$, defined around an equilibrium point (see Tab. 4-1), are considered and using Eqn. (4-9), the slip dynamics can be linearized and Eq. (4-10) obtained. For the complete procedure see [19].

$$\bar{\mu} = \left.\frac{\partial \mu(\lambda)}{\partial \lambda}\right|_{\lambda=\bar{\lambda}} \tag{4-9}$$

Table 4-1: Nominal linearization conditions for stability analysis

Variable	Steady-state value
$\bar{\lambda}$	0.03
$\bar{T_b}$	$850Nm$
$\bar{v}$	$25m/s$
F_z	$m_c g$
Road conditions	Dry asphalt

$$\delta\dot{\lambda} = \left[\frac{1}{v}\left(\frac{m_c g \mu(\bar{\lambda})}{m_c}\right) - m_c g \bar{\mu}\left(\bar{\lambda}\left(\frac{1-\lambda}{m_c} + \frac{R_w^2}{I_w}\right)\right)\right]\delta\lambda + \left[\frac{R_w}{vI_w}\right]\delta T_b \tag{4-10}$$

The transfer function $G\lambda(s)$ from δT_b to $\delta\lambda$ is given by:

$$G_{\lambda s} = \frac{\left[\frac{R_w}{vI_w}\right]}{s + \left[\frac{1}{v}\left(g\bar{\mu}(\bar{\lambda})\left((1-\bar{\lambda}) + \frac{m_c R_w}{I_w}\right) - g\mu(\bar{\lambda})\right)\right]} \tag{4-11}$$

Based on the transfer function model 4-11, local stability around the equilibrium point ($\bar{\lambda} = \lambda_{opt}$) and minimum-phase properties of the linearized system can be analyzed. Doing so some interesting features displayed by the open-loop braking dynamics can be explained. The pole of $G_{\lambda(s)}$ is given by:

$$s_{pole} = -\frac{1}{v}\left(g\bar{\mu}(\bar{\lambda})\left((1-\bar{\lambda}) + \frac{m_c R_w}{I_w}\right) - g\mu(\bar{\lambda})\right) \tag{4-12}$$

Hence, the stability condition is:

$$\bar{\mu}(\bar{\lambda})\left((1-\bar{\lambda}) + \frac{m_c R_w}{I_w}\right) > \mu(\bar{\lambda}) \tag{4-13}$$

Noting that, since $(1-\bar{\lambda}) \ll \frac{m_c R_w^2}{I_w}$ and $\frac{I_w \mu(\bar{\lambda})}{m_c R_w^2} \approx 0$, the stability condition can be reduced to $\bar{\mu}(\lambda) > 0$. In other words, $G\lambda(s)$ is unstable if the equilibrium point λ is beyond the peak of $\mu(\lambda)$.

A further analysis that can be performed to obtain more information about the wheel corner dynamics features is to plot how the stability margins for the open loop system change as the velocity and normal load change. Despite the longitudinal vehicle speed not being present in the pole's expression and, hence, not affecting the stability and minimum-phase properties of the linearized braking dynamics, the velocity at which the vehicle is travelling still influence the wheel behaviour. Indeed, the velocity acts as a time scale on the wheel dynamics. As a matter of fact, notice that the pole is characterized by the multiplying factor $1/v$. Figure 4-2a shows the magnitude and phase plots of the frequency response associated with $G\lambda(s)$ (at nominal linearization conditions reported in table 4-1) for three different values of v. As can be noticed, the angular frequency of the pole for $v = 3m/s$ is a one order of magnitude larger than that for $v = 30m/s$. Clearly, this scaling effect must be taken into account in the design

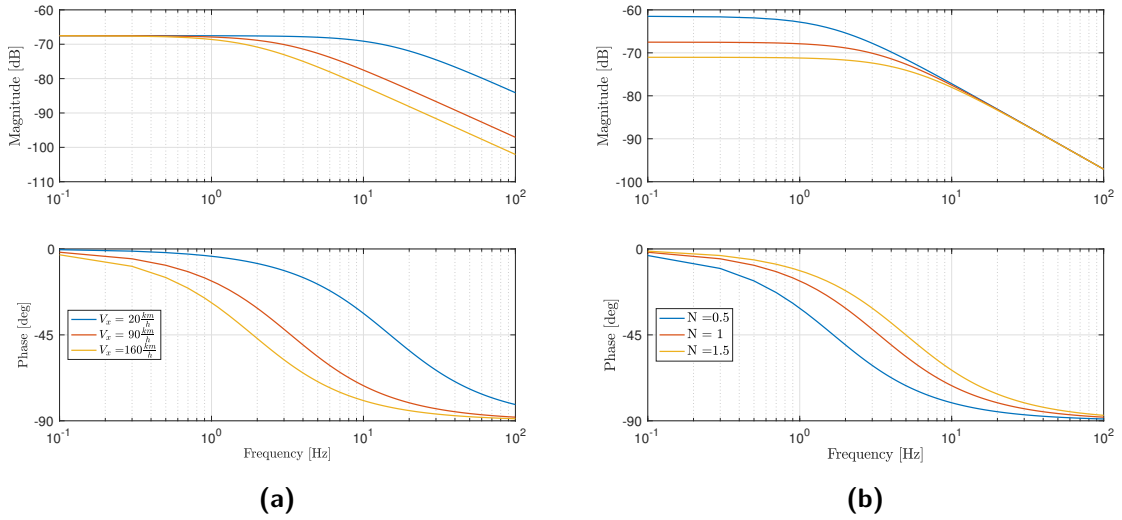

Figure 4-2: Magnitude and phase Bode plots of the frequency response associated with $G\lambda(s)$ for: (a) Different longitudinal speed values, (b) Different longitudinal vertical loads

of a braking controller. On the other hands, as can be seen in Figure 4-2b, the vertical load mainly affects the low frequency behaviour of $G\lambda(s)$. As low frequency demand does not usually represent a problem for ABS controllers, the effect of the normal load changes is not as critical as for velocity ones.

4-2-3 Corner dynamics simulation environment

As discussed, this first simulation environment should be as simple as possible for fast computations but at the same time account for the main elements that are expected to affect the controller performances. With this in mind, Eqn. (4-7) is used to describe the dynamics of wheel around its y-axis and that of the chassis in the longitudinal direction. In order to incorporate the full complexity of the tire behaviour, MF-swift is used to obtain the value of F_x. T_b on the other hand, is calculated by applying the EHB transfer function to the torque prescribed by the controller. Moreover, some noise is superimposed on the state signals T_b, v and ω to replicate sensor behaviour. Lastly, the slip λ is calculated as in (2-16).

4-2-4 Prediction model

For the corner braking control prediction model, Eqn. 4-8 can be used after some small changes to include brake system dynamics. It was noticed, in fact, that although the controller would still work if brake system limitations are not taken into account in the prediction, including them significantly improves the performances. As seen in Chapter 2, EHB dynamcis can well be represented by a first order transfer function with delay. Since the delay is only present when the brake application is initiated, and at the same time ABS brake only intervenes when the vehicle is already braking, the delay part can be neglected in the prediction model. Additionally, because `ACADO` needs the system to be described by means of continuous

Table 4-2: State and input bounds for wheel corner controller

Variable	Unit	Lower-bound
Upper-bound		
T_b	[Nm]	0
3500		
λ	[-]	0
1		
v	[m/s]	0
53		
dT_b	[Nm/s]	-35000
42000		

time differential equations, the frequency domain needs to be abandoned in favour of time domain. The actuator dynamics can then be described by the following expression:

$$T_{b_{\text{act}}} = T_{b_{\text{cmd}}} + \tau_{\text{act}} dT_{b_{\text{cmd}}} \tag{4-14}$$

where $T_{b_{\text{act}}}$ is the actual brake torque realized by the actuator, $T_{b_{\text{cmd}}}$ is the commanded one, $dT_{b_{\text{cmd}}}$ is the requested torque increment w.r.t. the previous shooting grid increment $(K-1)$ and τ_{act} is the time constant value for Electro–Hydraulics Brakes, set to $\tau_{act} = 16ms$. Including the actuator dynamics not only improves the controller performances, but also gives additional benefits. The first of them is the possibility of imposing an upper and lower bound on the torque rate of change. Moreover, as torque is now a state and not the control input, its weight in the cost function can be set to zero while at the same time having the additional degree of freedom of being able to change the importance of torque rates on the overall cost.

By combining Eqn. (4-2) with (4-14), and rearranging the equations to the implicit formulation needed by `ACADO Toolkit`, the final prediction model is obtained:

$$\begin{bmatrix} \dot{T}_{b_{cmd}} - dT_{b_{cmd}} \\ \dot{\lambda} + \frac{1-\lambda}{vm_c} + \frac{R_w^2}{I_w v} F_x - \frac{R_w}{vI_w}(dT_{b_{cmd}}\tau + T_b) \\ \dot{v} - \frac{F_x}{m_c} \end{bmatrix} = \begin{bmatrix} 0 \\ 0 \\ 0 \end{bmatrix} \tag{4-15}$$

where $x_{k_0} = [T_{b_{cmd}}, \lambda, v]'$ and F_x is fed online every T_s.

4-2-5 State and input bounds

Following the previous discussion regarding the benefits of including constraints, in this section upper and lower bounds imposed in the MPC formulation will be discussed. Choosing the right constraints not only makes the controller faster but also prevents some infeasible solutions to be picked as the optimal one. For ease of reading, the values are reported in Tab. 5-1; however, the reasoning related to their choice is explained in the next paragraphs.

As the focus of this work is braking dynamics, the slip should be constrained such that the MPC only searches for optimal solutions in the range [0 1]. In this way, all those scenarios in which the wheel's longitudinal velocity is greater the the vehicle's one are left out.

For what concerns the vehicle velocity on the other hand, the lower-bound should be set to 0 to prevent the vehicle from going backwards while the upper-bound value is set equal to the maximum speed the vehicle is capable of achieving.

Brake torque limits are also fairly easy to set. The lower bound is placed at $0Nm$ as negative values would mean that a driving torque is applied. The upper-bound is again set at the system's maximum achievable brake torque. The specific value can be calculated from Eqn. (2-22) by assuming the maximum brake pressure to be $P_i = 160bar$ and maximum disc-pad friction coefficient to be $\mu_i(v, p, T) = 0.5$. Given the differences in sizing between front and rear brakes, two different values are found. In this case, as the corner simulation should be representative of the front, the value is chosen to be $T_{b,max} = 3500Nm$.

Lastly, limits for the brake torque rate of change are also set at the system maximum capability. Torque rates are dependent on pressure increase/decrease limitations of the actuator. Since that EHB pressure rate increase is around $1300bar/s$ and assuming the system is 70% slower in damping pressure, again using Eqn. (2-22) for conversion, the torque rate bounds are set to $dT_{b,max} = 42000Nm/s$ and $dT_{b,min} = 30000Nm/s$.

4-2-6 Additional considerations

Since this first controller implementation is mainly focused on understanding the basics of MPC applied to ABS, a series of simplifications is made:

- The driver is not taken into account - meaning that the brake manoeuvre is initiated by the controller itself via step change of the reference state;
- Since the driver is not in the loop, no activation logic is needed;
- No reference adaption is taken into account - the slip target is manually set at the optimal point (peak of the $\lambda - F_x$ curve for the specific tire and friction coefficient);
- No automatic scheduling of the weight matrices is yet implemented - weights are changed manually based on the velocity range and friction coefficient of the manoeuvre;
- No low speed ABS mode is yet considered - simulations are simply ended when the controller is not capable of controlling the wheel dynamics anymore.

The above simplifications limit the variability of the problem by a substantial amount, allowing the designer to obtain good understanding of the cause-effect relationship of each parameter. Nonetheless, taking these elements into account is a fundamental aspect of implementing a ABS controller applicable to a real life situation. For this reason, all the features left out for this first implementation will be introduced for the final controller discussed in 5.

4-3 Corner braking control - implementation

This section introduces the tools used to define the OCP. First the modelling environment for setting up the Non-Linear Programming (NLP), `ACADO Toolkit`, is discussed. `ACADO` does

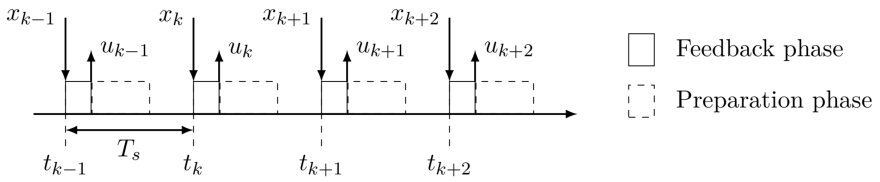

Figure 4-3: Task scheduling of the acsRTI scheme. After the preparation phase the algorithm waits for incoming measurements (x_k) and executes the feedback phase. The solution (u_k) is then directly applied to the system

not solve the problem itself but rather prepares it for a quadratic programming solver, in this case `qpOASIS`, in a systematic sequential manner. After general introduction of the tools, some more information is given on how to handle the case in which the QP solver does not find a feasible solution.

4-3-1 `Acado toolkit`

As mentioned, the OCP formulation is implemented withing `ACADO Toolkit`. `ACADO` is a open-source software environment for automatic control and dynamic optimization entirely written in C++. It supports auto generation of efficient and self contained C code [53]. In this work, the tool is used as a modelling environment to define the optimal control problem in a syntax that resembles that in (4-3).

Embedded integrators with efficient sensitivity propagation are a crucial part of the algorithmic tools necessary to implement real-time optimal control. One of the most appealing features introduced by `ACADO` is the task scheduling of the Real Time Iteration (RTI) scheme which splits one iteration into the following two parts:

- A preparation phase, where the NLP is linearized, discretized and condensed;
- A feedback phase, where the condensed QP is solved by the solver.

Figure 4-3 shows the typical task scheduling approach in the RTI scheme. The solution found in the feedback phase is then applied to the system and the next iteration starts again with the linearization problem. This iterative approach is also known as Sequential Quadratic Program (SQP).

The preparation phase can be time-consuming as it consists of many floating points operations. Nonetheless, since operations are independent from the optimization's initial state ($\widetilde{x_0}$), preparation can be executed before measurements arrive. Doing so, the feedback state phase (after a new initial state is measured) is only dedicated to solving the OCP. In this way, real-time performances within the milli- or micro-seconds range can be achieved depending on the application [54].

When modelling the OCP with `ACADO toolkit`, one first has to set the prediction horizons and shooting interval. Furthermore, either a single or multiple shooting approach needs to be selected. Subsequently, the nonlinear dynamical system introduced in section 4-2, can

be implemented in its continuous time form and constraints can be set. Finally the weights should be tuned.

ACADO takes the prepared linearized continuous time OCP and discretizes it over an equidistant time grid from T_0 to T_P with shooting intervals. The optimal control problem from (4-3) then can be rewritten as:

$$\begin{aligned}\min_{\substack{x_{k_0},\dots,x_{k_0+N_P}\\ x_{k_0},\dots,x_{k_0+N_P}\\ x_{k_0},\dots,x_{k_0+N_P}}} \frac{1}{2}\sum_{k=k_0}^{k_0+N_p-1} &(y_k - y_{\text{ref}})' Q (y_k - y_{\text{ref}}) + (u_k - u_{\text{ref}})' R (u_k - u_{\text{ref}}) \\ &+ \frac{1}{2}(y_{k+N_P} - y_{\text{ref}})' P (y_{k+N_P} - y_{\text{ref}})\end{aligned} \tag{4-16}$$

in which $Q \in \mathbb{R}^p_{\geq 0}$, $R \in \mathbb{R}^m_{\geq 0}$, $P \in \mathbb{R}^p_{\geq 0}$. From this discretized from, one of two approaches can now be taken:

- Either the resulting QP is solved in the current form using structure exploiting solvers such as FORCES Pro or qpDUNES;
- Or the QP problem undergoes a further procedure called condensing (see Appendix A) and the resulting condensed form can be solved by a dense QP solver.

In this work, the QP is further condensed and solved by qpOASES, an open-source implementation of the recently proposed online active set strategy [55].

4-3-2 QP OASES

qpOASES is a structure-exploiting active-set QP solver that supports warm start and particularly suited for model predictive control applications. The algorithm is capable of effectively solving condensed QP of the from:

$$\min_{\tilde{u}} \frac{1}{2}\tilde{u}'\tilde{H}\tilde{u} + \tilde{u}'\underbrace{\tilde{F}\tilde{x}_0}_{\text{g}} \tag{4-17a}$$

$$\text{subject to} \quad \tilde{G}\tilde{u} \leq \underbrace{\tilde{l} - \tilde{E}\tilde{x}_0}_{\text{w}} \tag{4-17b}$$

in which $\tilde{H}$ and g are the condensed Hessian and gradient of the quadratic program respectively and $\tilde{G}$ is the condensed constraint matrix. For the condensed Quadratic Problem problem the Karush–Kuhn–Tucker (KKT) conditions become:

$$\tilde{H}\tilde{u} + g - \tilde{G}'\mu = 0 \tag{4-18a}$$

$$\mu_i(G_i\tilde{u} - w_i) = 0 \qquad i = 1,\dots,m \tag{4-18b}$$

$$\mu \leq 0 \tag{4-18c}$$

$$\tilde{G}\tilde{u} - w \leq 0 \tag{4-18d}$$

The active-set algorithm solves (4-17) by finding a solution for the active subset ($\widetilde{G}_A$) of $\widetilde{G}$. For this active subset, the solution to the dense inequality constrained QP of (4-17) is reduced to solving an equality constrained QP. The solution can then be found by solving the following Linear Program (LP):

$$\begin{bmatrix} \tilde{H} & \tilde{G}'_A \\ \tilde{G}_A & 0 \end{bmatrix} \begin{bmatrix} \tilde{u}^{opt} \\ -\mu_A^{opt} \end{bmatrix} = \begin{bmatrix} -g \\ w_A \end{bmatrix} \tag{4-19}$$

whose matrix is invertible. Older versions of the QP solver could only deal with positive definite Hessian matrices. However, by applying a regularization procedure, `qpOASES v3.0` can now also solve (4-19) for positive definite matrices [52].

The combination of `ACADO toolkit` and `qpOASES` is in general fairly quick and if the prediction model is kept within reasonable complexity real-time requirements are easy to meet. Nonetheless, if this is not the case, `qpOASES` offers two possibilities to limit the amount of calculation being performed at every time step:

- Limiting the number of Maximum Working Set Recalculations;
- Early termination of the optimization procedure.

In general both ABS formulations were well withing real-time on the PC used to develop this work. However, as it will be further discussed, in the beginning of the braking manoeuvre, when the controller behaves as a driver reference torque follower, iterations to find the optimal solution take too long. Therefore, using either, early termination of limiting the number of working set calculations might be beneficial.

Overall, both proposed corner and full car ABS controllers deliver feasible results at decent speeds when the selected controller frequency and prediction horizon N_P are used. Nonetheless, if the controllers were to be run on less capable hardware, as a `dSPACE` or automotive ECU, structure exploiting QP solvers (e.g. `qpDUNES`) might be beneficial [56].

4-3-3 Controller settings

In this section, controller settings will be explained. Once the problem is set up, the two main parameters influencing the MPC performances are: prediction horizon (N_p) and sampling time (T_s). Since the optimization is required to run real-time, hence faster than T_s (see Fig. Figure 4-3), the choice for an optimal T_s and N_p is not trivial. Increasing the prediction horizon has a positive correlation with the total computational time. On the other hand, the choice of T_s determines what that real-time threshold actually is. Moreover, as `ACADO` does not allow separately defined prediction and control horizon, the chosen N_p not only defines the number of prediction steps but also that of control moves.

A typical rule of thumb in control system design states that sampling interval T_s should be between four and ten times faster than the process dead time. Here, four times faster is generally considered to be barely adequate and ten times faster to be the best. Conceptually, this ensures that the controller is running at a fast enough rate to adequately handle changes in the signal being controlled. As is not uncommon for the slip dynamics to be exceeding 20

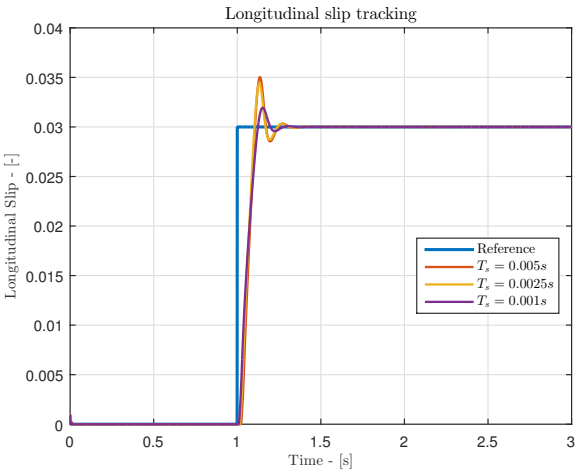

Figure 4-4: Longitudinal slip tracking comparison for different values of T_s

Hz, a good starting point for our investigation is to only consider controller frequencies larger than about 200 Hz, that is $T_s = 0.005$ s. A confirmation of this intuition is found by looking at sample times of commercially available ABS, which are indeed generally between 200 and 350 Hz. As higher frequencies generally mean better performances, it is now a matter of seeing how fast the controller frequency can set to without exceeding the real-time threshold.

A series of tests was performed with three different sampling intervals ($T_s = 5$, 2.5, 1 ms). The test consisted of applying a step reference signal for the slip. A fixed value of 25 steps is used for the prediction horizon horizon. The sampling time difference results in the actual look ahead time changing, specifically $T_{LH} = 25$ ms, $T_{LH} = 62.5$ ms and $T_{LH} = 125$ ms for $T_s = 1$ ms, $T_s = 2.5$ ms and $T_s = 5$ ms respectively. Attention is focused on how the reference is tracked and how the time needed for performing the prediction and solving the optimization compares to the specific sampling time. For ease of comparison, the tracking performances are plotted on the same graph, see Figure 4-4. For ease of reading on the other hand computational time is shown in three different plots, Figure 4-5. Considering the final implementation needs to control the full vehicle instead of a single corner, a multiplication factor of four is applied to the computational time of the corner controller when compared to the real-time threshold.

As can be seen, although slip tracking is fairly good for each of the three frequencies, the smaller the time step, the smaller is the initial overshoot. The effect is quite minute; however, keeping into account the substantial difference in look-ahead time, it is surprising to see how well the controller with $T_s = 1$ ms, an consequent look ahead time of 25 ms, tracks the reference. Nonetheless, looking at Figure 4-5c it is clear that, at least with the current settings, real-time performances are not achieved. Although the situation significantly improves for the controller run at $f = 285Hz$, there are still some events (e.g. the controller initialization or the first instances of the braking) in which the input generation is to slow compared to T_s. Finally, for $T_s = 5$ms the prediction plus optimization time is well within real-time. Based on the above consideration, it was chosen to use $T_s = 5$ms, equivalent to a controller frequency of 250 Hz for future development.

Now that T_s is fixed, the attention can be focused on selecting the best prediction and

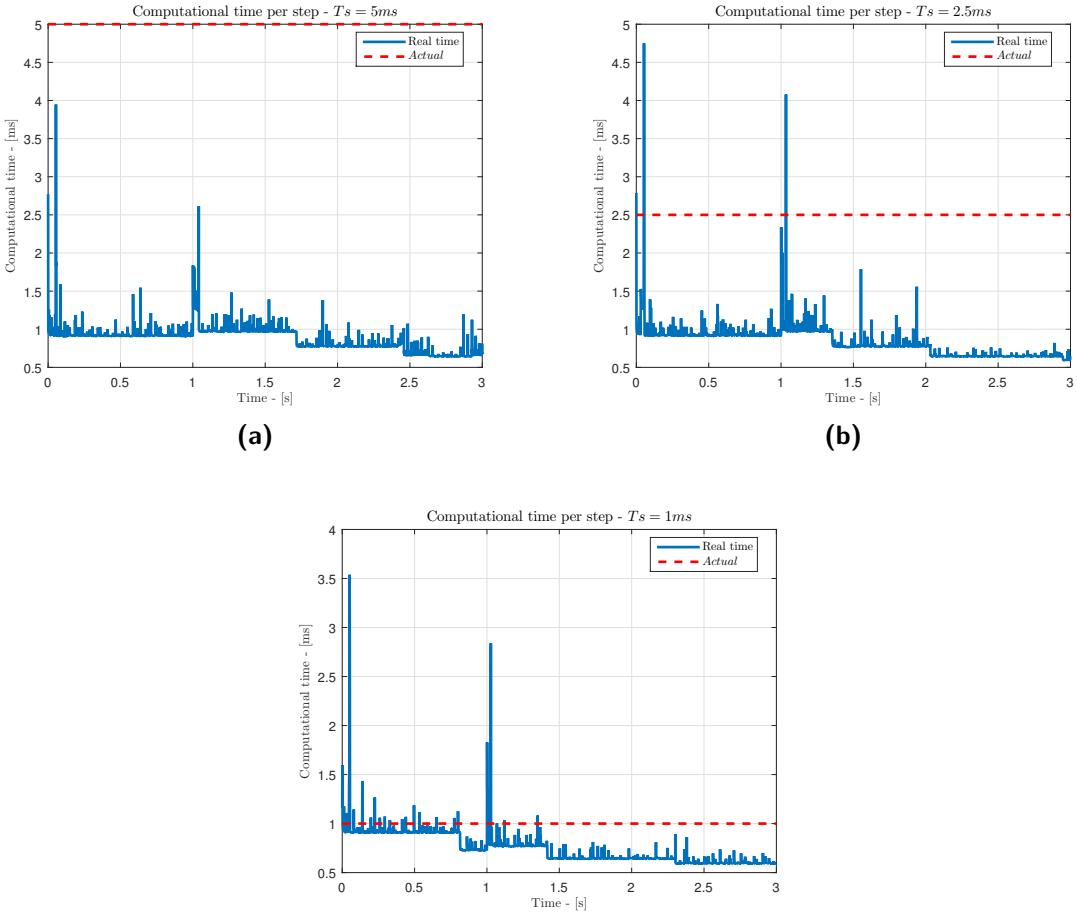

Figure 4-5: Computational time needed to generate input for each step. $T_s = 5$ ms (a), $T_s = 2.5$ ms (b), $T_s = 1$ ms (c)

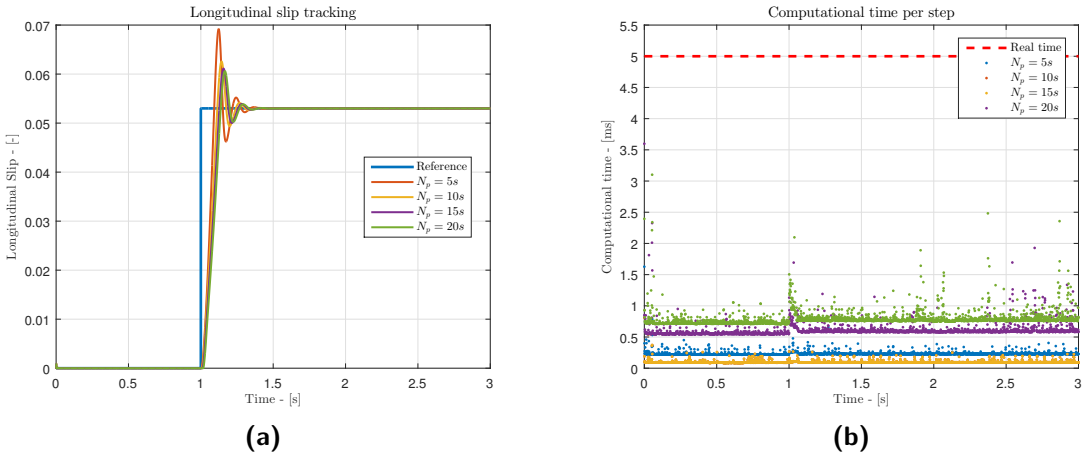

Figure 4-6: Effect of different prediction horizons on: Slip tracking (a), computational time (b)

consequent control horizon. The idea here is to increase N_p until either the real-time boundary becomes too close or no improvement is seen in making N_p larger. Figure 4-6a and Figure 6-2b shows tracking performance and computational time resulting from different choices of N_P. Specifically, the following were evaluated: N_p = [5,10,15,20] samples, corresponding to T_p = [25,50,75,100]ms. It can be noticed that overshoot decreases as the prediction horizon increases; this is true up to a certain point (in this case $N_p > 30$), after which no real benefit is seen anymore. On the other hand, increasing the number of prediction steps makes the time needed to output a control move higher as the number of predictions increases and, consequently, that of variables to be optimized. Based on this analysis, a $N_p = 20$ was selected since this was found to be the point after which the improved tracking was not balancing the increase in computational time.

As a note, the simulations results shown above are preformed on PC with the following processor and RAM: Intel(R) Core i7-4770HQ @ 2.20 GHz and 16 GB of RAM. Only a very small amount of the available RAM is used while the processor speed was found to be about 0.5 GHz. These values are needed to run both the controller and the simulation environment. This is by no means an accurate way of assessing the processing power or memory needed to run the controller; however, it can provide an initial idea of the feasibility of it.

Once the core of the MPC is fixed, performances can then be improved by modifying a series of additional settings (e.g. integrator type, termination tolerance, etc.). As these settings are mainly based on trial and error, they will not be explained, nonetheless, they are reported in 4-3.

4-3-4 Handling of infeasibility

Although the controller has been design to return feasible solutions for every scenario, it can occur that the NLP or the QP becomes infeasible. Generally there are two types of infeasibility:

- The nonlinear online optimization itself can be insfeasible, for example due to initial conditions that violates state constraints set in the OCP formulation;

Table 4-3: `ACADO Toolkit` solver settings

Variable	Value
Prediction horizon (N_p)	20
Sampling time (T_s)	5 ms
Number of SQP iterations	1
Max number of working set recalculations	60
Shooting type	Multiple shooting
Condensing type	Full condensing
Hessian approximation	Gauss Newton
MPC integrator	Implicit Runge Kutta 2^{nd} order
Termination Tollerance	10^{-7}

- The underlying QP becomes infeasible, for example due to constraints linearization.

Currently the solution of the QP solver is only used when the a success flag being returned is either zero or 1, meaning the solution is either successful or the maximum number of working set recalculations was hit. In this second case, using the solution returned by the QP solver is useful since this is both feasible and closer to the optimum than the previous time-step solution. The warm-start of the next time-step will then try to bring the solution closer to the optimal.

In case the return flag is any other value, the solution is discarded and the last successful solution used. This is not a true guarantee that the system will recover from this state but it is assumed that this approach is still superior compared to choosing an infeasible solution.

4-4 Weights sensitivity

Once the controller and solver settings are defined, additional performance can be extracted from properly tuning the weights. As already mentioned, MPC comes with the sizable advantage of having much fewer weights compered to other, non-model based, control strategies. Additionally, instead of being based on complex heuristics, weights are clearly associated with control variables which mikes the whole tuning process significantly simpler.

By referring to Eqn. 4-16, its observed that weights are evidently associated with states and control inputs. As seen, the state is $x = [T_b, \lambda, v]$ and the control input $u = [dT_b]$. The weight on the torque should clearly be zero, as any penalization would prompt the controller to brake less. Diversely for the velocity, this reasoning is not that straight forward. In fact, by proper setting of the reference some benefit could be obtained. The velocity target could be chosen as follows:

$$v_{ref}(t) = v(t) - a_{max}T_s$$

where a_{max} is the maximum achievable deceleration based on the current friction coefficient. After experimenting however, since the reference in `ACADO` can only be defined at the beginning of each prediction step (and not throughout the prediction), this approach does not bring any additional performance. The weight on the longitudinal slip is therefore the only state related parameter that should be set different from zero. Intuition tell us that on one hand increasing

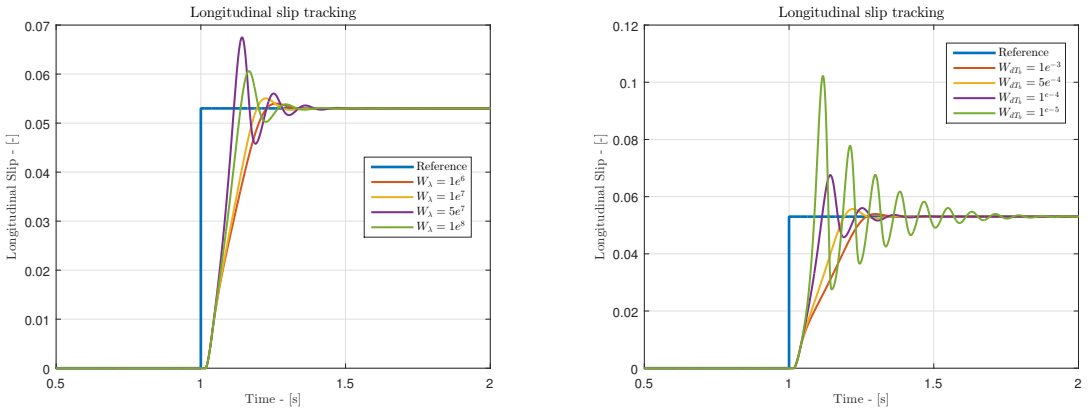

Figure 4-7: Effect of different: W_λ (a), $W_{dT_b}(b)$

this weight would improve the tracking and make the response to change in the reference signal faster; on the other it would make the controller more nervous and, consequently more prone to robustness issues. To investigate the actual effect of W_λ, a series of tests was performed with a step change in λ_{ref}. Both stage and terminal weights are set to the same value and the weight for the control input fixed to $W_{dTb} = 1 \times 10^{-4}$. The following were investigated: $W_\lambda = [1 \times 10^6, 1 \times 10^7, 5 \times 10^7, 1 \times 10^8]$. Results, shown in Figure 4-7a, are in line with what discussed earlier. Keeping in mind the final controller will be employed on everyday condition, bumpy roads included, the controller should not be tuned to be overly reactive. In this sense, $W_\lambda = 5 \times 10^7$ seem a good compromise.

Once the weight related to the longitudinal slip tracking error is selected, a further degree of freedom is given by the selection of the weight associated to the control input. As increasing this value penalizes fast variations of torque, this should make the controller less prone to oscillations and if tuned properly should reduce overshoot while maintaining an high cost on the tracking errors which is associated with precision. Again a step reference change is used to confirm what just said with W_λ fixed to 5×10^7. Figure 4-7b clearly shows how W_{dT_b} could be used to slacken the controller and to reduce overshoot. Smaller values make the control input change faster but more nervous, while higher values decrease the prescribed torque rate. The optimal seem to be found in the interval $W_{dT_b} = [1 \times 10^{-4}, 5 \times 10^{-4}]$, a value equal to 2×10^{-4} is hence selected. Since the effect of the control input weight is so well contained, it was chosen to only act on this weight in order to adapt the controller response to different friction coefficient and vehicle velocity. In particular, on higher frictions coefficient a rapid change in brake torque, associated with a lower value of W_{T_b} is desired. On the other hand, on low friction surface, a smoother control is to be preferred. In a similar fashion, when at higher speeds, where the slip dynamics natural frequency is lower, a smaller value can be used for W_{T_b}. Oppositely, when the dynamics becomes more unstable a quicker control action is to requested.

Lastly, the terminal weights need to be addressed. The slip error terminal weight should be significantly higher than its stage value as this would encourage the optimizer to lean towards an optimal control sequence that at the end of the prediction (and control) horizon achieves perfect tracking of the reference. Similarly, as the aim is to be in a steady state condition

at the end of the prediction time span, meaning the change in torque should be zero, the terminal weight for the torque rate should be significantly higher than its stage value.

4-5 Summary

Chapter 4 introduced the NMPC for corner control. First a discussion of the theoretical concepts behind model predictive control was presented. Specifically: prediction model, optimization and RTI-scheme were discussed. The brake corner model was then introduced and analyzed from stability point of view. Bode plots for the linearized system model highlighted relevant aspects that will need to be taken into account for the full vehicle ABS control. The just presented equations describing corner dynamics are then casted into a form that is suitable for their use as the controller's prediction model. State and inputs bounds, as well as model assumptions and simplifications, are also explained. The OCP was formulated in `ACADO Toolkit` and solved by `QP Oases`. The working principle of the two software's were discussed. Implementation continued with the discussion about controller frequency and prediction horizon selection, as well as some other settings for the optimizer. Lastly, the effect of weights accodiated with each state and control input was investigated.

Chapter 5

Final ABS controller

Despite the fact that single corner control can provide very good insight in ABS design, extension of the controller to the full vehicle behaviour is a fundamental step needed to quantify how good a design is on real world conditions.

As it will be discussed, extending from one wheel control, is not simply a matter of repeating the equations four times. When dealing with the full vehicle behaviour, complex couplings between wheels are displayed, some of which should be accounted for in the prediction model. In addition, the driver should now be taken into account, meaning a supervisory logic shall be implemented to activate the controller only when it is needed and leave the driver in full control in non-safety critical braking manoeuvres. Furthermore, despite the controller showing excellent dynamic performance and tracking ability, to obtain the correct vehicle behaviour, references should also be chosen appropriately and adapted to the current conditions. These as well as some other important considerations, will be explained in the following sections.

5-1 Prediction model

The prediction model is the start item of the controller extensions. It discriminates between what effects are to be taken into account and what others can be neglected.

As for the simpler one wheel implementation, the system's states are kept as: wheel brake torque $T_{b,ij}$, wheel slip λ_{ij} and chassis longitudinal velocity v. However, given we have four wheels instead of one, the number of state variables shifts to nine from the previous three. Furthermore differential equations, describing each state variable, need to be extended to account for additional effects. Load transfer is the most significant one, however differences in brake corner designs also result in more limited brake capabilities for rear actuators compared to front ones.

The prediction model in its implicit form is shown in Eqn. (5-1). The state vector is now: $x = [T_{b_{FL}}, \lambda_{FL}, T_{b_{FR}}, \lambda_{FR}, T_{b_{RL}}, \lambda_{RL}, T_{b_{RR}}, \lambda_{RR}, v]$.

$$\begin{bmatrix} \dot{T}_{b_{FL}} - dT_{b_{FL}} \\ \dot{\lambda}_{FL} + \frac{1-\lambda_{FL}}{v\left(m_{fr}+\frac{m_s a_x h}{2L}\right)} + \frac{R_w^2}{I_w v} F_{x_{FL}} - \frac{R_w}{v I_w}(dT_{b_{cmdFL}}\tau + T_{b_{FL}}) \\ \dot{T}_{b_{FR}} - dT_{b_{FR}} \\ \dot{\lambda}_{FR} + \frac{1-\lambda_{FR}}{v\left(m_{fr}+\frac{m_s a_x h}{2L}\right)} + \frac{R_w^2}{I_w v} F_{x_{FR}} - \frac{R_w}{v I_w}(dT_{b_{cmdFR}}\tau + T_{b_{FR}}) \\ \dot{T}_{b_{RL}} - dT_{b_{RL}} \\ \dot{\lambda}_{RL} + \frac{1-\lambda_{RL}}{v\left(m_{rr}-\frac{m_s a_x h}{2L}\right)} + \frac{R_w^2}{I_w v} F_{x_{RL}} - \frac{R_w}{v I_w}(dT_{b_{cmdRL}}\tau + T_{b_{RL}}) \\ \dot{T}_{b_{RR}} - dT_{b_{RR}} \\ \dot{\lambda}_{RR} + \frac{1-\lambda_{RR}}{v\left(m_{rr}-\frac{m_s a_x h}{2L}\right)} + \frac{R_w^2}{I_w v} F_{x_{RR}} - \frac{R_w}{v I_w}(dT_{b_{cmdRR}}\tau + T_{b_{RR}}) \\ \dot{v} - \frac{F_{x_{FL}}+F_{x_{FR}}+F_{x_{RL}}+F_{x_{RR}}}{m_t} \end{bmatrix} = \begin{bmatrix} 0 \\ 0 \\ 0 \\ 0 \\ 0 \\ 0 \\ 0 \\ 0 \\ 0 \end{bmatrix} \tag{5-1}$$

The augmentation equation ($\dot{T}_{b_{ij}}$) is kept equal to that in Eqn. (4-15). The chassis longitudinal dynamics ($\dot{v}$) now accounts for the additional forces generated by the four tires as well as for the fact that the mass is now the full vehicle's one. Most changes are made in the slip equations. The base structure is still the same as in Eqn. (4-15) but, in order to account for the variability in corner weight associated with longitudinal acceleration, static weight transfer is added/subtracted to the static corner mass depending on the chassis acceleration direction. The algebraic equations describing actuators dynamics are kept the same but allowed values for the brake torque and torque rates limited differently front and rear. Lastly, tire forces are fed online and used both for the individual slip equation and chassis longitudinal dynamics.

Constraints

Constraints for states and inputs are based on the same considerations made in Chapter 4. Additionally, it was chosen to limit the torque rates of the rear wheels (in the pressure increasing direction only) compared to that of the front ones. In terms of actuator capabilities, this should not be the case, since both front and rear brake calipers are served by the same high pressure accumulator and type of proportional valves; However, for safety reasons it is advisable that in the event of a lock up, rear wheels would follow the front ones to prevent the vehicle from spinning out.

For ease of reading, bounds imposed are reported in Table 5-1.

5-2 Reference state generator

Dynamic behaviour of a controller and how well this is able to track a reference signal is surely very important; however, how the reference is defined is also a key aspect. By referring to Eqn. (4-16), it is apparent that a reference signal should be defined for each of the nine states and four inputs that the controller processes. Some of these references are fairly simple to choose (e.g. reference torque rate and torque values), others, on the other hand, take a fair amount of work to be defined.

Table 5-1: State and input bounds for full vehicle controller

Variable	Unit	Lower-bound	Upper-bound
$T_{b_{fr}}$	[Nm]	0	3500
$T_{b_{rr}}$	[Nm]	0	1700
λ_{ij}	[-]	0	1
v	[m/s]	0	53
$dT_{b_{fr}}$	[Nm/s]	-35000	42000
$dT_{b_{fr}}$	[Nm/s]	-35000	35000

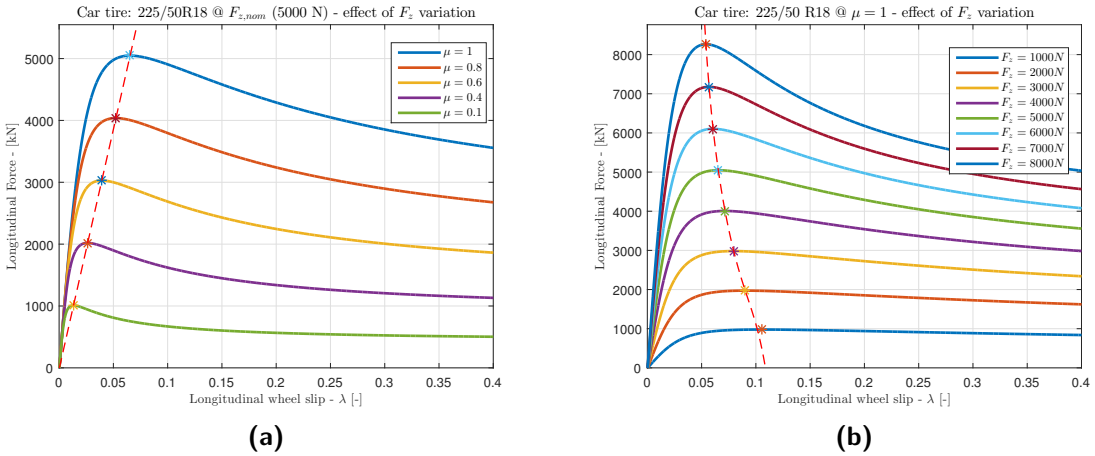

Figure 5-1: Effect of friction coefficient (a) and load (b) variations on tire's longitudinal force - slip curves

Torque rates targets are chosen as $dT_{b,ij_{trg}} = 0$, since the aim is to reach the a stable equilibrium for the longitudinal slip and remain in that location. $T_{b,ij_{trg}}$ is selected to be the controller output at the previous time step for similar reasons. The velocity target state could be chosen in multiple ways. A theoretically good one is to take the velocity at the previous time step and subtract the maximum feasible deceleration given by the average friction coefficient of the four tires multiplied by gravity ($a_{x_{max}} = \mu_{avg} g$). As mentioned though, this was; however, not found to bring any performance benefits and could lead to problems in situations in which the friction coefficient is very noisy or variable (e.g. bumpy roads or mu transitions). For this reason it was decided to opt for $v_{trg} = 0$, equivalent to the vehicle being at rest.

By far the most complex reference to generate is the target slips. It is obvious that this should coincide with the slip value at which the longitudinal force is maximum. However, tires present substantial amount of non-linearity and this point is practically never the same. It is well known that tire longitudinal forces are dependent on load conditions, friction coefficient, suspension angles, inflation pressure and so on (as well as lateral slip conditions, not accounted for in this work). These variables drastically affect the shape, and hence peak location, of the force characteristic. Following investigation, it was found that the most variability in the peak location is given by load and friction variations and that, consequently, suspensions angles and pressure influences could safely be neglected for this applications.

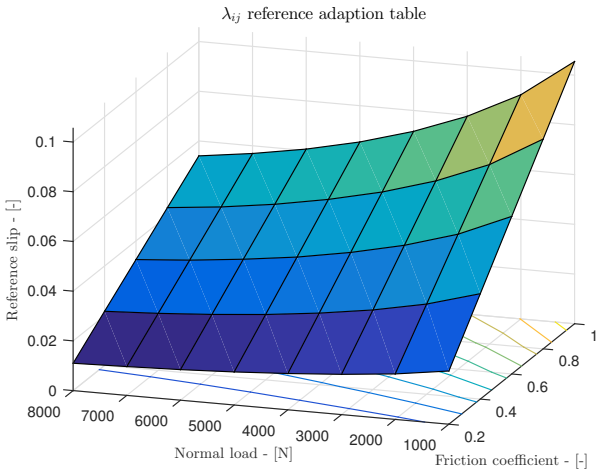

Figure 5-2: Reference longitudinal slip look-up table

Figure 5-1a and Figure 5-1b show how friction coefficient scaling and load variation respectively affect the shape of the $F_x - \lambda$ curves for the standard tire mounted on the simulated vehicle. An increase in friction coefficient is associated with a shift of the peak towards higher values of slip. As can be seen by the superimposed fitting, for the specific tire the peak shift is linearly proportional to the increase in friction coefficient. By referring to Figure 5-1b the effect of load variation can be appreciated as well. Higher loading of the tire has a negative correlation with the amount of longitudinal slip associated to the force peak. Contrary to the friction case, this time the relationship is nonlinear.

Two approaches could now be taken, either an analytical relation dependent on tire normal load and friction coefficient could be identified by fitting the tire model output, or, a simpler two dimensional look-up table could be implemented by running a series of simulation for different input conditions. The first approach could be more beneficial if different tires are to be used and a more general relationship is needed. In this specific case the other hand, the main objective is to evaluate the performance advantage associated with the new proposed design. It was therefore decided that opt for a look-up table approach as it doesn't involve fitting. The result of this process is shown in Figure 5-2. As can be seen, the trends discussed in the previous paragraphs are encountered again.

While on smooth roads, the look up table alone manages to produce a smooth reference of the controller to track; on bumpy roads however, due to the tire normal load vibrations, the output of the reference generator is rather variable and noisy. The ABS controller then starts overreacting to this variability and performance are affected. A low-pass filter was thus inserted downstream to the reference generation. The cut off frequency was chosen to be $f_{c_{ref}} = 6.5Hz$ so to eliminate the vibration but at the same time keep the controller responsive to friction jumps.

5-3 Activation logic and controller integration

The controller presented in the previous chapter initiates the brake manoeuvre by itself, following a step change in the reference state for the slip. Despite this being an effective way

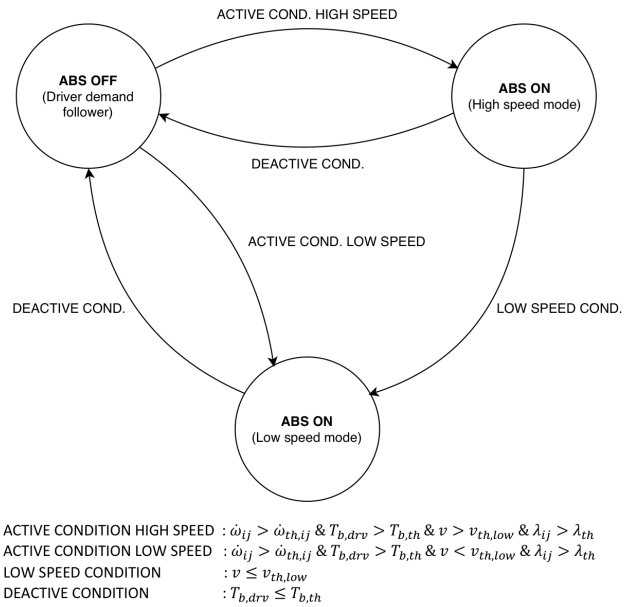

Figure 5-3: Supervisory state machine logic

of preliminary checking the controller's behaviour, a supervisory logic activating the controller and switching between modes must be developed if the driver wants to be taken into account. Moreover, since the transition from manual brake application to ABS can be responsible for problems in the controller's or vehicle's doings, it is essential to implement them if actual controller wants to be simulated.

As this research uses electronically controlled brakes meaning there is no physical connection between the brake pedal and hydraulic pressure generator, it was decided to keep the model predictive controller active at all times and switch between three controller modes:

- **ABS Off** - tracks the driver torque request during normal braking;
- **ABS On** - takes over control and prescribes brake torques based on slip references;
- **ABS On low speed** - keeps the brake torques constant when the wheel slip dynamics is too fast to control.

This is not the usual approach, since even in market-available hybrid vehicles mounting the EHB system, the ABS and brake control logics are kept as separate functions. However, having the two controllers together reduces the overall design complexity and cost, and it is beneficial from a communication delay point of view. A schematic state machine representation, illustrating the three ABS modes and the possible transitions between them is shown in Figure 5-3.

As this research focuses on straight line braking and does not consider the possibility of significantly different road conditions among wheel pairs, ABS activation is not individual to each corner but rather front and rear activations are considered. It is advisable; however, to change this when taking into account lateral dynamics.

In order to decide whether or not the slip is about to go unstable and, ABS should consequently activate, variables are compared to some predefined bounds in a rule - based fashion. Furthermore, additional conditions are checked to prevent mis-interventions. The most intuitive way of identifying an unstable situation would be to compare the slip signal against the one producing the highest longitudinal force for the specific loading and friction conditions. If the actual slips overcome the optimal slip then the ABS is activated. Despite this approach being theoretically correct, it tends to result in late interventions. Once the friction peak is passed, in fact, it takes a significant amount of under-braking to bring the slip back from the unstable region, thus activating ABS just before the slip peak is to be desired. Since the wheel angular acceleration does not present the relaxation behaviour that the tire slip does, is thus a good way of anticipating an unstable condition. The lower the threshold value the earlier the ABS activates. On the other hand, to prevent mis-interventions on bumpy roads and lower friction surfaces, the activation threshold cannot be too low. Additionally, threshold values should be distinguished between front and rear wheels due to sizing and brake distribution differences.

Despite proper selection of the wheel angular acceleration thresholds, mis-interventions can be prevented by a series of plausibility checks to make sure the driver is actually braking and intervention is not triggered by external factors:

- Brake torque requested by the driver is non-zero and high enough to lock on polished ice - ($T_{b,drv} \leq T_{b,th} = 450Nm$);
- The wheel slip signal is positive and in the rage of possible unstable values ($\lambda_{ij} \leq \lambda_{th} = 0.02$);
- Vehicle velocity is higher than a minimum threshold at which the system dynamics is to fast to control ($v = v_{th} = 1ms$).

A simple deactivation logic is also implemented to make sure that the controller does not freeze in the **ABS On** state. Whenever the torque requested by the driver is below $T_{b,th}$, the supervisory logic switches gives back control. A more sophisticated deactivation logic, accounting for those situations in which the driver doesn't fully release the brake but the wheel behaviour is not unstable anymore, should be implemented if the controller was to be employed on a real vehicle. Clearly; however, this would be outside the scope of this research work.

Lastly, it is safer to keep the prescribed brake torque at a constant value and consequently lock, rather then having the controller mis-behaving and potentially under-braking when the system dynamics is too unstable to control. This situation usually happens at very low speed and it is common to all ABS controllers. How good and precise a specific controller is, and at what frequency this is run, only affect the speed at which it is needed to switch to its low speed mode. The limit velocity for the NMPC is quite low, which is a measure of the controller's goodness. After experimenting on multiple friction coefficients a value of $3km/h$ was found to be the earliest the slip oscillation couldn't be kept stable anymore. An excess value of $v_{th} = 1ms$ was therefore selected.

Table 5-2: State and input weights for the *ABS OFF* controller mode

Variable	Unit	Weight
$T_{b_{fr}}$	[Nm]	50
$T_{b_{rr}}$	[Nm]	50
λ_{fr}	[-]	0
λ_{rr}	[-]	0
v	[m/s]	0
$dT_{b_{fr}}$	[Nm/s]	1×10^{-5}
$dT_{b_{rr}}$	[Nm/s]	5×10^{-5}

5-4 Cost function weight scheduling

Switching between ABS modes is done by online adjustment of the cost function's weights. In addition, the relative importance of states and inputs in the optimization cost is also adjusted online in relation to environmental conditions. In this section, the reasoning behind weight selection and adjustment is explained. Attention is first put on implementation of the three different controller modes, and later shifted onto the velocity scheduling implemented for the ABS On mode.

In order to satisfactorily track the driver request while normal braking is performed, null weights are chosen for the wheel slips λ_{ij} and chassis velocity v. On the other hand, relatively high equal weights are put on the states $T_{b_{ij}}$. Additionally, small weights are selected for the inputs $dT_{b_{ij}}$. Per se these would not be necessary as very little variability is present in the driver request; however, having slightly higher weights for the rear torque rates ensures stability in the event of late activation as the front wheels would be faster to lock. Settings for the ABS Off mode are reported in Table 5-2. It needs to be noted that the controller takes the three squared matrices Q, R and P seen in Eqn. (4-16). However, off diagonal terms, associated with two different states/inputs are all set equal to zero for simplicity. Furthermore, matrices Q and P, corresponding to stage and termination cost respectively, are set to be equal as no real improvement could be obtained by differentiating them due of the chosen relatively long prediction horizon. Matrices are then reshaped into the two line vectors W and W_n seen in Figure 5-4, for implementation purposes in `ACADO`. Specifically, W contains the elements from Q and R and W_n those in P.

As already discussed, in the ABS On - Low speed mode the brake torque applied to each wheel is kept constant to prevent any unwanted under-braking that might be caused by the controller being unable to do its job. Achieving this is simply a matter of setting all the weights but those corresponding to the torque rates equal to zero. $W_{dT_{b_{ij}}}$ are then chosen as very high values to prevent any unwanted torque increase/decrease. Front and rear weights are not different in this case because the rear wheels locking-up before the front ones would only result in a small body side slip angle which the driver which the driver should be able to easily correct. Weight values for this mode are reported in Table 5-3.

In ABS On the focus is put onto tracking the wheels slip reference values as closely as possible. No penalty is therefore associated with torque states $T_{b_{ij}}$ or chassis velocity v. On the other hand, high values are inserted on the diagonal of Q and R in the positions corresponding to front and rear wheel slips λ_{ij}. The respective values are one order of magnitude apart because

Table 5-3: State and input weights for the *ABS ON - Low speed* controller mode

Variable	Unit	Weight
$T_{b_{fr}}$	[Nm]	50
$T_{b_{rr}}$	[Nm]	50
λ_{fr}	[-]	0
λ_{rr}	[-]	0
v	[m/s]	0
$dT_{b_{fr}}$	[Nm/s]	5×10^5
$dT_{b_{rr}}$	[Nm/s]	5×10^5

Table 5-4: State and input weights for the *ABS ON - High speed* controller mode

Variable	Unit	Weight
$T_{b_{fr}}$	[Nm]	0
$T_{b_{rr}}$	[Nm]	0
λ_{fr}	[-]	5×10^8
λ_{rr}	[-]	3.5×10^7
v	[m/s]	0
$dT_{b_{fr}}$	[Nm/s]	$a_{fr}v^4 + b_{fr}v^3 + c_{fr}v^2 + d_{fr}v + e_{fr}$
$dT_{b_{rr}}$	[Nm/s]	$a_{rr}v^4 + b_{rr}v^3 + c_{rr}v^2 + d_{rr}v + e_{rr}$

of already mentioned stability concerns, different loading conditions and torque variations. In particular, as can be seen from Figure 5-1b, higher normal loads are associated with more pronounced peaks, while lower loads with generally flatter curves. This means that for front tires, usually subjected to higher loading conditions, it will be more difficult to track the optimal wheel slip and thus will require more control effort. Additionally, as the front actuators operate on brake torque intervals that are wider compared to the rear one, higher weights in the cost are imposed to λ_{FL} and λ_{FR} compared to λ_{RL} and λ_{RR}.
Referring to the frequency analysis made in Chapter 4, it is clear that the system's dynamics changes significantly as the velocity changes. To cope with this effect, two approaches can be taken. The first one consist on tuning the controller with the spotlight on low speed (below $50km/h$) and then use the same weights in the high speed region. The second, which involves more effort but results in better adaption, is to tune the controller on multiple velocity ranges. Once the optimal weights for each velocity band are identified, polynomial fitting can be employed to identify a continuous curve passing by those points. The latter is the selected approach for this work. Four velocity bands were chosen as [200-100, 100-50, 50-20, 20-1]. The controller weights were the identified as described later in section 5-5 and the Matlab function *polyfit* used to fit the coefficients of a 4^{th} order polynomial. The procedure was repeated for front and rear wheels. For ease of reading, weights associated with the ABS On controller mode are shown in Table 5-4. Coefficients from the fitting procedure on the other hand, are reported below:

$$a_{fr} = -0.00001 \times 10^{-5}, \quad b_{fr} = 0.00140 \times 10^{-5}, \quad c_{fr} = -0.05393 \times 10^{-5},$$
$$d_{fr} = 0.92319 \times 10^{-5}, \quad e_{fr} = 0.59698 \times 10^{-5},$$
$$a_{rr} = -0.25 \times 10^{-6}, \quad b_{rr} = 4.30 \times 10^{-6}, \quad c_{rr} = -5.18 \times 10^{-6},$$
$$d_{rr} = 183817.33 \times 10^{-6}, \quad e_{rr} = -46124.61 \times 10^{-6},$$

5-5 Controller tuning

In the previous chapter, basic effect of changing the weights associated to states and control inputs was shown. An indicative optimal value was also selected for each weight. Once the controller is extended it however, the tuning needs to be done again. Values selected for the corner model are used as starting point for finding the new controller weights.

In order to make the job easier it is best practice to objectivize the results by means of performance indicators. Specifically, since the tracking performance wants to be assessed, two indices, both focusing on the wheel slip error are used:

- Root Mean Squared Error (RMSE). It is a quadratic scoring rule that measures the average magnitude of the error. Taking the square root of the average squared errors has some interesting implications for RMSE. Since the errors are squared before they are averaged, the RMSE gives a relatively high weight to large errors. This means that tuning based on RMSE is to be used when large errors are particularly undesirable, as it is in our case.

$$RMSE_{ij} = \sqrt{\frac{1}{T_f - T_i} \int_{T_i}^{T_f} (\sum_k \lambda_k - \lambda_k^*) dt} \tag{5-2}$$

- Integral Time-weighted Absolute Error (ITAE). It integrates the absolute error multiplied by the time over time. In this way, errors which exist after a long time are weighted higher than those at the start of the response. The ITAE tuning produces systems which settle much quicker than if other tuning metrics were used. This characteristic is evidently to be desired given the high instability of the controller variable.

$$ITAE_{ij} = \sum_k \int_{T_i}^{T_f} (t(\lambda_k - \lambda_k^*)) dt \tag{5-3}$$

In Eqn. (5-2) and (5-3), the ij stays for either front or rear and k represents the wheel identifier ($FL = 1$, $FR = 2$, $RL = 3$, $RR = 4$). Hence, $k = [1, 2]$ and $k = [3, 4]$ when the indicator refers to the front and read axle respectively.

Tuning was done by performing a series of brake manoeuvres keeping the slip reference fixed. Tests were repeated with different friction conditions and multiple initial velocities so to span the full range of real life possibilities. Based on RMSE and ITAE value, the weights presented in section 5-4 were identified.

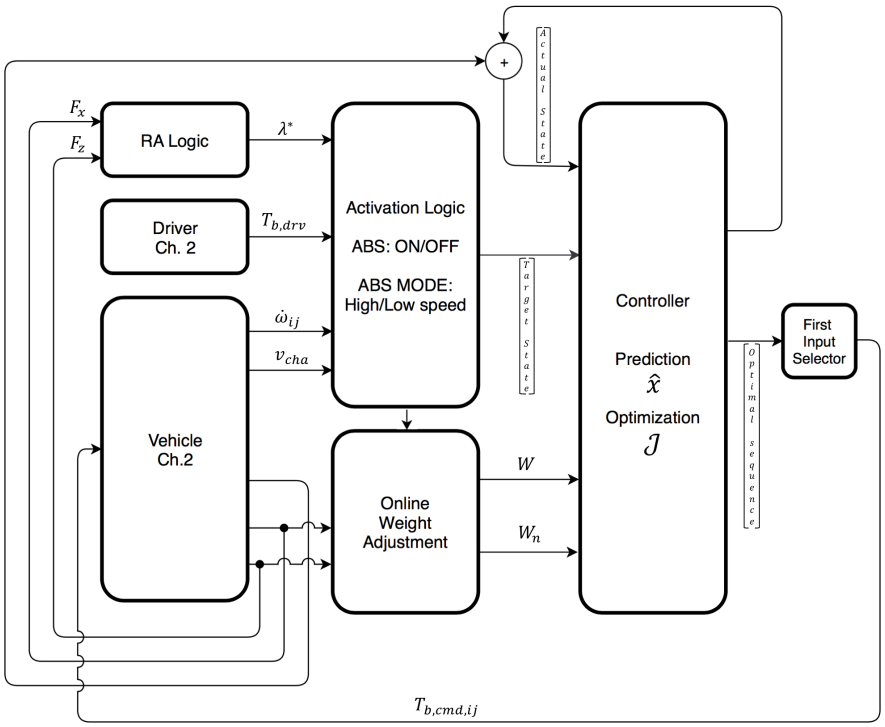

Figure 5-4: Schematic overview of controller subsystems and connections

5-6 Subsystem connection

The elements presented in the previous sections need to be connected appropriately in order for the controller to work.
Figure 5-4 shows how each subsystem is connected to the others and what signals are interchanged. As can be seen, the reference adaption block reads longitudinal and normal force signals at each time step and, after calculating the friction coefficient, outputs target wheel slips λ^* for each wheel based on μ_{ij} and $F_{z,ij}$. This slip target, together with the other signals coming from the vehicle and driver subsystems, is then passed to the activation logic and mode selection block.

Based on the state machine presented in section 5-3, the controller's mode as well as the target state are then calculated based on current conditions. The prescribed mode is then implemented by the online weight adjustment block via proper selection of the entries of the weight matrices W and W_n. When in ABS On mode, the block also obtains the estimated chassis velocity from the vehicle and schedules the slip gains according to the relations presented in the previous section.

Current state, target state, online longitudinal force measurements and cost weights are then passed to the NMPC which, based on the prediction model and online optimization problem, finds the optimal control inputs.

The control inputs then act as a target for the low level ABS controller, which operates the hydraulic unit so to track the reference coming from the NMPC. Brake corner pressures are then applied to the vehicle which closes the loop.

At each controller time step the loop is then repeated. It needs to be noted that the elements shown in Figure 5-4 are simulated with different time steps to replicate the real case scenario as best as possible. Vehicle and its subsystem are simulated with variable step size solvers, normally operating much below $1ms$, to well catch their highly nonlinear behaviour. On the other hand, the driver is simulated with a fixed step size of $1ms$. Lastly, the controller and sensors run at a frequency of $250Hz$ equivalent to $5ms$, which is how they would function in real life.

5-7 Summary

Chapter 5 discussed the extension of the single corner model seen in 4 to the full vehicle. Several additional components had to be designed to be next to the NMPC core. The prediction model is undated to suit the full car. Additional equations are implemented as well as respective state and input bounds. A reference state generator for the NMPC was developed and its working principles are well explained. Next to it a ABS activation logic was formulated and implemented using a supervisory state machine. Based on the findings of Chapter 4 weight scheduling was realized to keep adapt to system dynamics alteration by velocity changes. Additionally implementation of the modes transitions is also performed in this block. Controller tuning, although fairly quick and easy, was realized using rigorous performance indicators. Lastly, the subsystem connection and set-up of a unified simulation environment is explained.

Chapter 6

Controller assessment

After exploiting how the controller was designed and its initial promising performance, how this would work on passenger cars and everyday conditions still remains an open question.

ABS braking absolute performance strongly depends on the vehicle's characteristics. A good way to assess the controller's performance, also found in the majority of published papers on the topic, is to compare the proposed strategy with the current state of the art. In this case this coincides with the Rule Based logic provided by Toyota, whose working principle will be briefly explained.

Demonstrating the stability of the controller is also a key point that still remains untouched. Applying stability theory to advanced model based controllers, is not only extremely difficult and a research topic on its own, but often not possible. In addition, these procedures only prove the closed loop stability of the system model used in the analysis and not of the real plant. Developing accurate enough models of the system in differential equation forms, next to what already done for the controller and simulation, is unthinkable. A comprehensive set of manoeuvres was therefore developed and the controller stability verified by tests.

Moreover, in order to obtain deep understanding of how the two controllers compare, a set of performance indicators was developed to analytically analyze results.

Lastly, simulation results are presented, analyzed and commented.

6-1 ABS braking scenarios

The goal of the manoeuvres selection is to span all possible conditions that might be encountered on the road by customers. This; however, does not mean every possible ABS braking scenario should be simulated. Attention is rather focused at identifying a restricted set of manoeuvres that is representative of a much larger set of possible conditions.

The simulated scenarios aim at evaluation of both performance and robustness of the presented controller. The final list of manoeuvres is shown in Tab. 6-1. Braking scenarios

Table 6-1: Simulated braking scenarios for controller assessment

Manoeuvre	Initial velocity [km/h]	Avg. friction [-]	Exit velocity [kmh]	Surface layout	Extra
High friction	130	0.9	0	Smooth	-
Mid friction	90	0.7	0	Smooth	-
Low friction	40	0.3	0	Smooth	-
μ-jump	120	$1.1 \rightarrow 0.6$	70	Smooth	Jump @ 100 km/h
μ-jump	60	$0.75 \rightarrow 0.35$	30	Smooth	Jump @ 40 km/h
μ-jump	70	$0.3 \rightarrow 1$	20	Smooth	Jump @ 50 km/h
Rough road	70	0.65	0	Red bricks	-
Rough road	40	0.3	0	Belgian cobblestones	-

are chosen based on the guidelines given by the United Nations in Regulation 13 (E/ECE/-TRANS/505/Rev.1/Add.12/Rev.8. 3. Regulation No. 13) and Toyota's internal knowledge.

The 8 selected manoeuvres can be seen as belonging to three major groups:

- Braking on smooth roads - The first three manoeuvres are targeted at evaluating the performance gain on smooth roads with constant friction conditions (a small variability is always present as discussed in Chapter 2). As the aim of this work is a complete evaluation of the braking performances in common driving conditions, three friction levels, associated with the following surfaces, are selected: dry asphalt, wet asphalt and peaked snow. It should be noted that, depending on surface condition, a range of friction coefficients can be associated with each surface (dry asphalt fine/coarse, new/old, etc.) and a average value was selected. Initial speed for each of the three decelerations is chosen in relation to relatable domains' speed limits (e.g. high-way, freeway, etc.) and advisable maximum speed associated with the friction condition.

- Friction jumps - The three μ-jump manoeuvres are also performed on smooth roads; however, contrary to the homogeneous friction ones, they are specifically intended for evaluation of the controllers transient behaviour. Friction transitions are commonly found on everyday roads and it is therefore key for the controller to be fast-adapting and robust to them. One can easily think to the situation in which, on a winter sunny day some ice patches are present on the road. If it is now imagined that a brake manoeuvre is initiated on dry asphalt and then the vehicle enters the ice patch, it is critical for the brake torque to be reduced fast enough to avoid wheel lock. Similarly, when at the end of the patch, the vehicle rejoins the dry asphalt, it is important to take quick advantage of the increased friction coefficient. To assess the controller behaviour in relation to transient conditions, two friction jumps in which the friction coefficient drops and one in which it raises are simulated. The speed at which the jump happens is selected based on common sense.

- Braking on rough roads - The last two manoeuvres are performed on rough surface. The objective is to quantify and compare eventual performance degradation associated when injection of high noise levels in the sensed signals. Road irregularities, in fact, transmit through the vehicle and cause variable band noise on the sensor readings. As frequency and amplitude are dependent on the road's shape it is usually difficult to filter the disturbance out. In combination with a reactive controller this can leave to severe tracking issues. As already mentioned in Chapter 2, the roads, part of Toyota's database, are laser-scanned and replicated in simulation using the Curved Regular Grid (GRG) technique. A segment of the Belgian cobblestone road and its 3D map are shown in Figure 2-12.

6-2 Benchmarking metrics

If simulation scenarios are the base of the analysis, performance metrics are its core. Although a general idea of how the controller is working can be gained by simply looking at the simulation results, understanding the relative margins and where these are created can only

be achieved by implementing effect-related performance indicators. For this work, a comprehensive list was drafted. Different KPI sets apply to each of the three groups of manoeuvres. In the following paragraphs each performance metric and the manoeuvres it applies to will be discussed.

Steady state and transient performances, as well as human factors and actuator wear, are evaluated on smooth roads by the following KPIs:

- ABS Index of Performance (ABSIP) - The ABSIP compares the braking distance achieved by the specific controller (NMPC/RB) to that of the case in which ABS is not present. The returned value, a brake distance reduction percentage, give a first rough idea of how effective the controller is throughout the braking manoeuvre.

$$ABSIP = \frac{d_{ABS}}{d_{skid}} \tag{6-1}$$

- Brake Distance (BD) - The brake distance is calculated as the velocity integral from the moment at which the brake pedal is first pressed (T_i) to that in which the vehicle speed equals the exit velocity reported in Table 6-1 (T_f). The aim is again that of comparing overall braking performance but this time with an absolute brake distance reading. Please note that the way brake distance is evaluated in automotive magazines is often different from the way this value is obtain. As most of the times the magazines's calculation is started after the vehicle is already at maximum deceleration, brake distance readings often tend to be shorter than the value in this work.

$$BD = \int_{t_i}^{t_f} v_{cha} dt \tag{6-2}$$

- Mean Fully Developed Deceleration (MDFF) - This is simply the mean longitudinal acceleration, $\bar{a}_x$, calculated in a time interval that goes from 90% to 5% of the vehicle speed at the beginning of the braking. The MFDD is specifically designed for assessment the vehicle deceleration performance throughout the entire ABS activation time.

$$MFDD = [\bar{a_x}]_{0.05V_0}^{0.9V_0} \tag{6-3}$$

- ABS efficiency (η_{ABS}) - This is the ratio of mean longitudinal acceleration to its theoretical maximum (average friction coefficient times gravitation acceleration). $\bar{a}_x$ is calculated from when the vehicle velocity equals 80% of its initial speed to when the vehicle is at 10% of its initial speed. This KPI is specifically designed for assessment of steady state deceleration performance. That is after when the first violent weight transfer and consequent pitching have already happened to a point where the low speed ABS is still deactivated and the controller modulating brake torques.

$$\eta_{ABS} = \frac{[\bar{a_x}]_{0.1V_0}^{0.8V_0}}{\bar{\mu} g} \tag{6-4}$$

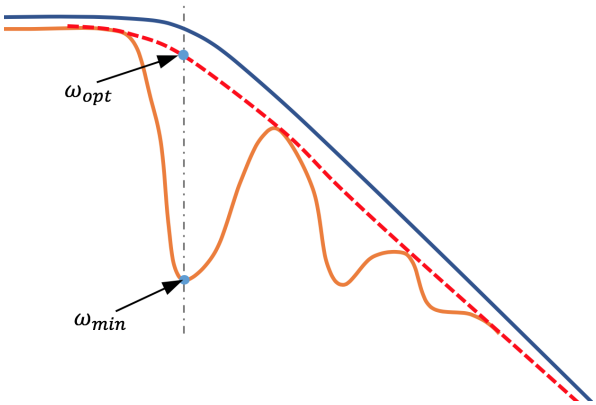

Figure 6-1: Illustration of the Peak to Peak KPI (PtP)

- Peak to Peak (ω_{peak}) - Quantifies the agility of the controller in transient conditions. This is done by focusing only on the first control cycle after ABS activation for manoeuvres 1-2-3-7-8. Omega peak is calculated in a similar fashion to a normalized slip error except that the vehicle velocity is not needed for the calculation and thus simulation results can be replicated more easily in real life. ω_{max} is the wheel angular velocity at either ABS activation or friction jump. ω_{opt}, on the other hand, is the optimal wheel speed obtained from the tire model. An illustration of these two points is shown in figure Figure 6-1.

$$\omega_{peak_{ij}} = \sum_{k} \frac{\omega_{max_k} - \omega_{opt_k}}{\omega_{max_k}} \tag{6-5}$$

- Integral Time-weighted Average of the longitudinal jerk ($ITAE_{J_x}$) - Aims at characterizing driving comfort. A negative influence on the driver's perception during ABS braking occurs owing to fluctuations in the realized brake force, which produces oscillations in the vehicle deceleration. That is: the lower the vehicle jerk, the better the comfort characteristics provided by the ABS are. Weighting the average with time, corresponds to taking the area between the jerk signal and zero (the ideal value that would be best). Additionally, taking the integral has the important advantage of filtering our outliers and spikes commonly originated by differentiating a noisy signal as their contribution to the area is zero. In this way the signal does not need to be heavily filtered to obtain a decent reading.

$$ITAE_{J_x} = \int_{t_i}^{t_f} t|J_x|dt \tag{6-6}$$

- $IACA_{T_b}$ - Calculates how much torque variation is prescribed by the controller. This is important for a first evaluation of potential issues related to actuator wear. Too much torque variation in fact can lead to premature degradation of both corner components and valves. Estimating how much this number should be to cause concerns is outside the scope of this thesis; however, comparing the indexes associated with the two controllers

and making sure the proposed logic's one is lower than the one associated with current logic can give a good estimate of the presence of possible implementation issues.

$$IACA_{T_b} = \frac{1}{t_f - t_i} \int_{t_i}^{t_f} |\delta T_b| dt \tag{6-7}$$

- Integral Pitch Variation (IPV) - The second of the human factor KPI on this list. Research has shown that the vehicle pitching motion affects the driver capabilities to estimate distances, it is therefore desirable for an ABS to be as smooth as possible in its control action. IPV is mostly relevant on high friction surfaces but it will be calculated for other manoeuvres as well.

$$IPV = \int_{t_i}^{t_f} |\dot{\psi}| dt \tag{6-8}$$

Performance metrics used for the friction jumps scenarios, contrary to those just seen, are only focused on analyzing the controllers' behaviour after the jump. Two key aspects are transient performance and lateral stability. The indices are as follows:

- Mean deceleration at jump ($\bar{A}_{jump}$) - Targeted at quantifying the overall deceleration performance during the the friction transitions. The calculation starts $0.2s$ before the front wheels experience the change in friction and ends $1s$ after the rear wheels have performed the jump.

$$\bar{A}_{jump} = \int_{i_{jump}-0.2s}^{f_{jump}+1s} a_x dt \tag{6-9}$$

- Recovery time (T_{rec}) - Quantifies how much time is taken by the controller to recover from the friction jump and go back to steady state conditions. The counter is started when the front wheels first experience the change in surface condition and runs until the longitudinal acceleration is inside a certain acceleration band. The band is identified as $\pm 5\%$ of the mean longitudinal acceleration after the jump.

$$T_{rec} = [t]_{i_{jump}}^{\pm 5\% \bar{A}_x} \tag{6-10}$$

- Peak to peak at jump ($\omega_{peak_{jump}}$) - Again targeted at quantifying the agility of the controller in transient conditions. However, the focus is this time put only on the first control cycle after the friction jump. Generally the first cycle is where most of the potential brake distance is lost, and it is therefore highly important to try minimizing this specific aspect. The metric is of particular interest for lower frictions coefficients where it takes significantly more time, and under-braking, to recover from the unstable part of the $\lambda - F_x$ curve. $\omega_{peak,jump}$ is calculated in the same way as for ω_{peak}. Again the k index in (6-11) ranges from 1 to 2 for the front wheels and from 3 to 4 for the rear ones.

$$\omega_{peak_{jump}} = \sum_k \frac{\omega_{max_k} - \omega_{opt_k}}{\omega_{max_k}} \tag{6-11}$$

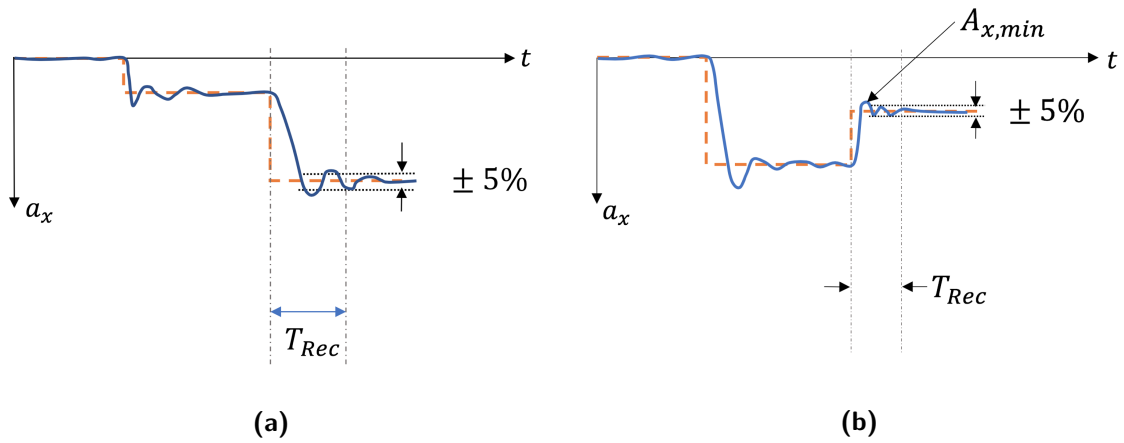

Figure 6-2: KPI illustration for: $\mu-$jump up manoeuvre (a), $\mu-$jump down manoeuvre (b)

- Maximum yaw rate at jump ($\dot{\psi}_{MAX}$) - Aims at quantifying the vehicle stability during the friction jump manoeuvre. It is not uncommon for a vehicle experiencing a sudden change in friction to exhibit some yawing. Yaw angles are usually not high since the wheel pairs undergo the friction transition at the same time. Nonetheless, the velocity at which the vehicle rotate should be contained in order to allow the driver to counter-steer. Although in this work only relative performance of the proposed controller is analyzed, it is worth mentioning that the usual threshold for acceptability is set around a value of $1 - 1.5 deg/s$.

$$\dot{\psi}_{MAX} = max\left[\dot{\psi}\right]_{i_{jump}}^{f_{jump}} \tag{6-12}$$

6-3 Benchmark rule-based logic

The approach Toyota, as well as most the other manufactures, are currently using is based on a large and very well tuned state machine. As mentioned in previous sections, this is due to the fact that to most of nowadays vehicles are equipped with normal hydraulics brakes which do not allow for continuous pressure modulation. The control is then based on a large number of heuristic rules built around experience that trigger the discrete transition from one state to the other. Each state is then associated with one of three fundamental control actions: increase, hold and decrease of pressure. Pressure increase/decrease can be done at different rates.

To obtain a basic idea of how such a control might be working in an ABS framework a good reference is "Brakes, Brake Control and Driver Assistance Systems Function" from Bosch GmbH [10]. In the book two scenarios are presented. The first discusses a high friction manoeuvre, the second a low adhesion one. Both of them will be summarized in the next paragraphs to give an idea on how rule - based ABS controllers work. As it will be seen, different frictions are associated with fundamentally different controller's behaviour. The supervisory logic of

the ECU detects the road conditions and adapts the ABS response characteristics to suit the specific friction coefficient.

- High adhesion braking - If the ABS sequence is activated on a road surface with high friction coefficient, only the wheel acceleration is selected as a control variable. Figure 6-3a shows the first two ABS control cycles on what could be a either wet or dry asphalt road. During the initial (uncontrolled) phase of braking, the wheel deceleration rises as a consequence of the brake pressure being applied by the driver. ABS is triggered once wheel deceleration passes the certain threshold level $-a$, at this stage the controller imposes a "maintain pressure" phase. Pressure is not directly reduced since the threshold $+a$ might sometimes be exceeded within the stable zone of the $\mu - \lambda$ curve and, in that case, some braking distance would be "wasted". As soon as the ABS is activated, a reference wheel tangential speed, v_{Ref}, is clipped and reduced according to a defined linear gradient. The reference speed is used as the basis for determining the slip switching threshold, λ_1.
  Phase 2 ends when the wheel speed v_R drops below a certain λ_1 threshold. At this point, the controller imposes to reduce pressure (phase 3). Pressure keeps decreasing as long as the wheel deceleration is above the threshold $-a$.
  When the threshold is overcome, another pressure-maintenance phase is initiated (phase 4). Pressure is maintained constant only until the wheel acceleration has increased so much that the relatively high threshold, $+A$, is overcome.
  The brake pressure is then increased (phase 5) as long as the acceleration remains above the threshold $+A$.
  In phase 6, the brake pressure is once again held constant since the acceleration is above the threshold (+a) but below $+A$.
  Once the wheel acceleration falls below the threshold $+a$, which is an indication that the wheel has returned to the stable zone of the $\mu - \lambda$ curve, the brake pressure is increased in stairway fashion (phase 7).
  Phase 7 terminates when $\dot{\omega} < -a$, the controller then switches to phase 8 where the brake pressure is then reduced immediately reduced (without a λ_1 signal being generated).
  Phase 8 ends when the wheel acceleration crosses the $-a$ again, at this the state is brought back to phase 3 and the loop 3 to 7 is continued until the end of the braking manoeuvre.

- Low adhesion braking - In contrast with good grip conditions, on a slippery road surface even very light pressures on the brake pedal are frequently enough to make the wheels lock up. Once the wheel is fully locked, it requires a much longer time to emerge from a high-slip phase and accelerate again. As a consequence, slips needs be to kept under closer attention that in the high friction case. Figure 6-3b shows a typical control cycle for road conditions with low levels of adhesion. For phases 1 to 3, the control sequence is the same as for high-adhesion conditions. Phase 4 starts with a short pressure-maintenance phase. When the wheel speed is lower than the slip switching threshold λ_1, the brake pressure is reduced until the wheel acceleration exceeds the threshold $-a$. A further short pressure-maintenance phase follows. Then, once again, the wheel speed is compared to the slip switching threshold λ_1 and, when higher, the pressure is reduced over another period of time. When the wheel acceleration exceeds

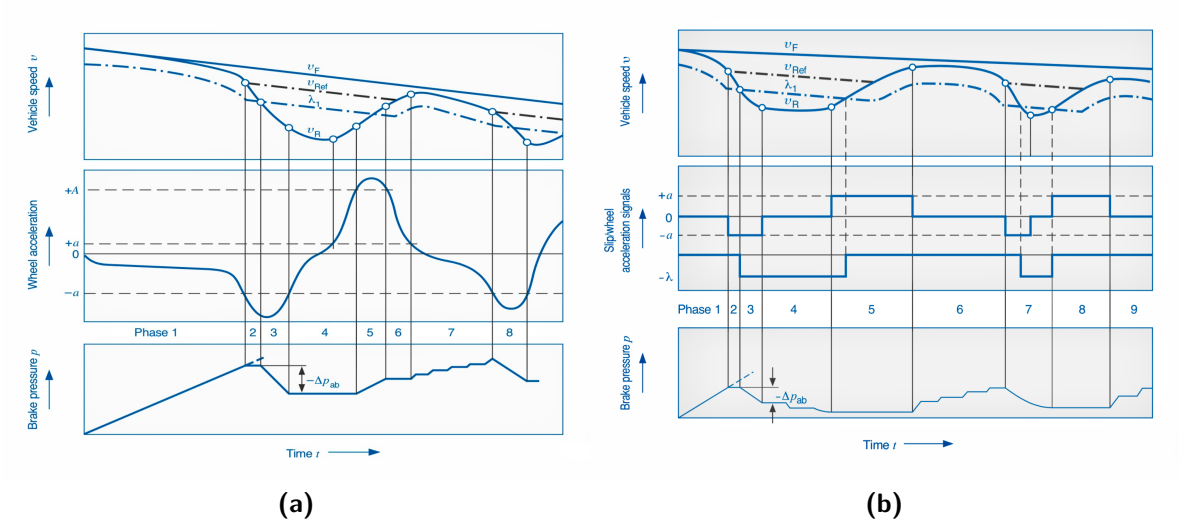

(a) (b)

Figure 6-3: Basic working principle of the benchmark rule based logic for: high-adhesion conditions (a), low-adhesion conditions (b). [10]

the threshold $+a$, another pressure-maintenance phase (phase 5) is initiated which lasts until the acceleration drops below the threshold $+a$ again. In phase 6, the incremental pressure-increase pattern seen in the preceding section takes place again until, in phase 7, triggered by the signal $-a$, pressure is released and a new control cycle starts. The next control cycles incorporate continual comparison of wheel speed with the slip switching threshold λ_1. Because of that continuous pressure release, the wheel retains a high level of slip for only a short period in comparison with the first control cycle. The loop 6-7-8 is then repeated until the end the braking manoeuvre.

The two examples just given, although already quite cumbersome, are a considerable simplification over what actually happens in the real controller. As previously mentioned, the actual state machines found on passenger vehicles end up having hundreds of states and a large variety of switching threshold to be tuned. Performances are surely remarkable but the tuning procedure represent a sizable hustle.

6-4 Results and comparison

After explanation of the various maneuvers and performance metrics, as well as a brief introduction of the benchmarking controller, it is now time to analyze results.

In order to keep the section clean, time history graphs are reported in appendix C and comparison radar charts in the summary at the end of the chapter rather then here. On the other hand, tables containing absolute and relative KPI readings summarizing how the NMPC compares to the current logic are presented in the section. In general, the reader is advised to consult the appendix and summary to get a quick graphical overview. On the other hand, here results are presented in a more analytical way by means of performance metrics only.

The first column in the tables, labeled as RB, concerns the current rule-based logic and reports the KPI absolute values. Column two relates to the absolute performance of the NMPC. The comparison tab reports the relative performance of the NMPC with respect to the rule - based control. Performance losses are marked in brackets while improvements do not present them, meaning *(15%)* indicates a loss in performance of fifteen percentage points and *7%* points out that the proposed controller is seven percent better than the current one. As mentioned earlier, a more graphical representation of how the two controllers compare can be found in Appendix C by means of radar charts.

Time history plots in Appendix C differs slightly between the two controllers due to confidentiality issues. In particular, the graphs related to the proposed controller are composed as follows:

- Brake torques are shown in the subplot 1, $T_{D,fr/rr}$ stands for the driver requested torqued in the front/rear while $T_{C,ij}$ is the torque delivered by the controller;
- Subplot 2 shows a comparison between chassis velocity V_{cha} and linearized wheel velocity $V_{wh,ij}$;
- Subplot 3 compares the achieved chassis longitudinal acceleration A_x to its theoretical maximum $A_{x_{MAX}}$ evaluated from the average friction coefficient;
- Subplots 4 and 6 show the slip distribution histograms for front left and rear right wheel. As all manoeuvres are performed in a straight line, it is safe to assume that wheels on the same axes will behave similarly;
- Front and rear slip time evolution in shown in subplot 5 and compared against their respective references;
- Subplot 7 concerns the angular velocities associated with front and rear wheels. Additionally, ABS activation is also shown;
- Lastly, in subplot 8, computational time is compared with the controller's sampling time.

For the benchmark logic on the other hand, a time history of the slip could not be shared due to confidentiality reasons. Additionally, the computational time would not be of any usage as the two controllers are based of fundamentally different philosophy. In place, the two additional histograms reporting the slip distribution during the simulation are shown. The optimal wheel slip is always between 2% and 10%, nonetheless, its actual value in relation to the manoeuvre can seen from the NMPC plots. However, it was chosen to keep them for the NMPC.

In the following pages results for each of the manoeuvres' groups are shown. Scenario specific comments are made as each result are presented, while more general comments, applicable to the whole group, at the end of each block.

Controller / KPI	RB	NMPC	Comparison
ABSIP - [%]	73.44	67.87	7.58%
Brake distance - $[m]$	87.11	80.51	7.58%
MFDD - $[m/s^2]$	7.92	8.47	6.49%
Peak to peak front - [%]	12.96	5.62	56.64%
Peak to peak rear - [%]	9.18	4.22	53.03%
η_{ABS} - [%]	87.9	96,2	8.63%
ITAE Jerk - $[\frac{m}{s^2}]$	111.1	89.9	$19,01\%$
$\dot{\phi}$ variation - $[\frac{deg}{s}]$	4.53	4,18	7.73%
IACA - $[\frac{Nm}{s}]$	7625	6921	9.23%

Table 6-2: Braking on smooth dry asphalt - 130-0 [km/h]

Braking on smooth road

In this subsection results obtained by testing the two controller on smooth, homogeneous friction surface are analyzed and discussed.

Dry asphalt - Results concerning the 130-0 km/h braking on high friction are shown in Table 6-2. As can be seen, an improvement is found for each of the indices. Before diving into the analysis, it is worth noticing how much the presence of ABS control can improve braking ability. Specifically, brake distance is reduced by more than 30% by the Nonlinear Model Predictive Control. The proposed controller allows the test vehicle traveling at 130 km/h to stop in only 67.87 m, which would mean a reduction of 5.57 m over the current control logic. Most of the advantage comes from the fact that the NMPC manages to stay much closer to the theoretical maximum feasible deceleration or precisely 96.2% of the available friction coefficient is exploited by the proposed control strategy. The rest is due to the improved initial transient, which by means of the *Peak to peak* metrics, is estimated to be in excess of 50% better. Lastly, jerk characteristics and consequent repetitive vehicle pitching are also improved by around 20% and 8% respectively, while the torque torque variation presents a reduction of about 9%.

Wet asphalt - In wet asphalt conditions, the NMPC is again outperforming the current controller in each of the selected fields. Improvement margins concerning steady-state braking are up by 50% compared to those on dry asphalt. As can be seen clearly by looking at the absolute η_{ABS} value, the effect is mostly due to the performance deterioration of the rule - based control rather than an improvement by the proposed controller. Nonetheless, the NMPC seems to behave slightly better in lower adhesion surface, about one percentage point gain is observed. Likewise concerning first cycle performance, the current logic degrades substantially particularly for the front wheels, while the proposed controller presents a minor

KPI \ Controller	RB	NMPC	Comparison
ABSIP - [%]	78.21	66.32	15.20%
Brake distance - $[m]$	54.29	46.04	15.20%
MFDD - $[m/s^2]$	5.67	6.74	15.88%
Peak to peak front - [%]	56.33	4.71	91.64%
Peak to peak rear - [%]	10.00	3,14	68.60%
η_{ABS} - [%]	81.9	97.2	15.74%
ITAE Jerk - $[\frac{m}{s^2}]$	99.99	30.21	69.79%
$\dot{\phi}$ variation - $[\frac{deg}{s}]$	5.64	4.32	21.45%
IACA - $[\frac{Nm}{s}]$	5878	5078	13.61%

Table 6-3: Braking on smooth wet asphalt - 90-0 [km/h]

improvement. The $ITAE_{J_x}$ related index is also largely improved, which is especially good as with a lower steady state deceleration jerkiness is much more perceivable. Lastly, pitch rate behaviour is improved by an excess of 21% and actuators are, in preliminary analysis, about 13% less stressed.

Packed snow - Despite the fact that tire used in the simulations is not meant to be used regularly on snow, some interesting findings can be achieved by analyzing the behaviour of the two controllers in this manoeuvre. By referring to Figure 5-1a, it can be noticed that as the friction coefficient decreases not only the peak shifts to lower slip ranges but also the curve gains a sharper shape. These two factors clearly mean that a controller that is not as precise will struggle more, as similar slip errors will now result in more under-/over- braking. The intuition is confirmed by Table 6-4. Steady state performance indicators related to the proposed are now about 25% higher than the benchmark. The NMPC manages to use 94% of the available friction compared to 71% of the rule - based controller, reducing the brake distance by roughly $7.5m$. Looking at the slip distributions for the two controllers in Figure **??** and Figure B-3, it is apparent how the NMPC does a much better job at keeping the slip close to the optimal point than the current RB control, which on average stays in correct bin roughly 25% of the time. Additionally, while the current logic is extremely close to locking the front wheels when the brakes are applied, the model predictive controller shows little to none overshoot as pointed out by the peak to peak indicator. Jerk and pitch rate metrics are improved by approximately 65% and the IACA is down to 29% less.

Summarizing what just seen, it is evident from the comparison column of the three tables just presented, that separation between controller performances increases as the friction coefficient goes down. This is to be attributed to three main factors: the increasing instability of the wheel dynamics as the friction conditions deteriorates; the longer time and under-braking

Controller / KPI	RB	NMPC	Comparison
ABSIP - [%]	84.00	61.38	26.93%
Brake distance - $[m]$	27.87	20.30	27.16%
MFDD - $[m/s^2]$	2.06	2.77	25.63%
Peak to peak front - [%]	90.96	0.02	99.98%
Peak to peak rear - [%]	34.57	0.02	99.94%
η_{ABS} - [%]	71.0	94.1	24.55%
ITAE Jerk - $[\frac{m}{s^2}]$	49.46	17,42	64.78%
$\dot{\phi}$ variation - $[\frac{deg}{s}]$	3.99	1.28	67.92%
IACA - $[\frac{Nm}{s}]$	3117	2213	29.00%

Table 6-4: Braking on smooth snow - 40-0 [km/h]

needed to the recover from unstable conditions; the lower initial speeds which cause the first cycle to happen in more unstable conditions. All of this effects mean that NMPC, being a smoother and more precise controller, is much more likely to outperform its rule - based counterpart in lower grip conditions.

Although the NMPC is outperforming the current logic generally everywhere, its main advantage is in the absence of first cycle overshoot, as particularly evident from the *Peak to peak indicators*.

Additionally, despite steady state related metrics being smaller than those targeted at transient behaviour, considering that in homogeneous friction conditions a much larger portion of the braking manoeuvre is spend in stationary conditions and hence even fewer percentage points correspond to remarkable improvements.

Jerk and pitch related indices also indicate a substantial gain. Although usually perceived as of secondary importance, human factors aspects are extremely relevant for automakers. Customers in fact would not be able to feel the benefit of a better tracking but surely will react to a smoother, safer-feeling, braking action.

Moreover, a possible concern point could have been related to actuator wear since the controller was tuned to be very reactive to slip errors but, as can be appreciated from the *IACA*, the metric is always below that of the benchmark controller.

The last item worth mentioning is related to real-time capabilities. Although, that concerning computational time is not a accurate analysis, it functions well in discovering possible issues. As can be noticed in any of the plots reported in C, when the controller behaves as a brake torque request follower, the real-time boundary is exceeded by the optimizer. After investigation of the optimization solver output, it was seen that many solutions are discarded because they do not satisfy the maximum actuator torque constraint. Since the driver request torque

is never exceeding the actuator capabilities, the constraint was removed to see if that would have fixed the issue. Not surprisingly, the problem was temporarily removed; however, this cannot be regarded as a permanent and an alternative solution is to be found. Lowering the weights associated with the torque target might be a solution to the problem; equally setting the optimally tolerance less tight could also be an alternative solution. In any case, given the problem is restricted to specific conditions and the controller is not running on dedicated hardware, it was chosen to leave it.

Braking on variable friction coefficient

Anti-lock Braking System (ABS) transient behaviour is analyzed in this subsection. As seen earlier, metrics focus only on how the controller reacts to the friction transition and consequent wheel and vehicle behaviour.

Dry to wet asphalt - Given the transient performances seen in the previous section, it is to be expected to find a similar situation is to be expected here. Nonetheless, it is both important to check this is the case as well as quantify the difference between the transient condition being right at the beginning of the braking manoeuvre or after the modulation is already happening. For this scenario a sightly "better" dry tarmac as well as a "worse" wet one than for group one since homologation rules by the UNECE Transport Division, prescribe friction jumps with minimum 0.5 friction coefficient difference between the two surfaces. As can be appreciated by the graphs in Figure B-4, the deceleration peak in the dry part of the manoeuvre for the NMPC controller is high enough to almost lift the rear wheels off the ground. AS the assessment in solely focused on the jump though, this does not constitute a problem. Observing the value of the minimum longitudinal deceleration for the proposed controller, which is an excess of 40% higher than the benchmark, it is clear deciding the control action based on optimization of a certain future time window ensures much less under-braking as a reaction to the jump in friction. Similarly, when attention is laid only on the first control cycle after the jump the advantage is seen again with *peak to peak* indicators being respectively 78% and 50% lower. Exciting the system less with torque variations also ensures a much shorter transition time, here about 38% shorter. Lastly, as motioned earlier, an effect to keep under control regardless of the longitudinal transition performance is the maximum yaw rate. In this case the NMPC ensures 50% more yawing stability than its rule - based equivalent.

Wet asphalt to packed snow - In this scenario again the friction coefficient are slightly changed to achieve a jump conform to what mandated by homologation rules. Similarly to what seen on homogeneous friction scenarios, relative performance difference spreads as the average friction coefficient goes down. The minimum recorded acceleration is now 2 m/s^2 lower for the RB control. *Peak to peak* difference is recorded at 85 and 65 percentage points for the front and rear respectively. On the other hand, steady state performance degradation is contained to only one percentage point more than in the previous case. Nonetheless, recovery time is identified to be 80% better. The cause of this difference is to be found in how the recovery time is identified. In fact, the counter is stopped only when the longitudinal acceleration signal does not exit the tolerance band anymore, despite the average value of the signal itself. Maximum yaw rate for the predictive controller is again well within the corresponding rule base value.

Controller / KPI	RB	NMPC	Comparison
$A_{x_{min}}@jump$ - $[m/s^2]$	2.52	4.38	42.47%
$T_{recovery}$ - $[ms]$	580	360	37.93%
$\bar{A}_x$ - $[m/s^2]$	4.07	5.88	30.78%
Peak to peak front - [%]	66.60	14.67	77.97%
Peak to peak rear - [%]	26.77	13.35	50.13%
$\dot{\psi}_{MAX}$ - $[deg/s]$	1.83	0.93	49.18%

Table 6-5: High speed $\mu-$jump (dry to wet asphalt)

Controller / KPI	RB	NMPC	Comparison
$A_{x_{min}}@jump$ - $[m/s^2]$	1.17	3.17	63.10%
$T_{recovery}$ - $[ms]$	480	100	79.17%
$\bar{A}_x$ - $[m/s^2]$	2.71	3.97	31.74%
Peak to peak front - [%]	81.17	12.36	84.77%
Peak to peak rear - [%]	28.69	9.87	65.60%
$\dot{\psi}_{MAX}$ - $[deg/s]$	1.12	0.39	65.18%

Table 6-6: Low speed $\mu-$jump (wet asphalt to packed snow)

KPI \ Controller	RB	NMPC	Comparison
$T_{recovery}$ - $[ms]$	550	300	45.45%
$\bar{A}_x$ - $[m/s^2]$	6.80	8.80	22.73%
Peak to peak front - [%]	12.94	4.43	65.77%
Peak to peak rear - [%]	12.78	3.07	75.98%
$\dot{\psi}_{MAX}$ - $[deg/s]$	1.65	0.36	78.18%

Table 6-7: $\mu-$jump (packed snow to dry asphalt)

Packed snow to dry asphalt - When moving to the μ-jump up transition, the minimum recorded deceleration is dropped as an indicator for obvious reasons. General trends found with the previous two manoeuvres are kept, but gains are slightly reduced. By looking at Figure **??** and B-6, the phenomenon is explicable by a better performance of the rule - based control rather than a loss from the NMPC. Recovery time of the proposed controller is measured at 300 ms, 45% better than the benchmark. Mean deceleration improves by around 23%. It is worth noticing that for the first time *peak to peak* comparison in the front is less favourable than in the rear, respectively 65% and 76%. Finally, the maximum yaw rate is again considerably lower for the proposed control strategy.

Overall, the Nonlinear Model Predictive Control proved to be superior to the rule - based logic on each of the simulated manoeuvres. The main takeaway is that robustness to friction transitions is verified. No strange behaviour or divergence with respect to the reference was found. This is the result of the optimal control problem remaining feasible throughout the friction transition.

The main problem related to friction jumps not yet discussed, can be clearly seen in Figure B-4, B-5 and B-6. As a result from the optimizer hitting the constraint while looking for an optimal solution, in the first few milliseconds after the front wheels enter the new friction surface the real time threshold is exceeded. The problem is analogous to what seen when the controller functions as a driver request follower and similar fixes could be tried to solve the issue. Moreover, it was observed that solutions very similar to the inputs later applied are outputted by the optimizer within the 5 ms. Intuition therefore suggests that, by playing with the termination tolerance, the problem could be solved.

Braking on rough roads

The main objective of this section is to check if performance is retained when high amount of noise are injected in the system by the road profile. Absolute controller performance degradation is assessed by simulating the controller twice, once on the rough surface and once on an equivalent scenario but for the absence of vertical wheel excitation. Performance

Controller / KPI	RB	NMPC	Comparison
Brake distance - [%]	-8.82	-3.04	65.53
η_{ABS} - [%]	-5.83	-3.84	34.13
Peak to peak front - [%]	-46.59	-16.32	64.97
Peak to peak rear - [%]	-24.15	-32.01	(24.55)
ITAE Jerk - [%]	-15.73	-61.93	(74.60)
IACA - [%]	-32.52	60.90	(46.60)

Table 6-8: Braking on rough roads - red bricks

metrics for the two are then compared by applying a selection of performance indicator used in the smooth road sections and checking how much these deteriorate. IPV was left out since the measurement was too affected by the road profile and a comparison with an equivalent sooth road would have been unfair. Similarly, the $MFDD$ was removed from the list because redundant with the η_{ABS} when results are expressed in percentage points.
The reduction in performance of the two controller are then compared. Again, the NMPC is kept as a reference and a spreadsheet-like convention is used: whenever the performance deterioration is higher than that of the benchmark the difference between the two is displayed in brackets; in the opposite situation instead, the difference is reported without.

Red bricks road - KPI for the ABS braking manoeuvre performed on dry red bricks road are shown in Table 6-8. As can be noticed by looking at the first two columns of the table, the expected performance degradation is indeed present. All of the metrics, in fact, have a negative sign indicating the deceleration performed on the equivalent smooth road shows a favourable behaviour.
Moreover, it is noticed how, despite the transient indicators being significantly worse, only a marginal loss is seen in those characterizing the full braking for both controllers. Switching to the comparison column, a mixed behaviour is detected: the proposed controller degrades less then the benchmark during the overall braking; however, the jerk, as well as the amount of torque change prescribed is significantly more. The explanation for this should be sought in the increased prediction model mismatch caused by the variability of the road profile. The controller tuning, still the same as for the previously seen scenarios, is perhaps a touch too aggressive and overreacts to the high frequency slip changes caused by the tire normal load variation. Since overall braking performance is still satisfactory, the tuning was not changed, yet, in case comfort or actuator wear would be found to be an issue by targeted investigation aggressiveness of the controller should be reduced.

Belgian cobblestones - Belgian cobblestones are much rougher than red brick, in addition, while on red bricks the $z-$ coordinate had a semi-sinusoidal character due to the bricks layout, on cobblestones the excitation is significantly more random. Lastly, the specific surface used for this test is quite old and presents some macroscopic bumps.
Despite the increased roughness, trends identified on red bricks are kept. Overall braking

Controller / KPI	RB	NMPC	Comparison
Brake distance - [%]	-6.71	-4.98	25.78
η_{ABS} - [%]	-2.50	-2.10	16.03
Peak to peak front - [%]	-10.72	-6.34	40.85
Peak to peak rear - [%]	-15.04	-7.85	47.81
ITAE Jerk - [%]	-24.38	-57.79	(57.81)
IACA - [%]	-36.11	73.29	(50.72)

Table 6-9: Braking on rough roads - Belgian cobblestones

performance deterioration for the NMPC is still within 5%. In spite of that, considerably higher torque fluctuations are needed to achieve it. Jerk performance is also notably affected; however, one could argue the difference is of minor as the ride is already quite rough.
When compared to the benchmark, degradation margins are similar with a slight advantage of the proposed controller except for the already discussed jerk and actuator wear possible issues.

All in all possible concerns related to model mismatch caused by system variability and noise were well addressed by simulation on rough roads. Deceleration-wise degradation is within the target identified by the benchmark controller. As the *IACA* of proposed controller was well of that of the benchmark, the need for some more investigation about the amount of allowable torque rate was uncovered. *Peak to peak* indicators also showed some degrading, however their absolute value is normally so small that in absolute terms this does not constitute any real issue.

6-5 Summary

Chapter 5 treats the assessment of the proposed for controller full vehicle by means techniques of simulation. A set of 8 braking scenario is identified and explained. 3 macro-groups are distinguished: braking performed on smooth roads and homogeneous friction coefficient; braking on friction transient conditions (μ-jumps); Braking of laser-scanned rough roads.

A set of KPI is identified for each of the 3 groups. The key elements being analyzed are: steady state performance, transient behaviour, comfort, actuator wear and lateral stability. Apart from absolute performances, the NMPC is also compared with the current industrial state of the art. The way this works is briefly explained by analyzing its control actions and how these are chosen in response to a specific friction coefficient. Lastly, both absolute and relative results are presented. A quick graphical recap of the relative performance between the NMPC and RB controllers on the previously mentioned manoeuvres in shown below.

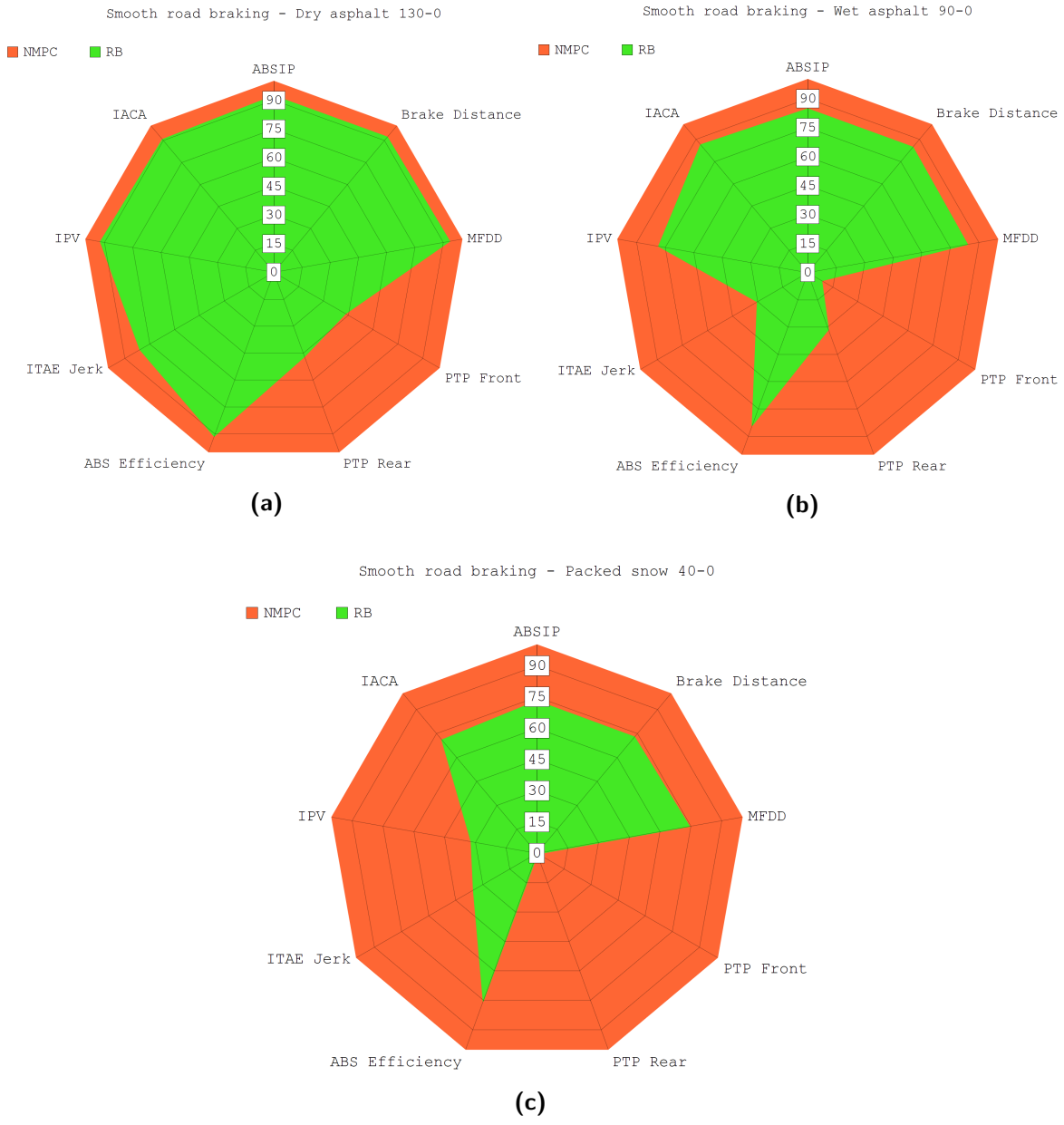

Figure 6-4: Relative performance radar plots scenarios on smooth roads. Dry asphalt (a), Wet asphalt (b), Packed snow (c)

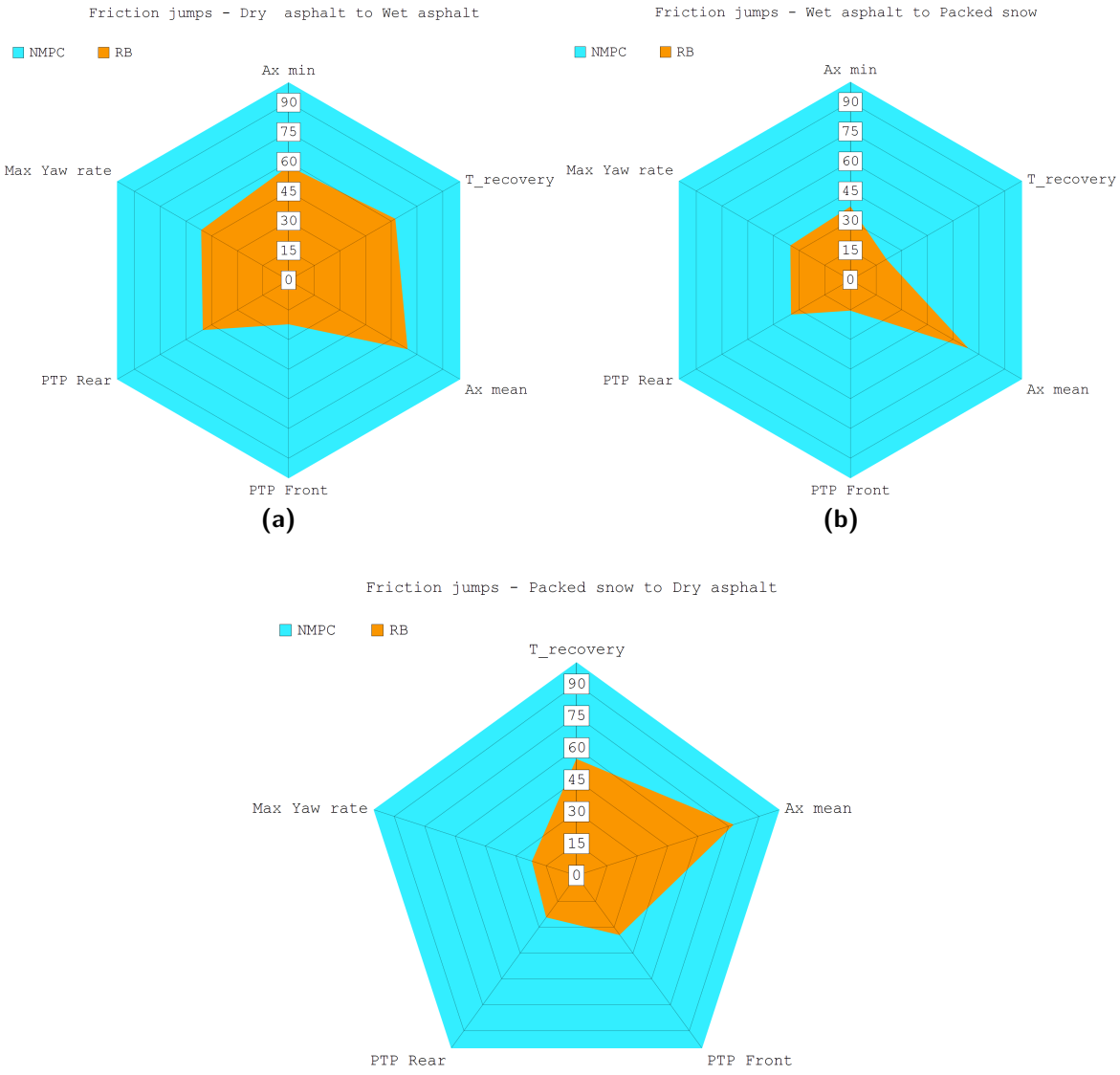

Figure 6-5: Relative performance radar plots for friction jumps scenarios.
Dry asphalt - Wet asphalt (a), Wet asphalt - Packed snow (b), Packed snow - Dry asphalt (c)

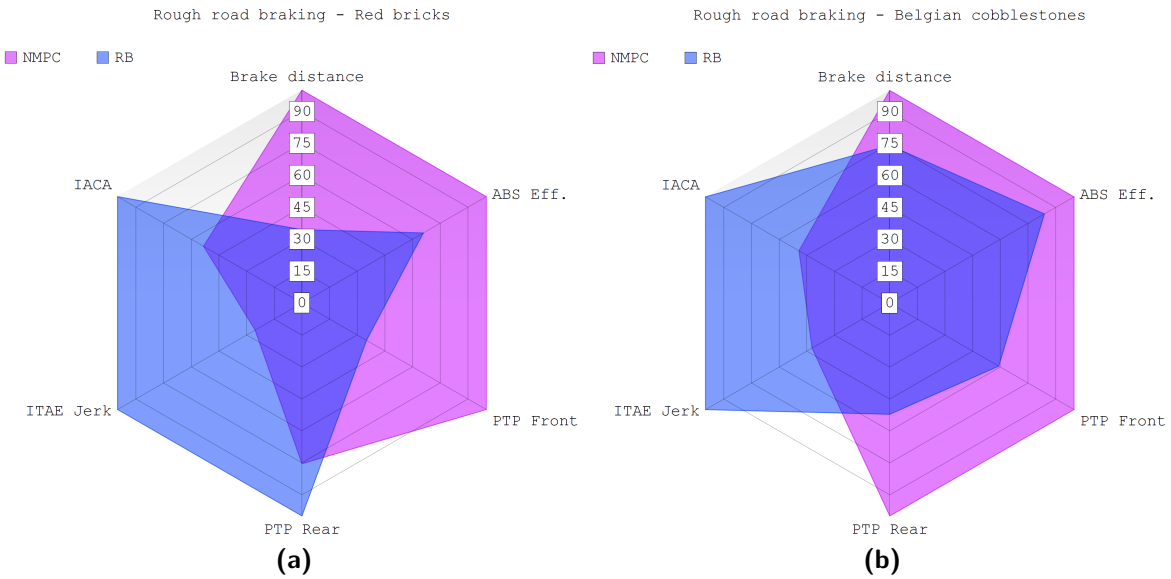

Figure 6-6: Relative performance radar plots for scenarios on rough roads. Red bricks (a), Belgian cobblestones (b)

Chapter 7

Conclusions and recommendations

7-1 Summary and conclusions

This thesis presents the design of a novel ABS algorithm based on nonlinear model predictive control. The model in the loop consists of 9 differential equations: four equations describe the rotational dynamic of each wheel in the $y-$direction; an additional four augmentation equations allow for controlling the torque rate instead of the brake torque; lastly one equation describes the chassis longitudinal dynamics. Effects related to brake actuator dynamics and longitudinal weight transfer are also taken into account. Lastly, online feed of wheel force data allows complete description of the tire dynamics.

All other subsystems necessary for the core nonlinear MPC were also developed. These include: an activation and supervisory rule-based logic, a reference state generator, and an online weight scheduler.
The supervisory logic is responsible for cycling through three possible controller states: ABS Off, ABS On, ABS On Low Speed. Whenever the ABS is inactive the NMPC acts as a driver brake torque request follower. Activation of the ABS controller is triggered based on some predefined wheel deceleration thresholds for front and rear wheel pairs. In a rage from $1m/s$ to maximum vehicle speed, the ABS operates as a slip target follower in its normal (high speed) mode. On the other hand, below $1m/s$, where the wheel dynamics is too unstable to control, the brake torque is kept constant to avoid any possible under-braking. The reference state generator sets the reference for the NMPC to follow based on the current controller mode as well as the estimated friction conditions and normal tire load.

Lastly, the weight scheduler implements the specific controller mode by means of cost function weights shifting. On top of that, in ABS On mode it also makes sure slip gains are adjusted according to the velocity the vehicle is currently at.

The controller is tested in an high-end simulation environment consisting of accurate modelling of the vehicle itself as well as its subsystems related to ABS. The vehicle is replicated by a multibody vehicle model enhanced with kinematics and compliance measurements. The vehicle model is the same Toyota uses for its usual MBD activities and its well validated

against experiments. A complex multiphysics model replicating the brake system non-linear behaviour is co-simulated in parallel to the vehicle model. Moreover, the rigid ring short wavelength tire model is employed to accurately reproduce tire behaviour when excited at high frequency. Lastly, sensor noise is taken into account by superimposing a with Gaussian noise coherent with the sensors' data-sheet to the signals coming from the vehicle.

To assess the proposed controller and identify the performance margins with respect to current industrial state of the art solutions, the nonlinear model predictive controller is benchmarked against a RB logic provided by Toyota.
The two controllers are then simulated on eight scenarios spanning different friction coefficients. In addition to common smooth road braking manoeuvres, this work also simulates friction transitions and rough roads. Friction transitions follow the homologation rules mandated by the transport division of the United Nations Economic Commission for Europe (UNECE). Rough pavements are existing laser-scanned road sections, replicated in simulation with CRG format. Since the control blackbox contained a series of other assistance systems together with ABS (i.e. ESC, EBD, AEB) simulation scenarios are only concerned with longitudinal dynamics. In other words, the driver model reference trajectory is always a straight line in the middle of the road; however, in case some yaw is caused by the controller doings, the driver model will countersteer as non-professional driver would do.

A comprehensive set of indicators specific to the manoeuvre type was also developed to accurately quantify the differences the two controllers and be able to clearly understand where the performance delta originates from. Some of the KPIs used are also targeted at evaluating robustness, human factors, as well as actuator wear.

The analysis showed that the proposed logic outperforms the current rule - based control on every manoeuvre. The improvements are mainly due to a much smoother and precise control action which destabilizes the wheel dynamics much less than the current logic does with its repeated control cycles (increase, decrease, and hold pressure). On the other hand, the NMPC modulates the brake torque continuously. Transient behaviour was found to be significantly improved thanks the optimization of future time steps performed by the controller based on the prediction model. On average the first ABS control cycle was found to be $\sim 75\%$ better than for the benchmark controller. Similarly, following a jump in the friction coefficient value, the NMPC was shown to be approximately 50% faster to recover from the friction jump. To a smaller extent, steady state tracking also improved by an average of 15%. Again, thanks to smoother and more precise control action, the velocity at which the controller needed to be switched to low speed mode was reduced by approximately 50%. Comfort levels and actuator abuse is reduced as well.

Regarding robustness aspects, no issues were ever found with the NMPC optimization problem failing to find a solution. Moreover, the proposed control strategy proved to recover friction jumps faster than the benchmark and with significantly lower vehicle jerk and yaw rate. The nonlinear model predictive controller showed lower performance degradation levels related to noise injection by the road profile. Minor real time concerns where highlighted at the beginning of the braking manoeuvre as well as for the first few milliseconds after a friction jump occurred. Their possible causes were discussed; however, considering the controller was not run on dedicated hardware but rather on a workstation together with the simulation of the vehicle and its subsystems, it was decided to leave this point open for future investigations.
Lastly, it is worth recalling that the NMPC comes with a considerably lower number of tuning

parameter (roughly two order of magnitude lower than the equivalent rule - based logic).

In conclusion, this research proved an application of a nonlinear model predictive approach in the field of anti-lock braking control to be extremely promising, and motivates future research targeted at clarifying all those points that still remain open. Despite the extent of this work, the conclusions drawn are applicable only to pure longitudinal dynamics context, nonetheless the use of wheel force information in the prediction model, as well are the model based approach itself, undoubtedly simplifies the extension of the controller and its results to a more general context.

7-2 Recommendation and future work

During the time span of this research multiple issues were faced and much learning was done. Despite the vast majority of the gained knowledge being applied as the work progressed, one aspect could have been improved if budget and time were no issue, is tire behaviour accuracy. As most of the simulations performed by automotive OEMs is concerned with lateral dynamics, much effort is spent in parameterizing the tire to an extent that is satisfactory for accurate simulation of lateral manoeuvres. Unfortunately though, when dealing with longitudinal slip dynamics, frequencies are a lot higher. Tire models able to accurately replicate this behaviour do exist and were actually used in this work. Nonetheless the number, and therefore cost, of the bench tests that are needed to properly populate the tire property file for the scope is very high and most of the time for pilot studies like this the budget is insufficient to do them all.
It is presumed that improved absolute results could be obtained if the tire was better parameterized, similarly though, it is believed relative results would not differ too much. To conclude on the point, it is important to understand the fundamental role of the tire model and tire property file in ABS simulation.

In addition to the just mentioned improvement that could be implemented in this research if circumstances allowed, as series of next steps should be taken to further investigate and develop the proposed Nonlinear Model Predictive Controller. The list can be divided in three major categories: functional implementation of new features and capabilities, testing of the controller, improvement and assessment of coupling robustness. Specifically:

- Functional implementation

    1. Extension to μ-split capabilities - The proposed controller is not capable of coping with conditions where different friction coefficients are present on the same axle. Due to the model based nature of the controller, together with the use of wheel force information, this is fairly straight forward to do. The prediction model front slip and longitudinal chassis dynamics equations should be modified to account for the effect of tire lateral forces being projected in the longitudinal direction when steering angles are considerable. In addition, a further equation should be added to the model to the describe the yaw behaviour of the chassis. Lastly, constraints and a target state for the yaw rate could be implemented to make sure stability is maintained during μ-split manoeuvres;

2. Implementation of brake torque target converter - As of now, the ABS NMPC prescribes a target torque then passed through a first order transfer function replicating the dynamics of the electro-hydrulic brakes. In reality though, those systems work with a target pressure rather than a target torque. A conversion block should therefore be implemented such that the torque requested to the controller is translated into a pressure requests that takes into account pad-disc friction coefficient variation;
3. Inclusion of additional safety measures - Additional consistency checks would be necessary before the controller is tested/deployed on a real vehicle. Being a critical safety system the ABS controller needs to be made fault-safe in case sensor provide a wrong information or stop reading the necessary signal. A possible way to achieve the necessary safety is by information redundancy and simplified controller running in parallel.

- Coupling robustness

1. Coupling with velocity estimator - Since the proposed controller is essentially slip based, coupling with a velocity estimator is a key element to be investigated. Despite the strong dependency of the controller on the velocity estimator, the two systems are fundamentally separated and any formulation of the estimator could be used. Coupling robustness verification could luckily be mostly done in simulation with little effort.
2. Effective radius estimation - The prediction model contains many parameters that need to be set appropriately, nonetheless, after investigation the system was found to be very robust to all parameter change except for the effective rolling radius. The slip equation in fact has a very strong dependency from it and excessive mismatch between the value the prediction model is using and the actual one leads to severe performance degradation. Fortunately, the controller is not significantly affected by small changes in its value, meaning a simple estimator updating the parameter each time the first few meters of a drive are completed is more than enough to fix the issue.

- Testing

1. Real time implementation for estimation of CPU requirements - Undoubtedly the first test needed to assess the controller's feasibility is the implementation on dedicated hardware (i.e. dSPACE). The presented simulation scenarios could then be run again with the compiled controller in the loop to clearly identify necessary hardware requirement, and eventual software modifications, to guarantee real time capabilities.
2. Hardware in the loop testing - A further necessary test towards the complete assessment and feasibility study is hardware in the loop testing. Specifically, the electro-hydraulic brake transfer function should be replaced by the real system and controller functionality verified again with the vehicle model running in parallel on host PC.
3. Field testing with load sensing bearings - After completion of the above mentioned points the NMPC anti-lock braking control would be ready to be deployed on

a prototype vehicle for the final verification. This would also be the first time the system is mated to one of its core design elements, the online feed of wheel force measurements by load sensing bearings (or any equivalent technology able to provide force information). The successful completion of the field tests would enshrine the end of the first prototypical phase for the system and this research work itself.

Appendix A

Condensing

The condensing of an optimal control problem has first been introduced by H.G. Bock. and K.J. Plitt [57] and has been used in the `qpOASES` solver [58] which is the quadratic program solver used in this work. This section summarizes the main working principle and serves as a backup for the explanation of the cause of the infeasibility. Let the discretized linear open-loop optimal control problem be presented in the following form:

$$\min_{\substack{x_{k_0},\ldots,x_{k_0+N_P} \\ x_{k_0},\ldots,x_{k_0+N_P} \\ x_{k_0},\ldots,x_{k_0+N_P}}} \frac{1}{2} \sum_{k=k_0}^{k_0+N_p-1} (y_k - y_{\text{ref}})' Q (y_k - y_{\text{ref}}) + (u_k - u_{\text{ref}})' R (u_k - u_{\text{ref}}) + \frac{1}{2}(y_{k+N_P} - y_{\text{ref}})' P (y_{k+N_P} - y_{\text{ref}}) \tag{A-1a}$$

subject to

$$x_{k_0} = \widetilde{x}_0 \tag{A-1b}$$
$$x_{k+1} = A x_k + B_{u_k} \tag{A-1c}$$
$$y_k = C x_k \tag{A-1d}$$
$$l \leq M y_k + N u_k \tag{A-1e}$$

The transformation of the parametric quadratic optimal control problem of A-1, to an OCP of a much smaller scale is called condensing. The evolution of states for the Np prediction steps can be expressed by evolving A-1d over all N_p steps. This then looks as follows:

$$x_{k+1} = Ax_k + B_{u_k} \tag{A-2a}$$
$$x_{k+2} = Ax_{k+1} + B_{u_{k+1}} = A^2x_k + AB_{u_k} + B_{u_{k+1}} \tag{A-2b}$$
$$\vdots$$
$$x_{k+N_p} = A^{N_p}x_k + \sum_{i=0}^{N_p-1} A^{N_p-1-i}B_{u_k} \tag{A-2c}$$

From A-2 a structure becomes visible. This structure can be summarized in the following augmented quantities:

$$\widetilde{x} \overset{\text{def}}{=} \begin{bmatrix} x_k \\ x_{k+1} \\ \vdots \\ x_{k+N_p} \end{bmatrix}, \qquad \widetilde{u} \overset{\text{def}}{=} \begin{bmatrix} u_k \\ u_{k+1} \\ \vdots \\ u_{k+N_p-1} \end{bmatrix},$$

$$\widetilde{Q} \overset{\text{def}}{=} \begin{bmatrix} Q & & & & \\ & Q & & & \\ & & \ddots & & \\ & & & Q & \\ & & & & P \end{bmatrix}, \qquad \widetilde{R} \overset{\text{def}}{=} \begin{bmatrix} R & & & \\ & R & & \\ & & \ddots & \\ & & & R \end{bmatrix},$$

$$\widetilde{A} \overset{\text{def}}{=} \begin{bmatrix} I \\ A \\ A^2 \\ \vdots \\ A^{N_p} \end{bmatrix} \qquad \widetilde{B} \overset{\text{def}}{=} \begin{bmatrix} 0 & & & \\ B & & & \\ AB & B & & \\ \vdots & \ddots & \ddots & \\ A^{N_p-1}B & \dots & AB & B \end{bmatrix},$$

,

$$\widetilde{M} \overset{\text{def}}{=} \begin{bmatrix} M & & & 0 \\ & M & & 0 \\ & & \ddots & \dots \\ & & M & 0 \end{bmatrix}, \qquad \widetilde{N} \overset{\text{def}}{=} \begin{bmatrix} N & & & \\ & N & & \\ & & \ddots & \\ & & & N \end{bmatrix}, \qquad \widetilde{l} \overset{\text{def}}{=} \begin{bmatrix} l \\ l \\ \dots \\ l \end{bmatrix}$$

Which are of the following dimensions: $\widetilde{x} \in \mathbb{R}^{(N_p+1)\cdot n_x}$, $\widetilde{u} \in \mathbb{R}^{N_p \cdot n_x}$, $\widetilde{Q} \in \mathbb{R}^{(N_p+1)\cdot n_x \times (N_p+1)\cdot n_x}$, $\widetilde{R} \in \mathbb{R}^{N_p \cdot n_c \times N_p \cdot n_u}$, $\widetilde{A} \in \mathbb{R}^{(N_p+1)\cdot n_x \times n_x}$, $\widetilde{B} \in \mathbb{R}^{(N_p+1)\cdot n_x \times N_p \cdot n_u}$, $\widetilde{M} \in \mathbb{R}^{N_p \cdot n_c \times (N_p+1)\cdot n_x}$, $\widetilde{N} \in \mathbb{R}^{N_p \cdot n_c \times N_p \cdot n_u}$, $\widetilde{l} \in \mathbb{R}^{N_p \cdot n_c}$. Using these augmented quantities, the linear parametric Quadratic Problem can be reformulated to the following form:

$$\min_{\tilde{u}} \frac{1}{2}\tilde{u}'\tilde{H}\tilde{u} + \tilde{u}' \underbrace{\tilde{F}\tilde{x}_0}_{\text{g}} \tag{A-3a}$$

$$\text{subject to} \quad \tilde{G}\tilde{u} \leq \underbrace{\tilde{l} - \tilde{E}\tilde{x}_0}_{\text{w}} \tag{A-3b}$$

In which $\widetilde{H} \overset{\text{def}}{=} \widetilde{B}'\widetilde{Q}\widetilde{B}+\widetilde{R} \in \mathbb{R}^{N_p \cdot n_u N_p \cdot n_u}$, $\widetilde{F} \overset{\text{def}}{=} \widetilde{B}'\widetilde{Q}\widetilde{A} \in \mathbb{R}^{N_p \cdot n_u n_x}$, $\widetilde{G} \overset{\text{def}}{=} \widetilde{M}\widetilde{B}+\widetilde{N} \in \mathbb{R}^{N_p \cdot n_c N_p \cdot n_u}$, $\widetilde{E} \overset{\text{def}}{=} \widetilde{M}\widetilde{A} \in \mathbb{R}^{N_p \cdot n_c N_x}$. The problem as described by A-3 is then called the condensed form of the original QP problem of A-1.

Appendix B

NMPC results

In this appendix time history charts for the NMPC ABS controller are presented. The following eight manoeuvres are shown:

1. Braking on smooth roads - Dry asphalt
2. Braking on smooth roads - Wet asphalt
3. Braking on smooth roads - Packed snow
4. Friction transitions - Dry asphalt to wet asphalt
5. Friction transitions - Wet asphalt to packed snow
6. Friction transitions - Packed snow to dry asphalt
7. Braking on rough roads - Red bricks
8. Braking on rough roads - Belgian cobblestones

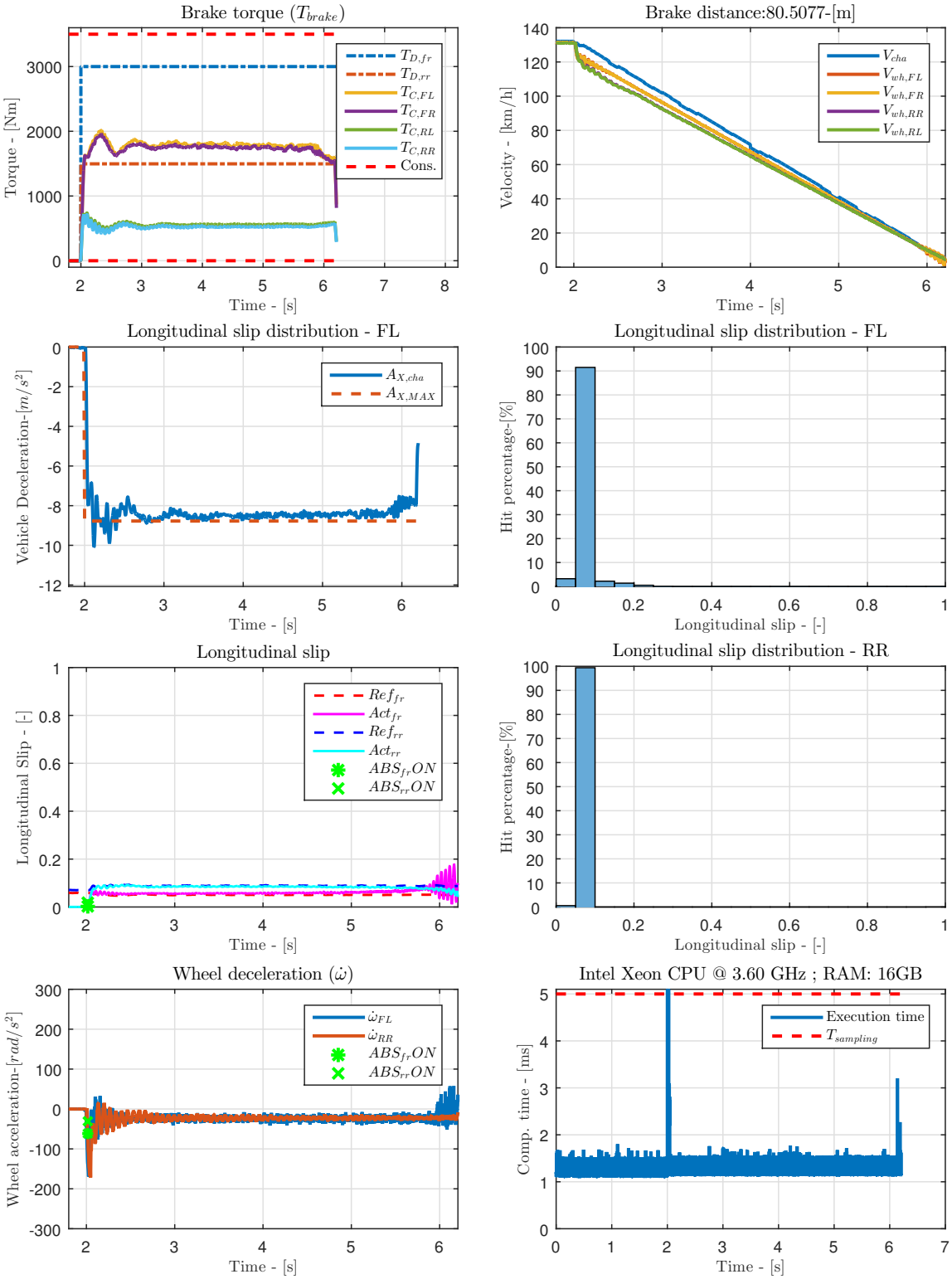

Figure B-1: Braking on dry asphalt - NMPC

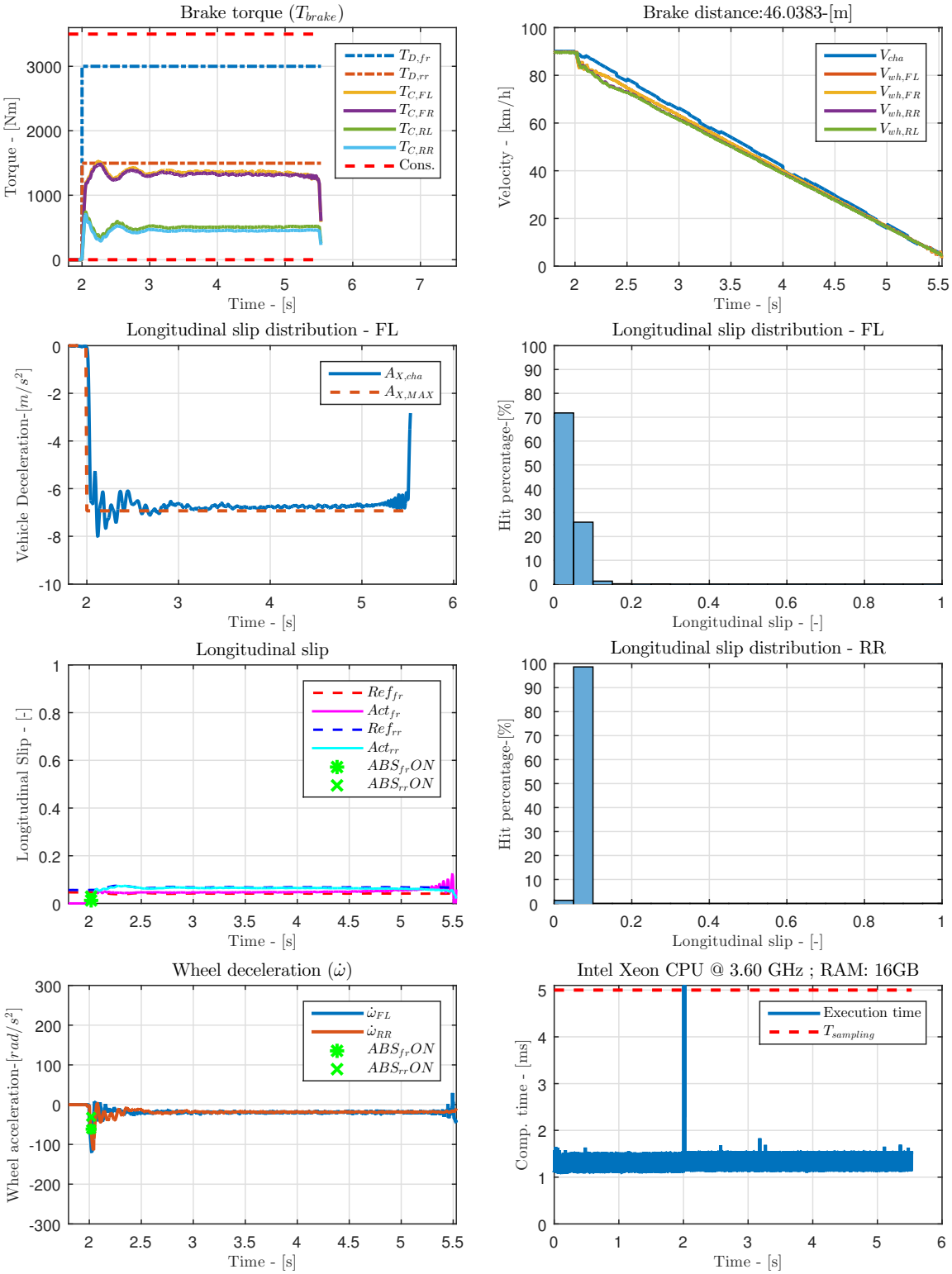

Figure B-2: Braking on wet asphalt - NMPC

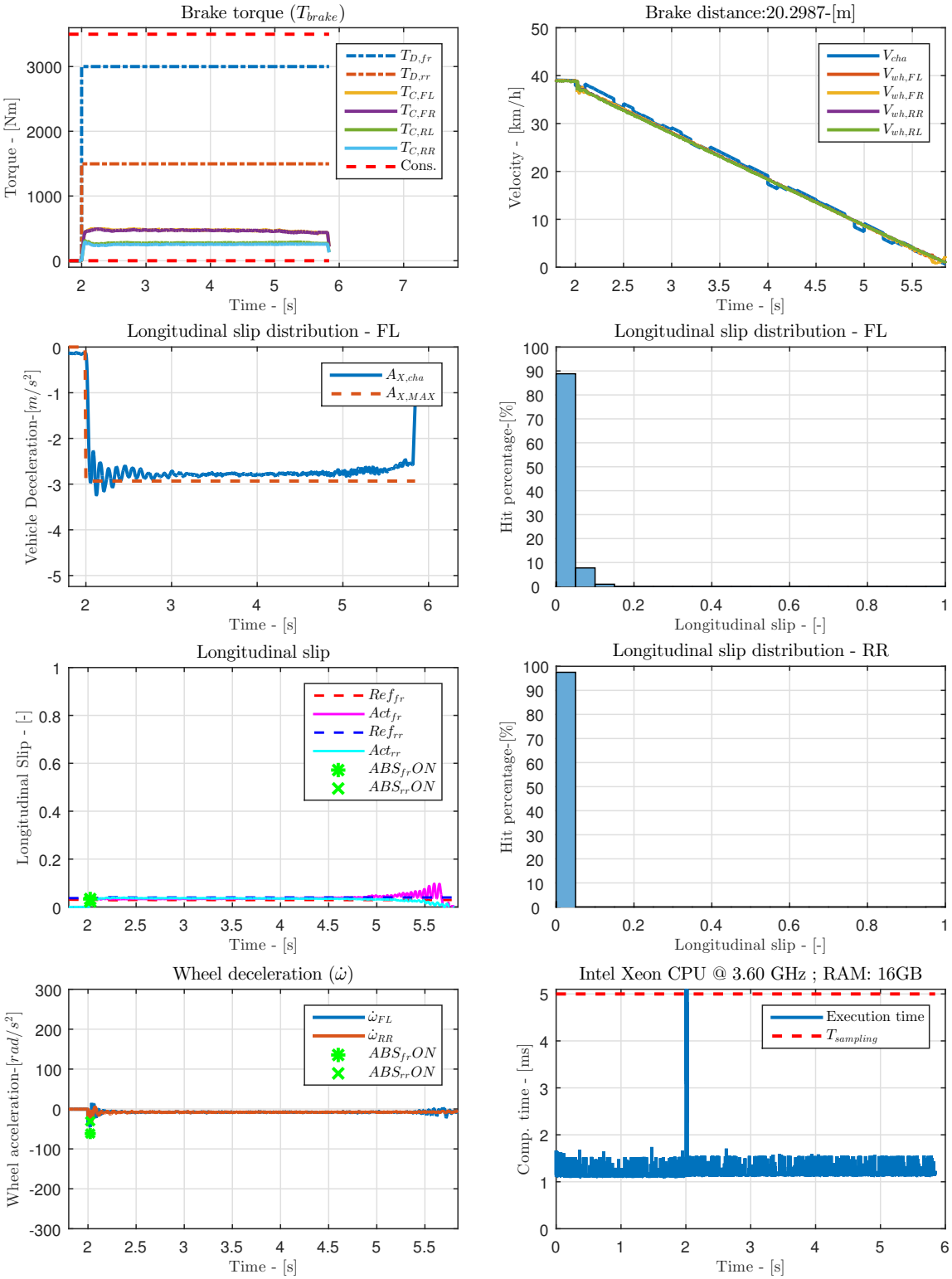

Figure B-3: Braking on packed snow - NMPC

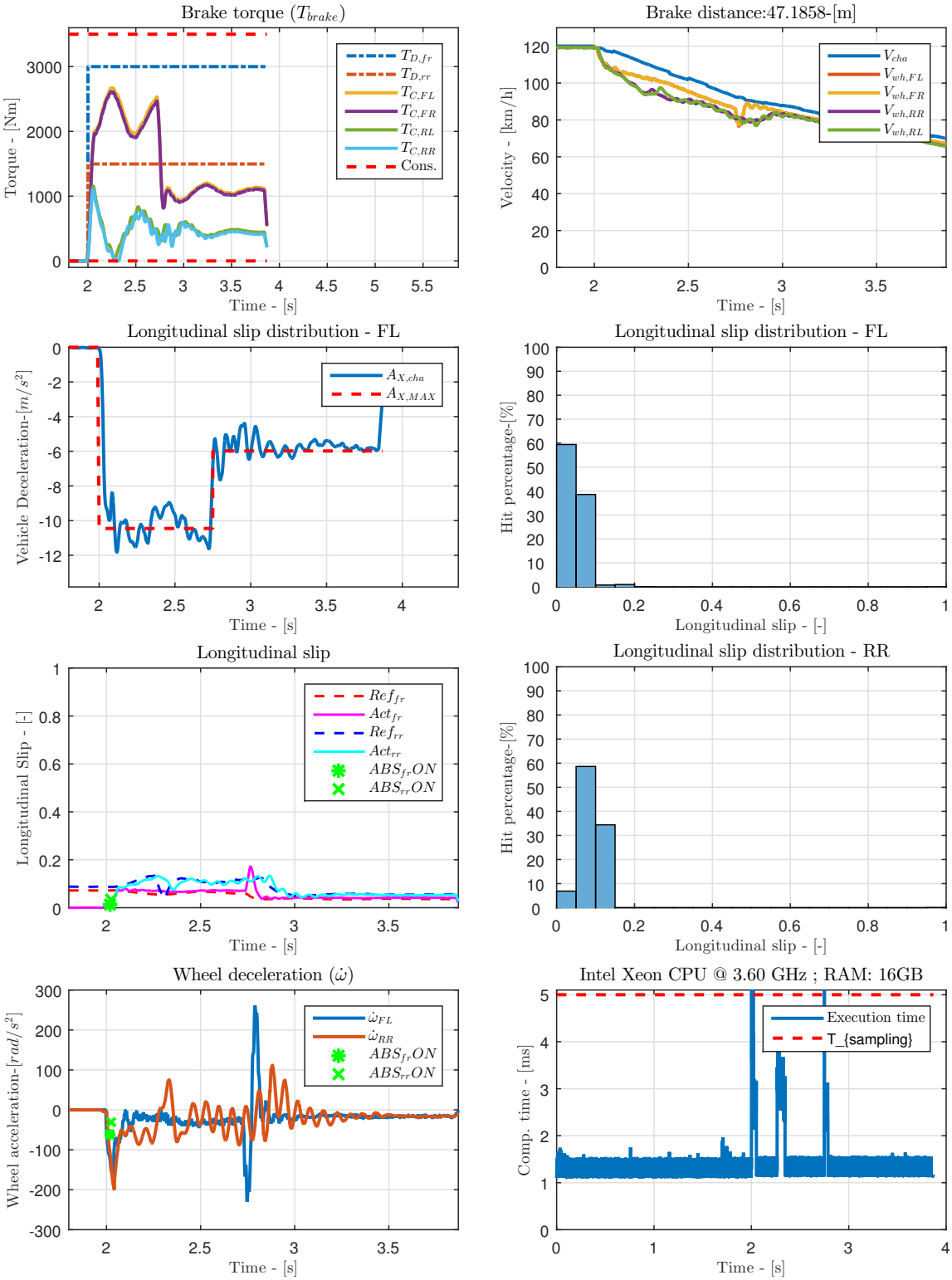

Figure B-4: Friction jump dry-wet asphalt - NMPC

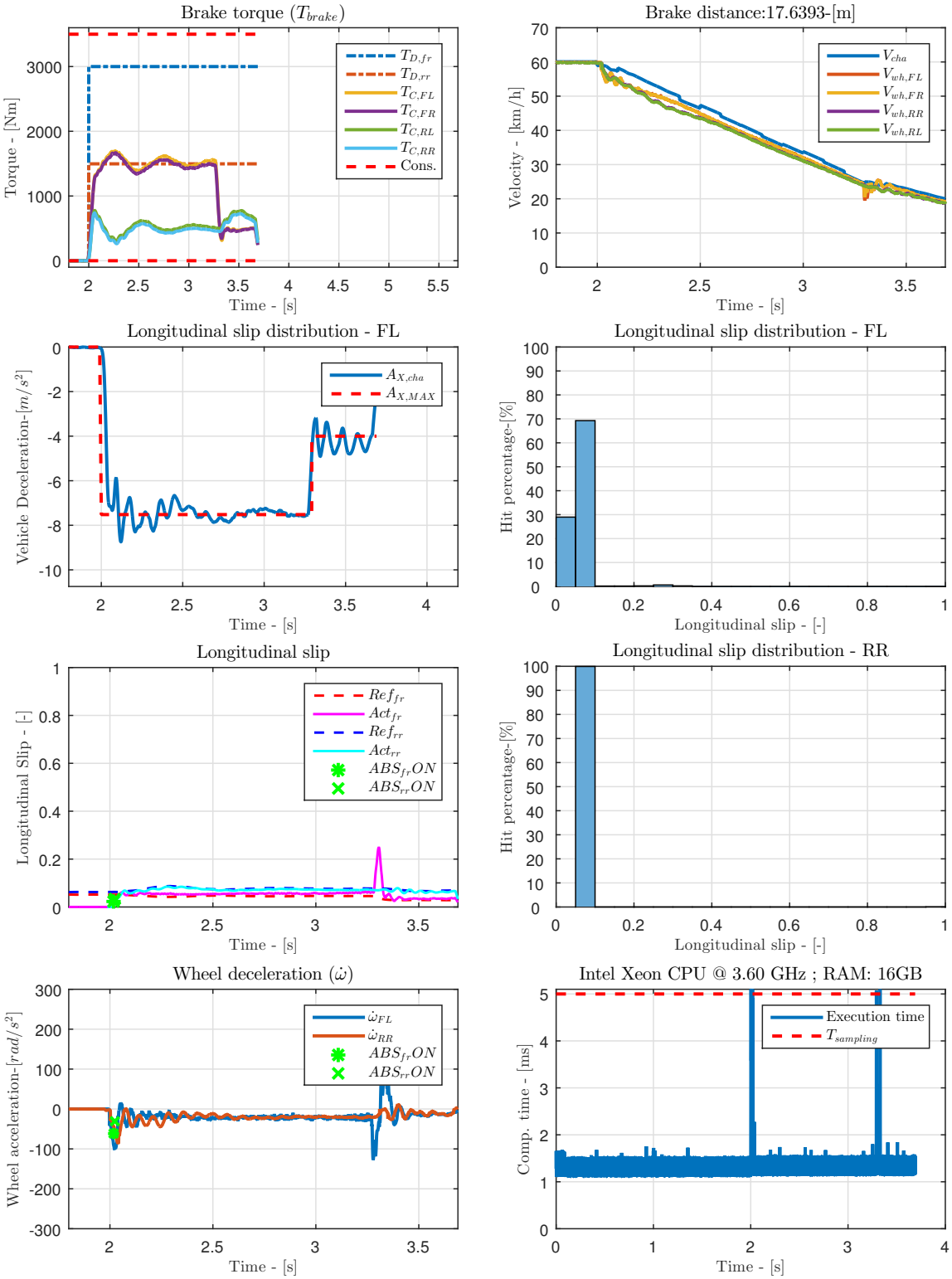

Figure B-5: Friction jump wet asphalt - packed snow - NMPC

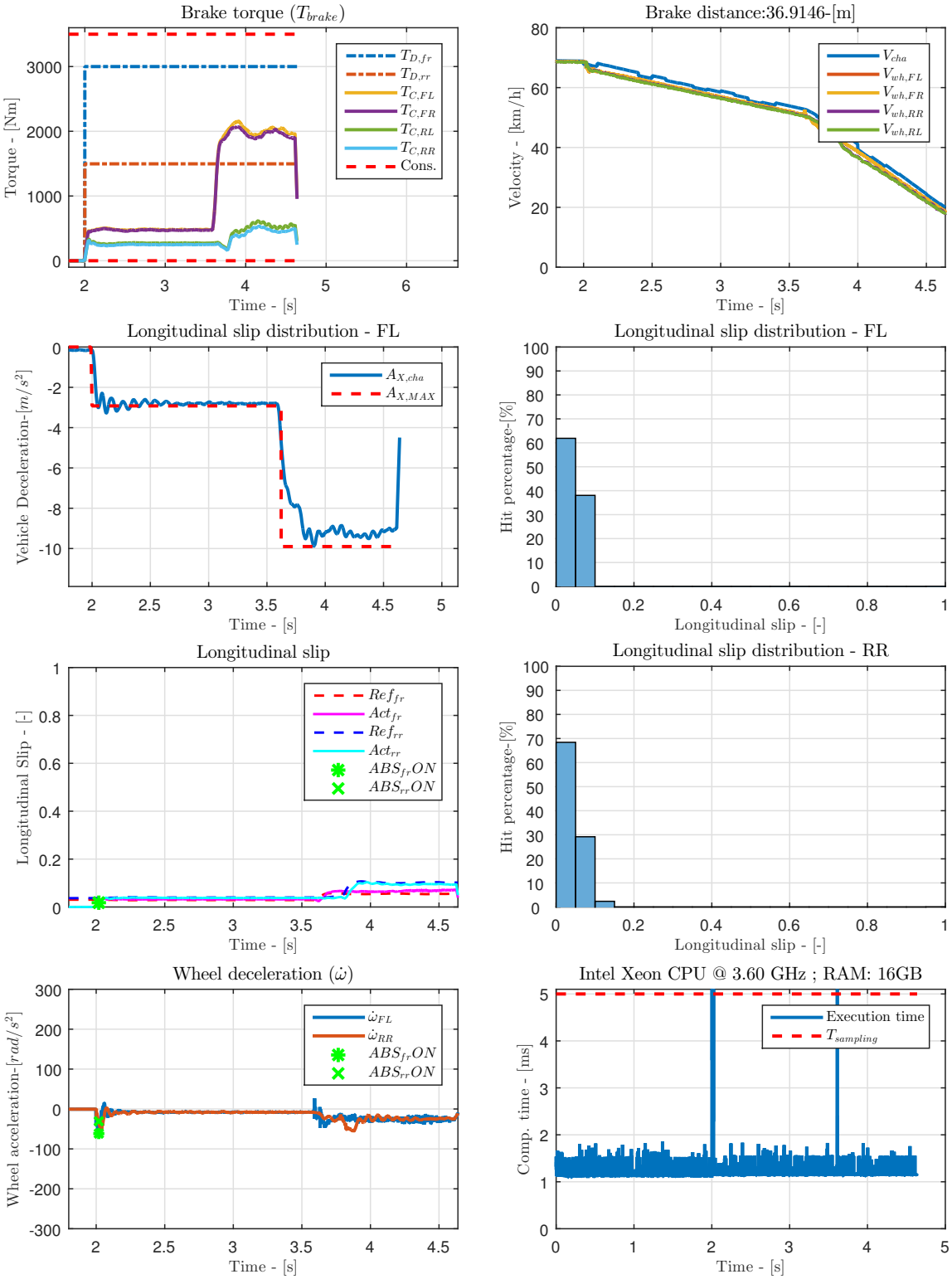

Figure B-6: Friction jump packed snow - dry asphalt - NMPC

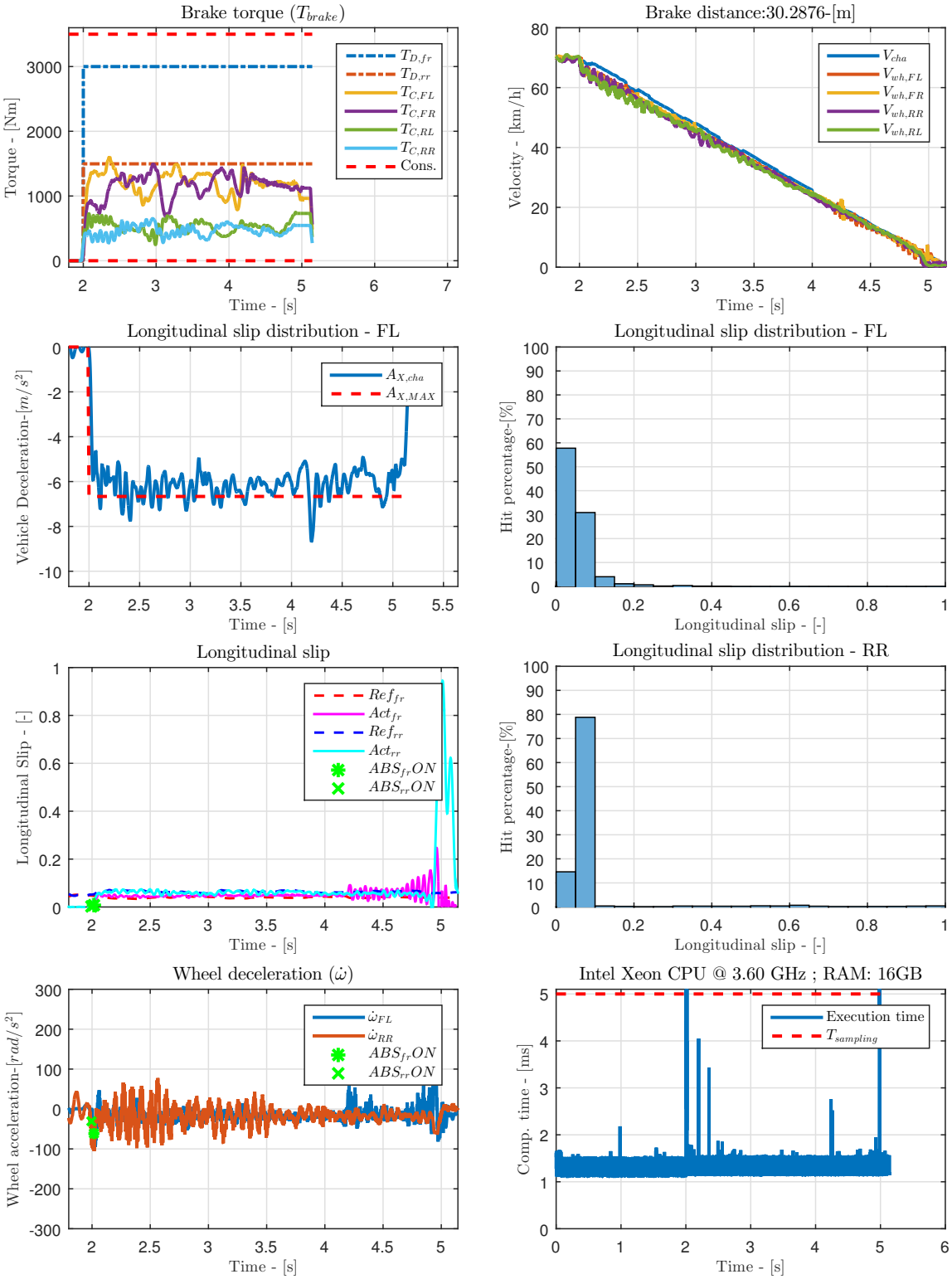

Figure B-7: Braking on red bricks - NMPC

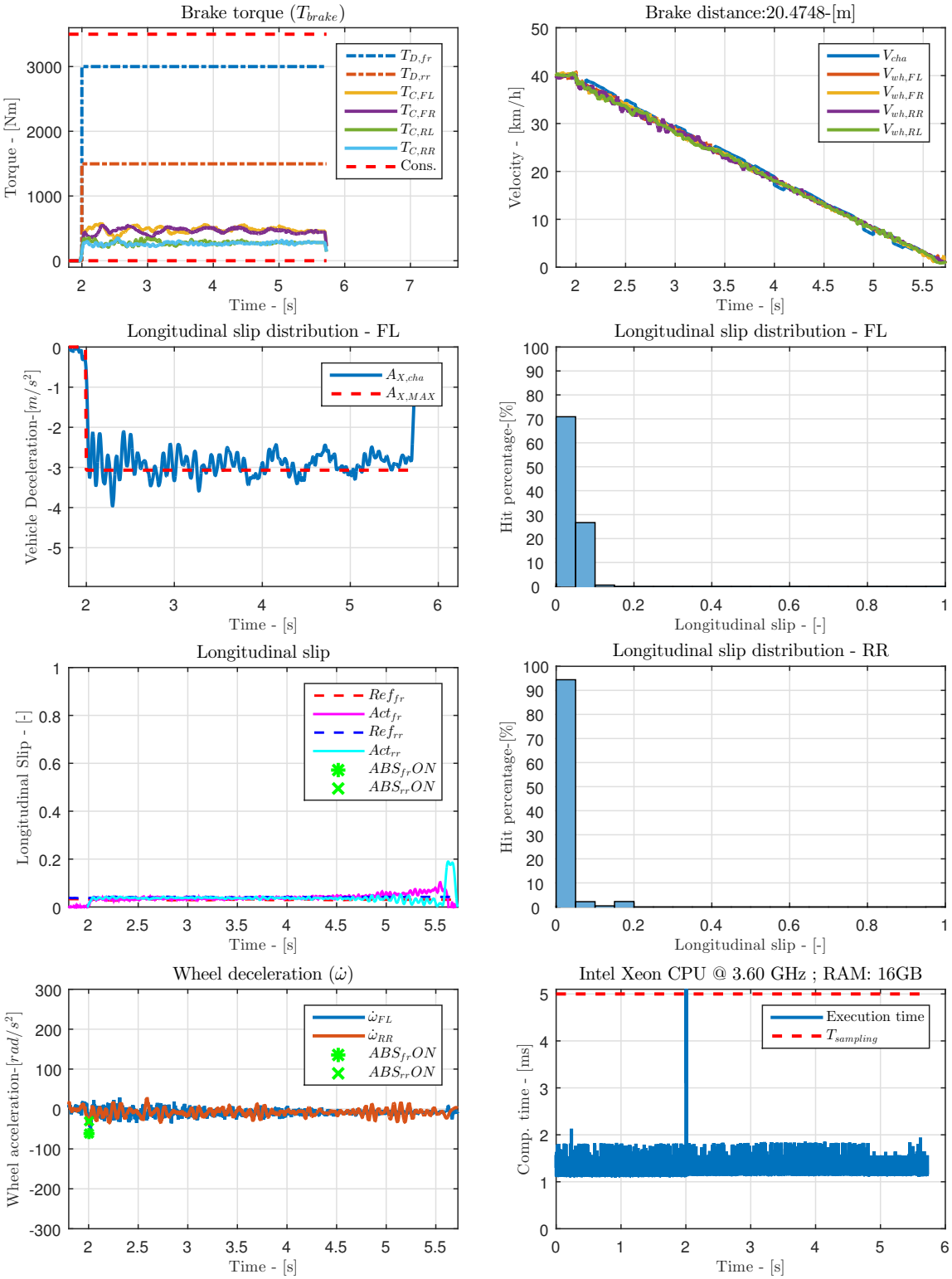

Figure B-8: Braking on Belgian cobblestones - NMPC

Appendix C

Benchmark RB controller results - NOT INCLUDED

This appendix contains confidential information and could therefore not be shared.

In this appendix time history charts for the NMPC ABS controller are presented. The following eight manoeuvres are shown:

1. Braking on smooth roads - Dry asphalt
2. Braking on smooth roads - Wet asphalt
3. Braking on smooth roads - Packed snow
4. Friction transitions - Dry asphalt to wet asphalt
5. Friction transitions - Wet asphalt to packed snow
6. Friction transitions - Packed snow to dry asphalt
7. Braking on rough roads - Red bricks
8. Braking on rough roads - Belgian cobblestones

Bibliography

[1] European Commission, "Statistics –accidents data." https://ec.europa.eu/transport/road_safety/specialist/statistics_en, 2017. (Accessed: 2018-06-18).

[2] M. P. Hagenzieker, J. J. Commandeur, and F. D. Bijleveld, "The history of road safety research: A quantitative approach," *Transportation Research Part F: Traffic Psychology and Behaviour*, vol. 25, pp. 150 – 162, 2014. Special Issue: The history of road safety research and the role of traffic psychology.

[3] M. Gerard, "Global chassis control and braking control using tyre forces measurements," Master's thesis, Delft University of Technology, 2011.

[4] D. Savitski, V. Ivanov, K. Augsburg, B. Shyrokau, R. Wragge-Morley, T. Pütz, and P. Barber, "The new paradigm of an anti-lock braking system for a full electric vehicle: Experimental investigation and benchmarking," vol. 230, 10 2015.

[5] W. Pasillas-Lépine, "Hybrid modeling and limit cycle analysis for a class of five-phase anti-lock brake algorithms," *Vehicle System Dynamics*, vol. 44, no. 2, pp. 173–188, 2006.

[6] V. Patil, "Generic and complete vehicle dynamic models for open-source platforms," Master's thesis, TU Delft, TU Chalmers, 2017.

[7] H. Pacejka, *Tire and Vehicle Dynamics*. Butterworth-Heinemann, third ed., 2012.

[8] A. Schmeitz, "Mf-tyre/mf-swift." http://publications.tno.nl/publication/34606988/ORSVMS/schmeitz-2013-mftyre-presentatie.pdf, 2013. (Accessed: 2018-08-01).

[9] O. Mikuláš, "A framework for nonlinear model predictive control," Master's thesis, Czech Technical University in Prague, 2016.

[10] Bosch GmbH, *Brakes, Brake Control and Driver Assistance Systems Function - Regulation and Components*. Springer Vieweg, first ed., 2014.

[11] ACEA, "Vehicles in use." http://www.acea.be/statistics/tag/category/vehicles-in-use, 2015. (Accessed: 2018-06-18).

[12] NHTSA, "Traffic stafety facts 2015 data." https://crashstats.nhtsa.dot.gov/#/DocumentTypeList/12, Sept. 2017. (Accessed: 2018-06-18).

[13] NHTSA, "Usdot releases 2016 fatal traffic crash data." https://www.nhtsa.gov/press-releases/usdot-releases-2016-fatal-traffic-crash-data, Oct. 2017. (Accessed: 2018-06-18).

[14] F. Wegman, "The future of road safety: A worldwide perspective," *IATSS Research*, vol. 40, no. 2, pp. 66 – 71, 2017. Special issue: The first global interactive forum on traffic and safety (2015) symposium on "diverse, regionally-rooted transport cultures".

[15] "Surface vehicle information report," tech. rep., SAE International, apr 2014.

[16] J. Y. Wong, *Theory of Ground Vehicles*. Wiley, fourth ed., 2008.

[17] Bosch GmbH, *Driving safety systems*. SAE International, second ed., 1999.

[18] G. Mauer, "Fuzzy logic controller for an abs braking system," vol. 3, pp. 381 – 388, 12 1995.

[19] S. Savaresi and M. Tanelli, *Active Braking Control Systems Design for Vehicles*. Springer, second ed., 2012.

[20] M. Schinkel and K. Hunt, "Anti-lock braking control using a sliding mode like approach," in *Proceedings of the 2002 American Control Conference (IEEE Cat. No.CH37301)*, vol. 3, pp. 2386–2391 vol.3, May 2002.

[21] S. M. Savaresi, M. Tanelli, C. Cantoni, D. Charalambakis, F. Previdi, and S. Bittanti, "Slip-deceleration control in anti-lock braking systems," *IFAC Proceedings Volumes*, vol. 38, no. 1, pp. 103 – 108, 2005. 16th IFAC World Congress.

[22] M. Gerard, W. Pasillas-L©pine, E. de Vries, and M. Verhaegen, "Adaptation of hybrid five-phase abs algorithms for experimental validation," *IFAC Proceedings Volumes*, vol. 43, no. 7, pp. 13 – 18, 2010. 6th IFAC Symposium on Advances in Automotive Control.

[23] S. Kerst, B. Shyrokau, and E. Holweg, "Reconstruction of wheel forces using an intelligent bearing," *SAE Int. J. Passeng. Cars – Electron. Electr. Syst.*, vol. 9, pp. 196–203, 04 2016.

[24] "Electric-vehicle control of individual wheel torque for on- and off-road conditions (e-vectoorc)." https://cordis.europa.eu/project/rcn/99412_en.html, 2015. (Accessed: 2018-20–16).

[25] X. Lu, Z. Zhou, and Y. Wang, "Design and comparative study of abs control strategies based on co-simulation," in *2015 IEEE International Conference on Cyber Technology in Automation, Control, and Intelligent Systems (CYBER)*, pp. 1665–1670, June 2015.

[26] U. Kiencke and N. L., *Automotive Control Systems for engine, driveline and vehicle*. Springer, 2005.

[27] Bosch GmbH, *Bosch Automotive Handbook*. Bentley Publishers, ninth ed., 2005.

[28] T. A. Johansen, J. Kalkkuhl, J. Ludemann, and I. Petersen, "Hybrid control strategies in abs," in *Proceedings of the 2001 American Control Conference. (Cat. No.01CH37148)*, vol. 2, pp. 1704–1705 vol.2, 2001.

[29] I. Ait-Hammouda and W. Pasillas-Lépine, "On a class of eleven-phase anti-lock brake algorithms robust with respect to discontinuous transitions of road characteristics," *IFAC Proceedings Volumes*, vol. 37, no. 21, pp. 551 – 556, 2004. 2nd IFAC Symposium on System Structure and Control, Oaxaca, Mexico, December 8-10, 2004.

[30] F. Pretagostini, "A survey on antilock braking systems control strategies," tech. rep., Delft University of Technology - Section of Intelligent Vehicles, 2018. Literature review.

[31] V. Ivanov, D. Savitski, and B. Shyrokau, "A survey of traction control and anti-lock braking systems of full electric vehicles with individually-controlled electric motors," *IEEE Transactions on Vehicular Technology*, vol. 64, no. 9, pp. 3878–3896, 2015.

[32] B. Shyrokau and V. Ivanov, "Alterable fuzzy sets in automotive control applications," *International Journal of Modelling Identification and Control*, vol. 3, pp. 153–181, 305-317.

[33] V. Ivanov, B. Shyrokau, D. Savitski, J. Orus, R. Meneses, J.-M. Rodriguez-Fortin, J. Theunissen, and K. Janssen, "Design and testing of abs for electric vehicles with individually controlled on-board motor drives," *SAE Int. J. Passeng. Cars - Mech. Syst.*, vol. 7, pp. 902–913, 08 2014.

[34] G. Venture, P. J. Ripert, W. Khalil, M. Gautier, and P. Bodson, "Modeling and identification of passenger car dynamics using robotics formalism," *IEEE Transactions on Intelligent Transportation Systems*, vol. 7, no. 3, pp. 349–359, 2006.

[35] H. Junjie, D. A. Crolla, M. C. Levesley, and W. J. Manning, "Coordination of active steering, driveline, and braking for integrated vehicle dynamics control," *Proceedings of the Institution of Mechanical Engineers, Part D: Journal of Automobile Engineering*, vol. 220, no. 10, pp. 1401–1420, 2006.

[36] J. D. Demerly and K. Youcef-Toumi, "Non-linear analysis of vehicle dynamics (navdyn): A reduced order model for vehicle handling analysis," in *SAE Technical Paper*, SAE International, 05 2000.

[37] C. Ghike and T. Shim, "14 degree-of-freedom vehicle model for roll dynamics study," in *SAE Technical Paper*, SAE International, 04 2006.

[38] S. B. Lu, S. B. Choi, Y. N. Li, M. S. Seong, and J. S. Han, "Global integrated control of vehicle suspension and chassis key subsystems," *Proceedings of the Institution of Mechanical Engineers, Part D: Journal of Automobile Engineering*, vol. 224, no. 4, pp. 423–441, 2010.

[39] B. Shyrokau, D. Wang, D. Savitski, K. Hoepping, and V. Ivanov, "Vehicle motion control with subsystem prioritization," *Mechatronics*, vol. 30, pp. 297 – 315, 2015.

[40] B. Shyrokau, D. Wang, and V. Savitski, Dzmitry Ivanov, "Vehicle dynamics control with energy recuperation based on control allocation for independent wheel motors and brake system," *International Journal of Powertrains*, vol. 2, pp. 153–181, 2013.

[41] J. Svendenius and B. Wittenmark, "Brush tire model with increased flexibility," *2003 European Control Conference (ECC)*, pp. 1863–1868, 2003.

[42] L. Li, F. Wang, and Q. Zhou, "Integrated longitudinal and lateral tire/road friction modeling and monitoring for vehicle motion control," *IEEE Transactions on Intelligent Transportation Systems*, vol. 7, pp. 1–19, March 2006.

[43] B. Shyrokau, D. Wang, K. Augsburg, and V. Ivanov, "Vehicle dynamics with brake hysteresis," *Proceedings of the Institution of Mechanical Engineers, Part D: Journal of Automobile Engineering*, vol. 227, pp. 139–150, 2013.

[44] S. Kerst, S. , B. Shyrokau, and E. Holweg, "Anti-lock braking control based on bearing load sensing," in *Eurobrake 2015*, 05 2015.

[45] S. Kerst, B. Shyrokau, and E. Holweg, "Wheel force measurement for vehicle dynamics control using an intelligent bearing," Sep 2016.

[46] J. Rauh, H. Schindler, L. Witte, T. Kersten, and W. Zipperer, "Opencrg - a unified approach to represent 3d road data in tyre simulation." https://www.vires.com/opencrg/docs/OpenCRG-Overview.pdf, 2008. (Accessed: 2018-08-05).

[47] J. Maciejowski, *Predictive Control with Constraints*. Prentice Hall, first ed., 2000.

[48] F. Borrelli, A. Bemporad, and M. Morari, *Predictive Control for Linear and Hybrid Systems*. Cambridge University Press, first ed., 2017.

[49] H. G. Bock, C. Diehl, K. Mombaur, and S. Sager, "Optimierung bei gewöhnlichen differentialgleichungen." https://wwwproxy.iwr.uni-heidelberg.de/groups/agbock/TEACHING/2015ws/NUM2/numerik2.pdf, 2014. (Accessed: 2018-08-10).

[50] F. Allgöwer, R. Findeisen, and Z. K. Nagy, "Nonlinear model predictive control : From theory to application," 2004.

[51] M. Diehl, *Real-Time Optimization for Large Scale Nonlinear Processes*. PhD thesis, Ruprecht-Karls-Universität Heidelberg, 2001.

[52] H. J. Ferreau, C. Kirches, A. Potschka, H. G. Bock, and M. Diehl, "qpoases: a parametric active-set algorithm for quadratic programming," *Mathematical Programming Computation*, vol. 6, pp. 327–363, Dec 2014.

[53] D. Ariens, B. Houska, H. Ferreau, and F. Logist, *ACADO for Matlab User's Manual*. Optimization in Engineering Center (OPTEC), 1.0beta ed., May 2010. http://www.acadotoolkit.org/.

[54] B. Houska, H. J. Ferreau, and M. Diehl, "An auto-generated real-time iteration algorithm for nonlinear mpc in the microsecond range," *Automatica*, vol. 47, no. 10, pp. 2279 – 2285, 2011.

[55] J. Ferreau, H. Bock, and M. Diehl, "An online active set strategy to overcome the limitations of explicit mpc," vol. 18, pp. 816–830, 05 2008.

[56] D. Kouzoupis, R. Quirynen, J. Frasch, and M. Diehl, "Block condensing for fast nonlinear mpc with the dual newton strategy," *IFAC-PapersOnLine*, vol. 48, no. 23, pp. 26 – 31, 2015. 5th IFAC Conference on Nonlinear Model Predictive Control NMPC 2015.

[57] H. Bock and K. Plitt, "A multiple shooting algorithm for direct solution of optimal control problems*," *IFAC Proceedings Volumes*, vol. 17, no. 2, pp. 1603 – 1608, 1984. 9th IFAC World Congress: A Bridge Between Control Science and Technology, Budapest, Hungary, 2-6 July 1984.

[58] H. J. Ferreau, "An online active set strategy for fast solution of parametric quadratic programs with applications to predictive engine control," Master's thesis, Ruprecht-Karls-Universität Heidelberg, 2006.

Glossary

List of Acronyms

3D	Three-Dimensional
ABS	Anti-lock Braking System
ACEA	European Automobile Manufacturers' Association
ADAS	Advanced Driver Assistance Systems
AEB	Autonomous Emergency Braking
ANFIS	Adaptive Network-based Fuzzy Inference System
CoG	Centre of Gravity
CRG	Curved Regular Grid
DoF	Degree of Freedom
EBD	Electronic Brake Distribution
ECU	Electronic Control Unit
EHB	Electro–Hydraulics Brakes
EMB	Electro –Mechanical Brake
ESC	Electronic Stability Control
E-VECTOORC	Electric-Vehicle Control of Individual Wheel Torque for On- and Off-Road Conditions
FBD	Free Body Diagram
FMI	Functional Mock-up Interface
FMU	Functional Mock-up Unit

FSM	Finite State Machines
HAB	Hydraulically Applied Brakes
HiL	Hardware In the Loop
IMU	Inertial Measurement Unit
IPC	Inter-Processor Communication
ISMC	Integral Sliding Mode Controller
ITAE	Integral Time-weighted Absolute Error
LP	Linear Program
KnC	Kinematics and compliance
KPI	Key Performance Indicators
KKT	Karush–Kuhn–Tucker
LUT	Look-Up Table
MBD	Model Based Design
MEMS	Micro Electro-Mechanical Systems
MF	Magic Formula
MPC	Model Predictive Control
NHTSA	National Highway Traffic Safety Administration
NLP	Non-Linear Programming
NMPC	Nonlinear Model Predictive Control
OCP	Optimal Control Problem
OEM	Original Equipment Manufacturer
PID	Proportional - Integral - Derivative
QP	Quadratic Problem
RB	Rule-Based
RHC	Receding Horizon Control
RMSE	Root Mean Squared Error
RSC	Roll Stability Control
RTI	Real Time Iteration
SDS	Spring Damper System

SQP	Sequential Quadratic Program
TCS	Traction Control System
TME	Toyota Motor Europe
VSC	Vehicle Stability Control

List of Symbols

α_{env}	Power dissipation coefficient to the environment, $[-]$
α_{ij}	Tire lateral slip angle, $[rad]$
β	Chassis side slip angle, $[rad]$
δ	Steering wheel angle, $[rad]$
δ_{ij}	Wheel steer angle, $[rad]$
$\dot{\omega}_{th,ij}$	Wheel angular acceleration threshold for activation, $[rad/s^2]$
λ	Longitudinal wheel slip, [-]
λ^*	Optimal longitudinal wheel slip, [-]
λ_{ref}	Reference longitudinal wheel slip, [-]
λ_{th}	Longitudinal wheel slip threshold for activation, [-]
μ	Tire-road friction coefficient, [-]
$\mu_{pad,ij}$	Disc-pad friction coefficient, [-]
ω_{ij}	Wheel angular velocity, $[rad/s]$
ϕ	Chassis pitch angle, $[rad]$
ψ	Chassis yaw angle, $[rad]$
τ	EHB actuator time constant, $[s]$
θ	Chassis roll angle, $[rad]$
λ^*	Optimal tire longitudinal wheel slip
a	Distance between front axle and total CoG, $[m]$
a_x	Chassis longitudinal acceleration, $[m/s^2]$
a_y	Chassis lateral acceleration, $[m/s^2]$
a_z	Chassis vertical acceleration, $[m/s^2]$
A_{pist}	Caliper piston area, $[m^2]$
b	Distance between rear axle and total CoG, $[m]$
c	Front suspension pitch damping coefficient, $[Nms/rad]$
c	Rear suspension pitch damping coefficient, $[Nms/rad]$
$c_{\theta f}$	Front suspension roll damping coefficient, $[Nms/rad]$
$c_{\theta r}$	Rear suspension roll damping coefficient, $[Nms/rad]$
c_{ij}	Damping coefficient of the corner, $[Nms/rad]$
C_{pd}	Heat capacity of the brake disc
$dT_{b,ij}$	Corner brake torque rate, $[Nm/s]$
$dT_{b,ref}$	Reference corner brake torque rate, $[Nm/s]$
$dT_{b_{cmd,ij}}$	Commanded corner brake torque rate, $[Nm/s]$
$F_{s,ij}$	Suspension force at the strut , $[N]$
$F_{x,ij}$	Longitudinal force at the chassis corner - ij = [FL,FR,RL,RR], $[N]$
$F_{x,i}$	Longitudinal tire force - i = [1,2,3,4], $[N]$
F_x	Chassis longitudinal force, $[N]$
F_x^{aero}	Aerodynamic longitudinal force, $[N]$

$F_{y,ij}$	Lateral force at the chassis corner - ij = [FL,FR,RL,RR], $[N]$
$F_{y,i}$	Lateral tire force - i = [1,2,3,4], $[N]$
F_y	Chassis lateral force, $[N]$
F_y^{aero}	Aerodynamic lateral force, $[N]$
F_z^{aero}	Aerodynamic vertical force, $[N]$
h_f	Height of the front roll center, $[m]$
h_p	Height of the pitch center, $[m]$
h_r	Height of the front roll center, $[m]$
h_s	Height of the CoG, $[m]$
h_{uf}	Height of front unsprung mass CoG above origin, $[m]$
h_{ur}	Height of rear unsprung mass CoG above origin, $[m]$
I_w	Moment of inertia of the vehicle corner about y-axis, $[kgm^2]$
$I_{xx,s}$	Moment of inertia of the sprung mass about x-axis, $[kgm^2]$
$I_{xy,s}$	Moment of inertia of the sprung mass about x- and y-axis, $[kgm^2]$
$I_{xz,s}$	Moment of inertia of the sprung mass about x- and z-axis, $[kgm^2]$
$I_{yy,s}$	Moment of inertia of the sprung mass about y-axis, $[kgm^2]$
$I_{yy,u}$	Moment of inertia of the unsprung mass about y-axis, $[kgm^2]$
$I_{yz,s}$	Moment of inertia of the sprung mass about y- and z-axis, $[kgm^2]$
$I_{zz,s}$	Moment of inertia of the sprung mass about z-axis, $[kgm^2]$
$k_{\phi f}$	Front suspension pitch stiffness, $[Nm/rad]$
$k_{\phi r}$	Rear suspension pitch stiffness, $[Nm/rad]$
$k_{\theta f}$	Front suspension roll stiffness, $[Nm/rad]$
$k_{\theta r}$	Rear suspension roll stiffness, $[Nm/rad]$
$k_{arb,i}$	Anti-roll bar stiffness of the corner, $[N/m]$
k_{ij}	Spring stiffness of the corner, $[N/m]$
k_t	Vertical stiffness of the tire, $[N/m]$
m_c	Vehicle corner mass, $[kg]$
m_d	Brake disc mass, $[kg]$
m_s	Vehicle sprung mass, $[kg]$
m_t	Total vehicle mass, $[kg]$
m_{ij}	Wheel assembly mass, $[kg]$
m_{uf}	Front unsprung mass, $[kg]$
m_{ur}	Rear unsprung mass, $[kg]$
N_p	Controller's prediction horizon, $[]-]]$
R_w	Wheel radius, $[m]$
t	Time, $[s]$
$T_{b,dvr}$	Driver brake torque demand, $[Nm]$
$T_{b,ij}$	Corner brake torque, $[Nm]$
$T_{b,ref}$	Reference corner brake torque, $[Nm]$
$T_{b,th}$	Brake torque demand threshold for activation, $[Nm]$

$T_{b_{act,ij}}$	Actual corner brake torque, $[Nm]$
$T_{b_{cmd,ij}}$	Commanded corner brake torque, $[Nm]$
T_{drag}	Tire drag torque, $[Nm]$
t_f	Front track width, $[m]$
T_p	Controller's look-ahead time, $[s]$
t_r	Rear track width, $[m]$
T_s	Controller sampling time, $[s]$
v	Chassis absolute velocity, $[m/s]$
v_x	Chassis longitudinal velocity, $[m/s]$
v_y	Chassis lateral velocity, $[m/s]$
v_{ref}	Reference chassis velocity, $[m/s]$
v_{thr}	Chassis velocity threshold for low speed ABS activation, $[m/s]$
W_λ	Optimization weight associated with longitudinal wheel slip - $[-]$
W_{dT_b}	Optimization weight associated with corner brake torque rate - $[-]$
W_{T_b}	Optimization weight associated with corner brake torque - $[-]$
W_v	Optimization weight associated with chassis velocity - $[-]$
x	Chassis position $x-$position - $[m]$
y	Chassis position $y-$position - $[m]$
z	Chassis position $z-$position - $[m]$
$z_{u,ij}$	Vertical displacement of the unsprung corner, $[m]$
P_{ij}	Brake pressure at the wheel, $[bar]$
P_{mc}	Brake pressure at the master cylinder, $[bar]$
SWF	Suspension force to wheel force, $[-]$
Q_{ij}	Thermal energy of the brake corner, $[J]$

a a_x a_y a_z A_{pist}

b

c_{ij} C_{pd}, $[kgm^2/Ks^2]$ c c $c_{\theta f}$ $c_{\theta r}$

$dT_{b_{cmd,ij}}$ $dT_{b,ij}$ $dT_{b,ref}$

$F_{s,ij}$ F_x F_x^{aero} $F_{x,i}$ $F_{x,ij}$ F_y F_y^{aero} $F_{y,i}$ $F_{y,ij}$ F_z^{aero}

h_f h_p h_r h_s h_{uf} h_{ur}

I_w $I_{yy,u}$ $I_{xx,s}$ $I_{xy,s}$ $I_{xz,s}$ $I_{yy,s}$ $I_{yz,s}$ $I_{zz,s}$

k_{ij} k_t $k_{arb,i}$ $k_{\theta f}$ $k_{\theta r}$ $k_{\phi f}$ $k_{\phi r}$

m_c m_d m_s m_t m_{ij} m_{uf} m_{ur}

N_p

P_{ij} P_{mc}

Q_{ij}

SWF

R_w

t $T_{b_{act,ij}}$ $T_{b_{cmd,ij}}$ $T_{b,dvr}$ $T_{b,ij}$ $T_{b,ref}$ $T_{b,th}$ T_{drag} t_f T_p t_r T_s

v v_x v_y v_{ref} v_{thr}

W_{dT_b} W_{T_b} W_v W_λ

x

y

z

$z_{u,ij}$

α_{ij} α_{env} β δ δ_{ij} λ λ^* λ_{ref} λ_{th} μ $\mu_{pad,ij}$ θ τ ϕ ψ ω_{ij} $\dot{\omega}_{th,ij}$